Published for SISSA by Springer

Received: March 27, 2020
Accepted: June 15, 2020
Published: July 7, 2020

Measurements of the production cross-section for a Z boson in association with b-jets in proton-proton collisions at $\sqrt{s} = 13$ TeV with the ATLAS detector

The ATLAS collaboration

E-mail: atlas.publications@cern.ch

Abstract: This paper presents a measurement of the production cross-section of a Z boson in association with b-jets, in proton-proton collisions at $\sqrt{s} = 13\,\text{TeV}$ with the ATLAS experiment at the Large Hadron Collider using data corresponding to an integrated luminosity of $35.6\,\text{fb}^{-1}$. Inclusive and differential cross-sections are measured for events containing a Z boson decaying into electrons or muons and produced in association with at least one or at least two b-jets with transverse momentum $p_{\text{T}} > 20\,\text{GeV}$ and rapidity $|y| < 2.5$. Predictions from several Monte Carlo generators based on leading-order (LO) or next-to-leading-order (NLO) matrix elements interfaced with a parton-shower simulation and testing different flavour schemes for the choice of initial-state partons are compared with measured cross-sections. The 5-flavour number scheme predictions at NLO accuracy agree better with data than 4-flavour number scheme ones. The 4-flavour number scheme predictions underestimate data in events with at least one b-jet.

Keywords: Hadron-Hadron scattering (experiments)

ArXiv ePrint: 2003.11960

https://doi.org/10.1007/JHEP07(2020)044

JHEP07(2020)044

Contents

1 Introduction

The measurement of the production rate of a Z boson in association with jets originating from b-quarks[1] ($Z + b$-jets) in proton-proton (pp) collisions provides an important test of perturbative quantum chromodynamics (pQCD). Current predictions for $Z+b$-jets production are known at next-to-leading-order (NLO) accuracy in pQCD, and they can be derived in either a 4-flavour number scheme (4FNS) or a 5-flavour number scheme (5FNS) [1–4].

[1] Unless otherwise mentioned, it is implicitly assumed that b-quark refers to both b-quark and $\bar{b}$-antiquark.

JHEP07(2020)044

In the 4FNS, b-quarks do not contribute to the parton distribution functions (PDFs) of the proton and, in QCD, they only appear in a massive final state due to gluon splitting ($g \to b\bar{b}$). In the 5FNS, b-quark density is allowed in the initial state via a b-quark PDF, with the b-quark typically being massless. Therefore, in the 5FNS the $Z + b$-jets cross-section is sensitive to the b-quark PDF and can be used to constrain it. The ambiguity among the schemes is an intrinsic property of the calculation and is expected to reduce with the inclusion of higher order perturbative corrections [3].

Furthermore, the measurement of $Z + b$-jets production provides a benchmark to test predictions from Monte Carlo (MC) simulations. These are commonly used to estimate the background contribution of $Z + b$-jet events to other topologies, such as the production of a Higgs boson decaying into a b-quark pair in association with a Z boson, or in searches for physics beyond the SM with signatures containing leptons and b-jets in the final state.

The $Z + b$-jets processes occur more rarely than the production of Z-boson events with inclusive jets (Z+jets) and they are more challenging to measure. The b-jets are identified by exploiting the long lifetime of b-hadrons produced in the quark hadronisation, and a higher level of background affects the measurement. The background is mainly composed of events with a Z boson associated with light-flavour jets or c-jets,[2] misidentified as b-jets, and events from the dileptonic decay of a $t\bar{t}$ pair.

Inclusive and differential cross-sections of $Z + b$-jets production have been measured in proton-antiproton collisions at the centre-of-mass energy of $\sqrt{s} = 1.96$ TeV by the CDF and D0 experiments [5–8] and at the Large Hadron Collider (LHC) [9] in $\sqrt{s} = 7$ TeV pp collisions by the ATLAS and CMS experiments [10–15], as well as in $\sqrt{s} = 8$ TeV pp collisions by the CMS experiment [16, 17]. The CMS experiment also recently released a measurement of the ratio of $Z + b$-jets to Z+jets cross-sections and the ratio of $Z + c$-jets to $Z + b$-jets cross-sections for events with at least one b-jet or one c-jet in $\sqrt{s} = 13$ TeV pp collisions [18].

This paper presents a measurement of the inclusive and differential production cross-sections of a Z boson, decaying into electrons or muons, in association with at least one or at least two b-jets using $35.6\,\text{fb}^{-1}$ of pp collision data collected by the ATLAS experiment at $\sqrt{s} = 13$ TeV in 2015 and 2016. For events with at least one b-jet, the differential cross-sections are presented as a function of the transverse momentum[3] (p_{T}) and the absolute value of the rapidity ($|y|$) of the leading b-jet, the p_{T} and the $|y|$ of the Z boson (Z p_{T} and Z $|y|$), and as a function of observables correlating the Z boson with the leading b-jet, namely the azimuthal angle between them ($\Delta\phi_{Zb}$), the absolute value of their rapidity difference (Δy_{Zb}), and their angular separation (ΔR_{Zb}). For events with at least two b-jets, the differential cross-sections are presented as a function of the p_{T} of the Z boson

[2] A c-jet is a jet originating from a c-quark.

[3] ATLAS uses a right-handed coordinate system with its origin at the nominal interaction point (IP) in the centre of the detector and the z-axis along the beam pipe. The x-axis points from the IP to the centre of the LHC ring, and the y-axis points upwards. Cylindrical coordinates (r, ϕ) are used in the transverse plane, ϕ being the azimuthal angle around the z-axis. The pseudorapidity is defined in terms of the polar angle θ as $\eta = -\ln\tan(\theta/2)$. Angular separation is measured in units of $\Delta R \equiv \sqrt{(\Delta\eta)^2 + (\Delta\phi)^2}$. When dealing with massive jets and particles, the rapidity $y = \frac{1}{2}\ln\frac{E+p_z}{E-p_z}$ is used, in which E is the jet or particle energy and p_z is the z-component of the jet or particle momentum.

JHEP07(2020)044

and as a function of observables built using the two leading b-jets, namely their p_{T} ($p_{\mathrm{T},bb}$), their invariant mass (m_{bb}), $p_{\mathrm{T},bb}$ divided by their invariant mass ($p_{\mathrm{T},bb}/m_{bb}$), the azimuthal angle between them ($\Delta\phi_{bb}$), the absolute value of their rapidity difference (Δy_{bb}), and their angular separation (ΔR_{bb}). The higher $\sqrt{s}$ leads to a large increase in the measured cross-section in comparison with previous ATLAS publications. This allows more extreme regions of phase space to be explored and new measurements to be performed in the rare two-b-jets configuration (i.e. $p_{\mathrm{T},bb}$ and $p_{\mathrm{T},bb}/m_{bb}$). Previous ATLAS measurements were compared with MC predictions based on leading-order matrix elements interfaced with a parton-shower simulation, which showed substantial mismodelling. Recent advances in this field permit this paper to compare the data with the latest MC predictions using next-to-leading-order matrix elements, which are expected to provide a better description of the data.

The experimental apparatus is described in section 2, and details of the data sample and the MC simulations are provided in section 3. The object definitions and the event selection at detector level are presented in section 4. Backgrounds that do not contain a real Z boson are estimated via MC simulations and validated in control regions in data or via data-driven techniques, while backgrounds containing a real Z boson and jets not originating from b-quarks are estimated with a fit to data distributions sensitive to the flavour of the jet (flavour fit); both are described in section 5. Distributions of the kinematic variables are presented in section 6. After background subtraction, the data are unfolded to particle level in a fiducial phase space, which is detailed in section 7. Systematic uncertainties in the unfolded data are discussed in section 8. The results are presented in section 9, and conclusions are drawn in section 10.

2 The ATLAS detector

The ATLAS detector [19] at the LHC covers nearly the entire solid angle around the collision point. It consists of an inner tracking detector surrounded by a thin superconducting solenoid, electromagnetic and hadronic calorimeters, and a muon spectrometer incorporating three large superconducting toroidal magnets.

The inner-detector system (ID) is immersed in a 2 T axial magnetic field and provides charged-particle tracking in the range $|\eta| < 2.5$. The high-granularity silicon pixel detector covers the vertex region and provides four measurements for most tracks, the first hit normally being in the insertable B-layer [20, 21]. It is followed by the silicon microstrip tracker, which provides eight measurements per track. These silicon detectors are complemented by the transition radiation tracker (TRT), which enables radially extended track reconstruction up to $|\eta| = 2.0$. The TRT also provides electron identification information based on the fraction of hits (typically 30 in total) with an energy deposit above the transition-radiation threshold.

The calorimeter system covers the pseudorapidity range $|\eta| < 4.9$. Within the region $|\eta| < 3.2$, electromagnetic calorimetry is provided by barrel and endcap high-granularity lead/liquid-argon (LAr) calorimeters, with an additional thin LAr presampler covering $|\eta| < 1.8$ to correct for energy loss in material upstream of the calorimeters. Hadronic

JHEP07(2020)044

calorimetry is provided by the steel/scintillator-tile calorimeter, segmented into three barrel structures within $|\eta| < 1.7$, and two copper/LAr hadronic endcap calorimeters. The solid angle coverage is completed with forward copper/LAr and tungsten/LAr calorimeter modules optimised for electromagnetic and hadronic measurements, respectively.

The muon spectrometer (MS) comprises separate trigger and high-precision tracking chambers measuring the deflection of muons in a magnetic field generated by the superconducting air-core toroid magnets. The field integral of the toroid magnets ranges between 2.0 and 6.0 T m across most of the detector. The precision chambers cover the region $|\eta| < 2.7$ with three layers of monitored drift tubes, complemented by cathode-strip chambers in the forward region, where the background is highest. The muon trigger system covers the range $|\eta| < 2.4$ with resistive-plate chambers in the barrel, and thin-gap chambers in the endcap regions.

Interesting events are accepted by the first-level trigger system implemented in custom hardware, followed by selections made by algorithms implemented in software in the high-level trigger [22]. The first-level trigger accepts events from the 40 MHz bunch crossings at a rate below 100 kHz, which the high-level trigger further reduces in order to record events to disk at about 1 kHz rate.

3 Data set and simulated event samples

3.1 Data set description

The data used in this measurement were recorded in 2015 and 2016 with the ATLAS detector at the LHC in pp collisions at $\sqrt{s} = 13$ TeV. The candidate events were selected by either a single-electron or single-muon trigger that imposed a minimum transverse energy (transverse momentum) threshold for the electron (muon) channel and quality and isolation requirements, which depended on the LHC running conditions. The threshold in 2015 was 24 (20) GeV for the electrons (muons), satisfying loose isolation requirements. Due to the higher instantaneous luminosity in 2016, the threshold was increased to 26 GeV for both the electrons and the muons, and a more restrictive isolation requirement was imposed on both leptons along with more restrictive identification requirements for electrons. Triggers with higher thresholds but with no isolation requirement or with loosened identification criteria were also used to increase the efficiency. Crossings of proton bunches occurred every 25 ns, the collisions achieved a peak instantaneous luminosity of 1.37×10^{34} cm^{-2}s^{-1}, and the mean number of pp interactions per bunch crossing (pile-up) was $\langle\mu\rangle = 24$. After applying criteria to ensure good ATLAS detector operation, the total integrated luminosity amounts to 35.6 fb^{-1}. The uncertainty in the combined 2015-2016 integrated luminosity is 2.1% [23], obtained using the LUCID-2 detector [24] for the primary luminosity measurements.

3.2 Simulated event samples for signal and background processes

MC simulations are used to describe signal events, to estimate the contribution of background processes, to unfold the data yield to the particle level, to estimate systematic uncertainties, and to compare predictions with the unfolded data distributions.

JHEP07(2020)044

An overview of all signal and background processes and the generators used for the production of nominal results is given in table 1 together with the theory uncertainty in the normalisation cross-sections corresponding to PDFs and scale variations.

Inclusive $Z(\to \ell\ell, \ell = e, \mu)$ production in association with both light- and heavy-flavour jets was simulated using the Sherpa v2.2.1 [25] generator. In this set-up, matrix elements at NLO for up to two partons, and matrix elements at LO for up to four partons, were calculated with the Comix [26] and OpenLoops [27, 28] libraries. They were matched with the Sherpa parton shower [29] using the MEPS@NLO prescription [30–33]. Sherpa uses the 5FNS with massless b- and c-quarks in the matrix element, but massive quarks in the parton shower. Samples were generated using the NNPDF3.0nnlo PDF set [34], along with the dedicated set of tuned parton-shower parameters developed by the Sherpa authors. In section 9, where several predictions are compared with the unfolded data, these samples are shown with their uncertainties and are referred to as Sherpa 5FNS (NLO). The uncertainties account for missing higher orders and are evaluated [35] using seven variations of the QCD factorisation and renormalisation scales in the matrix elements by factors of 0.5 and 2 and avoiding variations in opposite directions.

Additional $Z(\to \ell\ell)$ samples were produced with the LO matrix-element generator Alpgen v2.14 [36], interfaced with Pythia v6.426 [37] to model parton showers, using the parameter values of the Perugia2011C tune [38] for simulating the underlying event, and the CTEQ6L1 PDF set [39]. Matrix elements were calculated for up to five partons, and merged using the MLM prescription [40] with a matching scale of 15 GeV. Alpgen uses the 4FNS with massive b- and c-quarks in the matrix element and in the parton shower of Pythia. The matrix elements for the production of $Z + b\bar{b}$ and $Z + c\bar{c}$ events are explicitly included and a heavy-flavour overlap procedure is used to remove the double counting, between the matrix element and the parton shower, of heavy quarks from gluon splitting. The properties of b- and c-hadron decays were simulated with EvtGen v1.2.0 [41], as was done in all generated samples where the parton shower was simulated with Pythia. Photos++ v3.52 [42, 43] was used to simulate QED final-state radiation (FSR). The Alpgen samples are used in the analysis to estimate systematic uncertainties in the unfolding procedure and in backgrounds containing a genuine Z boson. In section 9 these samples are referred to as Alpgen + Py6 4FNS (LO). Samples of $Z(\to \tau\tau)$, $W(\to \ell\nu)$, and $W(\to \tau\nu)$ events were simulated with Sherpa, using the same set-up adopted for the signal samples.

The Z-boson and W-boson samples are normalised to the inclusive next-to-next-to-leading-order (NNLO) cross-section predictions provided by the FEWZ 3.1 program [44–47] with the CT14 PDF set. The K-factor applied to the Z samples to match the NNLO prediction is 0.975 for Sherpa and 1.196 for Alpgen.

The production of $t\bar{t}$ events with at least one W boson decaying leptonically was modelled using the Powheg-Box [48–51] v2 generator at NLO with the NNPDF3.0NLO [34] PDF set. The h_{damp} parameter, which regulates the high-p_{T} emissions against which the $t\bar{t}$ system recoils, is set to 1.5 m_{top} [52]. The events were interfaced with Pythia v8.230 [53] using the A14 tune [54]. The $t\bar{t}$ sample is normalised to the theory prediction at NNLO in QCD including the resummation of next-to-next-to-leading logarithmic (NNLL) soft-gluon terms [55–61]. Four additional $t\bar{t}$ samples were simulated to evaluate the un-

JHEP07(2020)044

certainty in this process, as described in [52]. One sample was produced with MadGraph5_aMC@NLO [62] and the same parton-shower model of the nominal $t\bar{t}$ sample in order to estimate the uncertainty due to the modelling of the hard scattering process. A second Powheg-Box sample showered with Herwig 7.13 [63, 64] was generated to evaluate the uncertainty due to the modelling of the parton shower and hadronization processes. A third sample was produced to simulate higher energy radiation with the factorisation and renormalisation scales changed by a factor of 0.5 while simultaneously increasing the h_{damp} value to 3.0 m_{top} and using the upper variation of the initial state radiation (ISR) from the A14 tune. The last sample simulates the lower energy radiation. It was generated with the renormalisation and factorisation scales varied by a factor of 2.0 while keeping the h_{damp} value at 1.5 m_{top} and using the ISR downward variation in the parton shower. The last two samples are also used to estimate the impact of FSR with parton-shower weights that vary the renormalisation scale for QCD emission in the FSR by factors of 0.5 and 2.0.

Single-top-quark events in the Wt-, s- and t-channels were generated using the Powheg-Box v1 generator interfaced with Pythia v6.4 [37]; the latter simulates parton showers, fragmentation, and the underlying event using the Perugia 2012 tune [38]. The CT10 PDF set was used [65]. The single-top samples for the t- and s-channels are normalised to cross-sections from NLO predictions [66, 67], while the Wt-channel sample is normalised to cross-sections from approximate NNLO predictions [68].

Diboson processes (WW, WZ, and ZZ) with one of the bosons decaying hadronically and the other leptonically were generated using Sherpa v2.2.1 with the CT10nlo PDF set. The matrix element includes up to one parton at NLO and up to three additional partons at LO. The samples are normalised to the NLO predictions [69].

Simulated events for $qq \to VH(\to b\bar{b})$ with $V = W$ or Z plus zero or one jet production at NLO were generated with the Powheg-Box v2 + GoSam + MiNLO generator [51, 70–72] with the NNPDF3.0NLO PDF set. The contribution from $gg \to ZH(\to b\bar{b})$ production was simulated using the LO Powheg-Box v2 matrix-element generator. The samples of simulated events include all final states where the Higgs boson decays into $b\bar{b}$ and the vector boson into a leptonic final state. The mass of the Higgs boson is set to 125 GeV and the $H \to b\bar{b}$ branching fraction is set to 58%. The $qq \to VH(\to b\bar{b})$ cross-section is calculated at NNLO (QCD) and NLO (EW), while the $gg \to ZH$ cross-section is calculated at NLO+NLL (QCD).

Generated events were processed with the ATLAS detector simulation [76], based on Geant4 [77], to simulate the detector response to final-state particles. To account for the effects of pile-up, multiple overlaid pp collisions were simulated with the soft QCD processes of Pythia v8.186 using the A2 tune [78] and the MSTW2008LO PDF set [79]. The distribution of the average number of interactions per bunch crossing in the simulation is weighted to reflect that in the data. Simulated events are processed with the same reconstruction algorithms as for the data.

3.3 Theoretical predictions

In addition to particle-level predictions from the fully simulated Sherpa and Alpgen samples described above, unfolded results from data are compared with six other predictions listed in table 2.

JHEP07(2020)044

Process	Generator	Order of cross-section calculation	Reference normalisation	Normalisation cross-section uncertainty
$Z \to \ell\ell$ ($\ell = e, \mu, \tau$) with $66 < m_{\ell\ell} < 116$ GeV	Sherpa	NNLO	[44–47]	5%
$W \to \ell\nu$ ($\ell = e, \mu, \tau$)	Sherpa	NNLO	[44–47]	5%
$t\bar{t}$	Powheg-Box	NNLO + NNLL ($m_{\text{top}} = 172.5$ GeV)	[55–61]	6%
Single top (t-, Wt-, s-channel)	Powheg-Box ($m_{\text{top}} = 172.5$ GeV)	NLO		6%
Dibosons $Z(\to \ell\ell) + Z(\to qq)$, $W(\to \ell\nu) + W(\to qq)$)	Sherpa	NLO	[69]	5%
Higgs $qq \to Z(\to \ell\ell) + H(\to b\bar{b})$ $gg \to Z(\to \ell\ell) + H(\to b\bar{b})$ $qq \to W(\to \ell\nu) + H(\to b\bar{b})$	Powheg-Box	NNLO QCD + NLO EW NLO + NLL NNLO QCD + NLO EW	[73–75]	3%

Table 1. Signal and background MC samples: the generator programs used in the simulation are listed in the second column, the order of the QCD calculation and the reference used for the calculations of the normalisation cross section are reported in the third and fourth columns. The normalisation cross-section uncertainty in the final column corresponds to PDFs and scale variations.

Two particle-level predictions (using specific parton-shower and matching predictions) were produced with the Sherpa v2.2.7 generator using NLO matrix elements [80]. The first sample, referred to as Sherpa Zbb 4FNS (NLO), includes $Z + b\bar{b}$ events generated in the 4FNS at NLO with massive b-quarks. It is interesting to compare this sample, which contains two b-quarks in the matrix elements, with the unfolded data even in the case of distributions with at least one b-jet, to understand if there are regions of the phase space that can be described with such a configuration. The second sample, referred to as Sherpa Fusing 4FNS+5FNS (NLO), contains the matrix elements at NLO for up to two partons, and matrix elements at LO for up to three partons. It includes both $Z + b\bar{b}$ events generated in the 4FNS at NLO with massive b-quarks, and Z+jets events generated in the 5FNS at NLO. They are combined according to the procedure described in ref. [81]. The combination is achieved by means of a dedicated heavy-flavour overlap removal procedure, the fusing technique, that acts as an additional step after the multijet merging algorithms. This procedure combines the advantages of inclusive 5FNS calculations with the higher precision of 4FNS calculations in regions of phase space where the b-quark mass sets a relevant scale. The two Sherpa samples use the NNPDF3.0nnlo PDF set with $\alpha_{\text{S}}(m_Z) = 0.118$ and the corresponding number of active quark flavours. Masses of c- and b-quarks are taken into account in the parton shower in all Sherpa samples.

Results are also compared with predictions from the LO matrix-element generator MadGraph5_aMC@NLO v2.2.2 [62] interfaced with Pythia v8.186 [53] with the A14 tune [54] to model the parton shower and underlying event. The matrix element includes up

JHEP07(2020)044

Generator	$N_{\text{max}}^{\text{partons}}$		FNS	PDF	Parton
	NLO	LO		set	Shower
Z+jets (including Z+b and Z+bb)					
Sherpa 5FNS (NLO)	2	4	5	NNPDF3.0nnlo	Sherpa
Sherpa Fusing 4FNS+5FNS (NLO)	2	3	5 (*)	NNPDF3.0nnlo	Sherpa
Alpgen + Py6 4FNS (LO)	—	5	4	CTEQ6L1	Pythia v6.426
Alpgen + Py6 (rew. NNPDF3.0lo)	—	5	4	NNPDF3.0lo	Pythia v6.426
MGaMC + Py8 5FNS (LO)	—	4	5	NNPDF3.0nlo	Pythia v8.186
MGaMC + Py8 5FNS (NLO)	1	—	5	NNPDF3.0nnlo	Pythia v8.186
Z+bb					
Sherpa Zbb 4FNS (NLO)	2	—	4	NNPDF3.0nnlo	Sherpa
MGaMC + Py8 Zbb 4FNS (NLO)	2	—	4	NNPDF3.0nnlo	Pythia v8.186

Table 2. Summary of theoretical predictions for the signal, including the maximum number of partons at each order in α_{S}, the flavour number scheme (FNS), the PDFs set and the parton shower. (*) Details of the merging between 4FNS and 5FNS in Sherpa Fusing 4FNS+5FNS (NLO) are available in ref. [81].

to four partons. Additional jets are produced by the parton shower, which uses the CKKW-L merging procedure [82], with a matching scale of 30 GeV. MadGraph5_aMC@NLO uses the 5FNS with massless b- and c-quarks in the matrix element, and massive quarks in the parton shower. The NNPDF3.0nlo PDF set is used with $\alpha_{\text{S}}(m_Z) = 0.118$. This prediction is referred to as MGaMC + Py8 5FNS (LO).

Two additional predictions were produced with MadGraph5_aMC@NLO v2.6.2, using matrix-element calculations with NLO accuracy. The first sample includes Z+jets events generated in the 5FNS with up to one parton at NLO, and massless b- and c-quarks; the second sample includes $Z + b\bar{b}$ events generated in the 4FNS at NLO, and massive b-quarks. Both samples were generated using the NNPDF3.0nnlo PDF set with $\alpha_{\text{S}} = 0.118$. They were interfaced to the Pythia v8.186 parton shower using the FxFx merging scheme [83], with a matching scale of 25 GeV. As in the previous case, massive c- and b-quarks are produced in the parton shower. The first sample is referred to as MGaMC + Py8 5FNS (NLO); the second is referred to as MGaMC + Py8 Zbb 4FNS (NLO).

An additional Alpgen prediction is used to test the sensitivity of the measurements to the parton structure of the proton. The Alpgen samples presented in section 3.2 are reweighted to the NNPDF3.0lo PDF set, using the prescriptions reported in ref. [84]. These predictions are referred to as Alpgen + Py6 (rew. NNPDF3.0lo). The predictions of LO MC generators, such as Alpgen + Py6 4FNS (LO) and MGaMC + Py8 5FNS (LO), with up to four or five partons in the matrix element, are still an interesting case to study as they allow comparison with the predictions of MC generators at NLO accuracy and with a smaller number of partons in the matrix element. Furthermore, they provide a benchmark in common with past analyses, such as in ref. [11].

JHEP07(2020)044

4 Event selection

Events selected in this analysis are required to have a signature consistent with a Z boson, decaying into two electrons or two muons, in association with at least one or at least two b-jets. Candidate events are required to have a primary vertex (PV), defined as the vertex with the highest sum of track p_{T}^2 with at least two associated tracks measured in the ID (ID tracks), each with $p_{\mathrm{T}} > 400$ MeV.

Electron candidates are reconstructed by matching a cluster of energy deposited in the EM calorimeter to a well-reconstructed ID track. Electrons are identified using a likelihood function based on variables describing the shape of the electromagnetic showers in the calorimeter, track properties, and track-to-cluster matching quantities [85]. Electrons must satisfy the 'tight' likelihood requirement. Electron candidates are required to have $p_{\mathrm{T}} > 27$ GeV and $|\eta| < 2.47$. Candidates in the transition region between the barrel and endcap electromagnetic calorimeters, $1.37 < |\eta| < 1.52$, are excluded.

Muon candidates are reconstructed by fitting a unique trajectory through the hits associated with a pair of matching tracks which are reconstructed separately in the ID and the MS; the energy loss in the calorimeter is taken into account in the combination procedure. Muons must satisfy the 'medium' identification criterion based on requirements on the number of hits and on the quality of the combined fit [86]. Muon candidates are required to have $p_{\mathrm{T}} > 27$ GeV and $|\eta| < 2.5$.

To select leptons originating from the primary pp interaction, the lepton tracks are required to have a longitudinal impact parameter (z_0) satisfying $|z_0 \sin(\theta)| < 0.5$ mm relative to the PV. The transverse impact parameter significance (d_0/σ_{d_0}) of the electron (muon) candidates must satisfy $d_0/\sigma_{d_0} < 5$ (3). In order to further suppress leptons from non-prompt processes or leptons from hadrons in jets, both the electron and muon candidates are required to satisfy p_{T}-dependent cone-based isolation requirements [86], which use information from ID tracks. The isolation requirements are set so that the scalar sum of the transverse momenta of the tracks in the isolation cone[4] around the lepton is less than 6% of the lepton p_{T}.

Jets are reconstructed, using the anti-k_t algorithm [87, 88] with radius parameter $R = 0.4$, from topological clusters of energy deposits in the calorimeter [89]. Jets are calibrated using a simulation-based calibration scheme, followed by in situ corrections to account for differences between simulation and data [90]. Events with jets arising from detector noise or other non-collision sources are discarded [91]. Furthermore, to eliminate jets containing a large energy contribution from pile-up, jets with $p_{\mathrm{T}} < 60$ GeV and $|\eta| < 2.4$ are required to have a significant fraction of their tracks with origin compatible with the primary vertex, as defined by a jet vertex tagger discriminant (JVT) [92]. Selected jets must have $p_{\mathrm{T}} > 20$ GeV and rapidity $|y| < 2.5$.

An overlap removal procedure is applied to electron, muon and jet candidates to prevent double counting. Any jet whose axis lies within $\Delta R = 0.2$ of an electron is removed. If a jet is reconstructed within $\Delta R = 0.2$ of a muon and the jet has fewer than three associ-

[4]The ΔR parameter of the isolation cone is defined by $\Delta R = \min(10\ \mathrm{GeV}/p_{\mathrm{T}}, 0.3)$ where p_{T} is the transverse momentum of the lepton candidate.

JHEP07(2020)044

ated tracks or the muon energy constitutes most of the jet energy, then the jet is removed. Any electron or muon of a given p_{T} reconstructed within $\Delta R = \min(0.4, 0.04 + 10\ \mathrm{GeV}/p_{\mathrm{T}})$ of the axis of any surviving jet is removed. Jets that survive the overlap removal procedure are removed if they are within $\Delta R = 0.4$ of the selected leptons.

The b-jets, defined as the jets containing at least one b-hadron, are identified using a multivariate algorithm, MV2c10 [93, 94]. This algorithm uses the impact parameter and reconstructed secondary vertex information of the tracks associated with the jets. Its output lies in the range $[-1, +1]$. A value close to $+1$ denotes a higher probability for the jet to be a b-jet. The b-jet candidates are selected if their MV2c10 output is greater than 0.8244. This selection corresponds to an efficiency of 70% for selecting jets containing b-hadrons, and misidentification rates of 0.26% and 8.3%, respectively, for light-flavour (u-, d-, s-quark and gluon) jets and c-jets, as estimated from a sample of simulated $t\bar{t}$ events. Other working points are defined by different b-tagging discriminant output thresholds; they are used to define control regions and to define the bins used in the flavour fit, as detailed in section 5.1.

In simulation, reconstructed jets are labelled as b-jets if they lie within $\Delta R = 0.3$ of one or more weakly decaying b-hadrons with $p_{\mathrm{T}} > 5$ GeV. Reconstructed jets not identified as b-jets are considered to be c-jets if they lie within $\Delta R = 0.3$ of any c-hadron with $p_{\mathrm{T}} > 5$ GeV. All other jets are classified as light-jets. Simulated Z+jets events are sequentially categorised depending on the labels of the jets, starting from b-jets, as follows: $Z+b$ when they have exactly one b-jet, $Z+bb$ when they have at least two b-jets, $Z+c$ when they have at least one c-jet, $Z+l$ when they have only light-jets. A similar classification is adopted for simulated W+jets events. In the distributions with at least one b-jet, the sum of $Z+b$ and $Z+bb$ samples is used to define the signal, and the Z+jets background is constituted by the sum of the $Z+c$ and $Z+l$ samples. In the distributions with at least two b-jets, the $Z+bb$ samples alone constitute the signal, while the sum of the $Z+b$, $Z+c$, and $Z+l$ samples form the Z+jets background.

The missing transverse momentum ($E_{\mathrm{T}}^{\mathrm{miss}}$), which may correspond to a neutrino escaping interaction with the detector, is defined as the negative vector sum of the transverse momentum of all identified hard physics objects (electrons, muons, jets), as well as an additional track-based soft term defined in ref. [95].

Events are required to have exactly two leptons[5] of the same flavour (ee or $\mu\mu$) but of opposite charge with their dilepton invariant mass in the range $76\,\mathrm{GeV} < m_{\ell\ell} < 106\,\mathrm{GeV}$. Events with $p_{\mathrm{T}}^{\ell\ell} < 150$ GeV must also have $E_{\mathrm{T}}^{\mathrm{miss}} < 60\,\mathrm{GeV}$. The requirement on the $E_{\mathrm{T}}^{\mathrm{miss}}$ value reduces by about 55% the background from $t\bar{t}$ events with dileptonic decay, while the signal is reduced by about 5%. Events passing the above selection and having at least one or at least two jets belong to the region referred to as the pre-tag region. The signal region is a subset of the pre-tag region. Events belonging to the signal region are assigned to two regions: those with at least one b-jet, referred to as the 1-tag region; and those with at least two b-jets, referred to as the 2-tag region, which is a subset of the 1-tag region.

A summary of the object selection and the event selection used in the analysis to define

[5] At least one of the lepton candidates is required to match the lepton that triggered the event.

JHEP07(2020)044

	Electron channel	Muon channel
Trigger	Single electron	Single muon
Leptons	Tight Isolated PV association: $\lvert d_0/\sigma_{d_0}\rvert < 5$, $\lvert z_0 \sin\theta\rvert < 0.5$ mm $p_{\mathrm{T}} > 27$ GeV $\lvert\eta\rvert < 1.37$ or $1.52 < \lvert\eta\rvert < 2.47$	Medium Isolated PV association: $\lvert d_0/\sigma_{d_0}\rvert < 3$, $\lvert z_0 \sin\theta\rvert < 0.5$ mm $p_{\mathrm{T}} > 27$ GeV $\lvert\eta\rvert < 2.5$
Jets	$p_{\mathrm{T}} > 20$ GeV and $\lvert y\rvert < 2.5$ $\Delta R(\text{jet}, \ell) > 0.4$	
b-jet	$p_{\mathrm{T}} > 20$ GeV and $\lvert y\rvert < 2.5$	

Regions				
	Pre-tag region	Signal regions	Z+jets Validation Region	$t\bar{t}$ Validation Region
Leptons	2 same-flavour, opposite-charge			1 e, 1 μ, opposite-charge
$m_{\ell\ell}$	76 GeV $< m_{\ell\ell} <$ 106 GeV			
$E_{\mathrm{T}}^{\mathrm{miss}}$	$E_{\mathrm{T}}^{\mathrm{miss}} <$ 60 GeV if $p_{\mathrm{T}}^{\ell\ell} <$ 150 GeV			
Jets	≥ 1 or ≥ 2 jets			
b-tagging efficiency working point selection	—	70%	≥ 1 b-jet at 77%–70%	70%
Number of b-jets	—	≥ 1 b-jets (1-tag region) ≥ 2 b-jets (2-tag region)	≥ 1 b-jets	≥ 2 b-jets

Table 3. Summary of object and event selections defining the signal regions and the validation regions for the main backgrounds of the analysis at detector level.

the signal regions and the validation regions for the main backgrounds, which are presented in section 5, is given in table 3.

4.1 Correction factors applied to simulation and corresponding uncertainties

Corrections are applied to simulated samples in order to ensure that the object selection efficiencies and the energy and momentum calibrations agree with data within the uncertainties associated with the corrections.

The electron and muon trigger efficiencies are estimated in data and simulation in order to determine simulation-to-data correction factors and their corresponding uncertainties. The average per-event correction factor is about 0.98 (0.93) for electron (muon) triggers; they are known with an uncertainty below 1% [85, 86]. Corrections to efficiencies for lepton reconstruction, identification, isolation and association with the PV in simulated samples are derived from data. Each per-lepton correction factor is close to unity and known with a precision that is better than 1% in the kinematic range considered [85, 86].

The energy scale of the electrons and the momentum scale of the muons in simulation are adjusted with correction factors that deviate from unity at the per-mil level and the resolutions are adjusted with correction factors that deviate from unity at the per-cent level in order to match lepton p_{T} and $m_{\ell\ell}$ distributions in data; the corresponding uncertainties are negligible.

JHEP07(2020)044

The jet energy scale (JES) is calibrated on the basis of the simulation including in situ corrections obtained from data [90]. The JES uncertainties are estimated using a decorrelation scheme comprising a set of 21 independent parameters, the largest of which may reach several per cent in specific corners of the phase space. The jet energy resolution (JER) uncertainty is derived by over-smearing the jet energy in the simulation by about 4% at $p_{\mathrm{T}} = 20$ GeV to about 0.5% at a p_{T} of several hundred GeV [96]. Simulation-to-data corrections and relative uncertainties are also applied to adjust the efficiency of the JVT requirement following the prescriptions of ref. [97]. The uncertainty in the scale and resolution of $E_{\mathrm{T}}^{\mathrm{miss}}$ is estimated by propagating the uncertainties in the transverse momenta of reconstructed objects and an uncertainty to account for soft hadronic activity in the event, as described in ref. [95].

Flavour-tagging efficiencies in simulation are scaled to match those measured in data for jets of all flavours as a function of the different b-tagging discriminant output thresholds, and of the jet p_{T} (and η for light-jets), using weights derived from control samples enriched in jets of each flavour [98]. In the case of b-jets, correction factors and their uncertainties are estimated from data using dileptonic $t\bar{t}$ events [98]. The correction factors for b-jets are close to unity. The uncertainties, described by a set of 28 independent parameters, are as low as 3% for jet p_{T} of about 60 GeV, but reach 10% for jet p_{T} of about 20 GeV and up to 20% beyond 300 GeV. In the case of c-jets, correction factors are derived using jets from W-boson decays in $t\bar{t}$ events [99]. The correction factors for c-jets range from about 1.2 to about 1.6. Their uncertainties, described by a set of 28 independent parameters, are about 20%–30% in the bulk of the phase space, but up to 100% for large jet p_{T} and for the b-tagging discriminant output threshold closest to +1. In the case of light-flavour jets, correction factors are derived using dijet events [100]. The correction factors for light-jets range from about 2 to about 3, with uncertainties described by a set of 36 independent parameters and ranging from 50% to 100%. An additional uncertainty of 30% is applied to the efficiency of b-tagging for simulated jets originating from pile-up interactions, which are less than 1% of the selected jets.

A variation in the pile-up reweighting of simulated events (referred to as pile-up uncertainty) is included to account for the uncertainty in the ratio of the predicted and measured inelastic cross-sections in the fiducial volume [101].

5 Background estimation

The main background in the 1-tag region is constituted by events with a Z boson produced in association with jets, where either a light-jet or a c-jet is misidentified as a b-jet; it is determined using a fit to data as detailed in section 5.1. Dileptonic $t\bar{t}$ events dominate in the 2-tag region. Smaller background contributions from the production of dibosons, a Higgs boson, a single top quark, a $Z \to \tau\tau$, or a $W \to \ell\nu$ are estimated using simulation, as described in section 3.2. Uncertainties in the normalisation cross-section of these predictions range from 4% to 6% depending on the process, as detailed in table 1. Background contributions from multijet events are estimated with a data-driven technique and found to be negligible, as described below.

JHEP07(2020)044

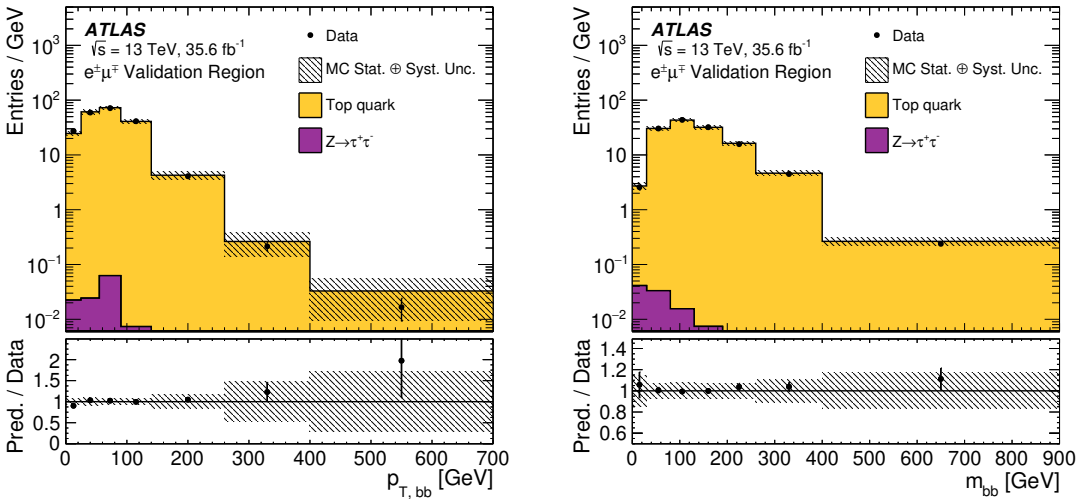

Figure 1. Transverse momentum (left) and invariant mass (right) of the di-b-jet system built with the two highest-p_{T} b-jets for events with at least two b-jets in the $t\bar{t}$ validation region. Systematic uncertainties of the predicted distributions are combined with the statistical ones in the hatched band, and the statistical uncertainty of the data is shown as error bars. The systematic uncertainties for the predictions account only for the yield and the shape of $t\bar{t}$ events.

The $t\bar{t}$ contribution is estimated using simulated events generated with Powheg-Box + Pythia normalised to the theoretically predicted cross-section, as discussed in section 3.2. An uncertainty of about 6% is assigned to the inclusive $t\bar{t}$ cross-section (see table 1), following the variation of the renormalisation and factorisation scales by a factor of 2.0, and the variation of the PDFs within their uncertainties. In addition, uncorrelated systematic uncertainties in the modelling of the distributions are derived by comparing the predictions from the nominal $t\bar{t}$ sample with the ones from the alternative samples described in section 3.2.

The modelling of $t\bar{t}$ production in the simulation is validated using a $t\bar{t}$-enriched region, which is selected by requiring that events have two leptons of different flavour ($e\mu$); all other selections are the same as in the signal region. As an example, figure 1 shows the $p_{\mathrm{T},bb}$ and the m_{bb} distributions for events with at least two b-jets. The total background from top quarks is the sum of $t\bar{t}$ and single-top events, where the latter are about 3% of the $t\bar{t}$ component in the validation region, and other backgrounds are negligible. Data and simulation agree well within the uncertainties which account for both the yield and shape uncertainties of simulated $t\bar{t}$ events and the statistical uncertainties of predictions and data.

Background contributions from multijet events in the electron and muon channels are estimated using a data-driven technique. Multijet-enriched control regions without b-tag and $m_{\ell\ell}$ requirements are used to derive the expected shape of this background. In the electron channel, the multijet-enriched control region is defined by applying the full signal event selection except for the electron identification and the d_0/σ_{d_0} cuts, and inverting the isolation selection for both electron candidates. In the muon channel, the multijet-enriched control region is defined by applying the full signal event selection but requiring

JHEP07(2020)044

both muon candidates to have the same charge. In both channels, contributions from non-multijet sources in the control regions are estimated from simulation and subtracted from the data, with the remaining distributions used as shape templates. A fit of the $m_{\ell\ell}$ distribution to data is then performed within the window of 60 GeV $< m_{\ell\ell} <$ 160 GeV in the one-jet and two-jets pre-tag regions separately and leaving the normalisation of the signal and of the multijet background templates free to float in the fit, while the normalisation of the other processes is fixed in the fit. The multijet background estimate in the pre-tag region is then extrapolated to the two signal regions using normalisation factors equal to the fraction of events in the multijet control region that satisfy the 1-tag and 2-tag requirements. Contributions from non-multijet processes are subtracted before estimating this fraction. Systematic uncertainties are assessed by varying the $m_{\ell\ell}$ range and the binning of the fit, excluding the Z-boson peak from the fit, performing the fit in the tagged regions in place of the pre-tag ones, and by allowing the other processes to be varied independently in the fit. The estimated size of the multijet background is consistent with zero within the statistical uncertainty even after considering all sources of systematic uncertainty. It is therefore neglected in the analysis.

5.1 Extraction of the cross-section for Z-boson production in association with light-jets and c-jets

The flavour fit used for the extraction of the yields of Z + light-jets and Z + c-jets backgrounds for the 1-tag and 2-tag selections is a maximum-likelihood fit to data based on flavour-sensitive distributions. The fit is done simultaneously in the electron and muon channels with templates derived from simulation.

In the 1-tag region, the b-tagging discriminant output of the leading b-jet is used as the flavour-sensitive distribution. This observable for events belonging to the signal region is distributed into three intervals that define the bins of the discriminant output distribution. Each bin corresponds to a certain range of b-tagging efficiency. The bins are numbered from 1 to 3, corresponding respectively to efficiencies of 60%–70% (bin 1), 50%–60% (bin 2) and <50% (bin 3) as estimated from simulated $t\bar{t}$ events. The light-flavour jet (c-jet) misidentification rates for the three bins are respectively 0.195% (5.4%), 0.048% (1.96%), and <0.017% (<0.94%). The signal template is built with simulated $Z+ \geq 1b$ events. The template shapes of the $Z+l$ and $Z+c$ samples are very similar (as shown in figure 2), hence those samples are combined to form a single template. All non-Z+jets backgrounds are combined into a single template, determined from the sum of their predicted contributions. The normalisations of the signal and of the Z+jets background are free to float in the fit, while the normalisation of the sum of the non-Z+jets backgrounds is fixed to their estimate.

In the 2-tag region the combination of the three bins of the b-tagging discriminant outputs of the leading and sub-leading b-jets produces a distribution with six bins that is used for the fit to data. The signal template is built with simulated $Z + bb$ events. Templates built with $Z + b$, $Z + c$ and $Z + l$ simulated events are combined into a single template. Because of the large rejection of light-flavour jets achieved in the 2-tag selection, the simulated $Z + l$ events in this region are not subjected to the b-tagging requirement. Instead they are weighted by a per-event probability that the jets pass the two-b-tags

JHEP07(2020)044

Generator	Signal SF	Z+jets background SF	Signal post-fit yield	Z+jets background post-fit yield	Signal + Z+jets post-fit yield
Sherpa	1.109 ± 0.003	0.861 ± 0.004	309 650 ± 810	166 640 ± 650	476 290 ± 750
Alpgen	1.480 ± 0.004	1.015 ± 0.002	297 670 ± 740	178 100 ± 400	475 810 ± 480

Table 4. Scale factors obtained for the fitted signal and Z+jet background for Sherpa and Alpgen fits, the total post-fit yields, and the statistical uncertainty, estimated with pseudo-experiments, from the fit for the 1-tag signal region.

Generator	Signal SF	Z+ jets background SF	Signal post-fit yield	Z+ jets background post-fit yield	Signal + Z+jets post-fit yield
Sherpa	1.18 ± 0.01	1.08 ± 0.04	23 440 ± 250	4780 ± 180	28 220 ± 200
Alpgen	1.18 ± 0.01	1.30 ± 0.05	23 650 ± 240	4550 ± 180	28 200 ± 200

Table 5. Scale factors obtained for the fitted signal and Z+jet background for Sherpa and Alpgen fits, the total post-fit yields, and the statistical uncertainty, estimated with pseudo-experiments, from the fit for the 2-tag signal region.

selection (procedure referred to as the *truth*-tagging). This probability is computed on the basis of the per-jet probabilities, which are assumed to be independent of each other [102]. As for the fit in the 2-tag region, the normalisations of the signal and of the Z+jets background are also free to float, while the normalisation of the other backgrounds is fixed to their estimate.

Tables 4 and 5 show the normalisation scale factors in the 1- and 2-tag regions obtained from the fit, together with the post-fit yields for the signal and Z+jet background samples generated with Sherpa or Alpgen. There is good agreement between the sum of the signal and background post-fit yields of Sherpa and Alpgen. The differences between Sherpa and Alpgen in the modelling of the Z+jet backgrounds after the flavour fit are taken into account in the systematic uncertainties as described below. The statistical uncertainty is estimated with pseudo-experiments.

Figure 2 shows the b-tagging discriminant bins after the fit in the 1-tag and 2-tag regions. In the upper panel of each figure, data are compared with the fit results obtained using templates derived from Sherpa samples for signal and Z+jet backgrounds. The lower panel shows the ratio of post-fit predictions to data using the Sherpa or Alpgen samples for signal and Z+jet backgrounds.

The Z+jets backgrounds predicted by Sherpa and corrected for the normalisation factor obtained from the fit are used as the nominal estimate in this analysis. Systematic uncertainties due to the object selection efficiencies and calibrations, discussed in section 4.1, affect the normalisation and the shape of Z+jets backgrounds. They are assessed by repeating the fit with the templates varied according to each of the systematic uncertainties. The fit is also repeated for each of the uncertainties affecting the $t\bar{t}$ and other backgrounds detailed above. An additional systematic uncertainty (referred to as the flavour fit uncertainty) in the normalisation of the Z+jets backgrounds is estimated by repeating the fit after separating the $Z + c$ from the $Z + l$ template in the 1-tag region,

JHEP07(2020)044

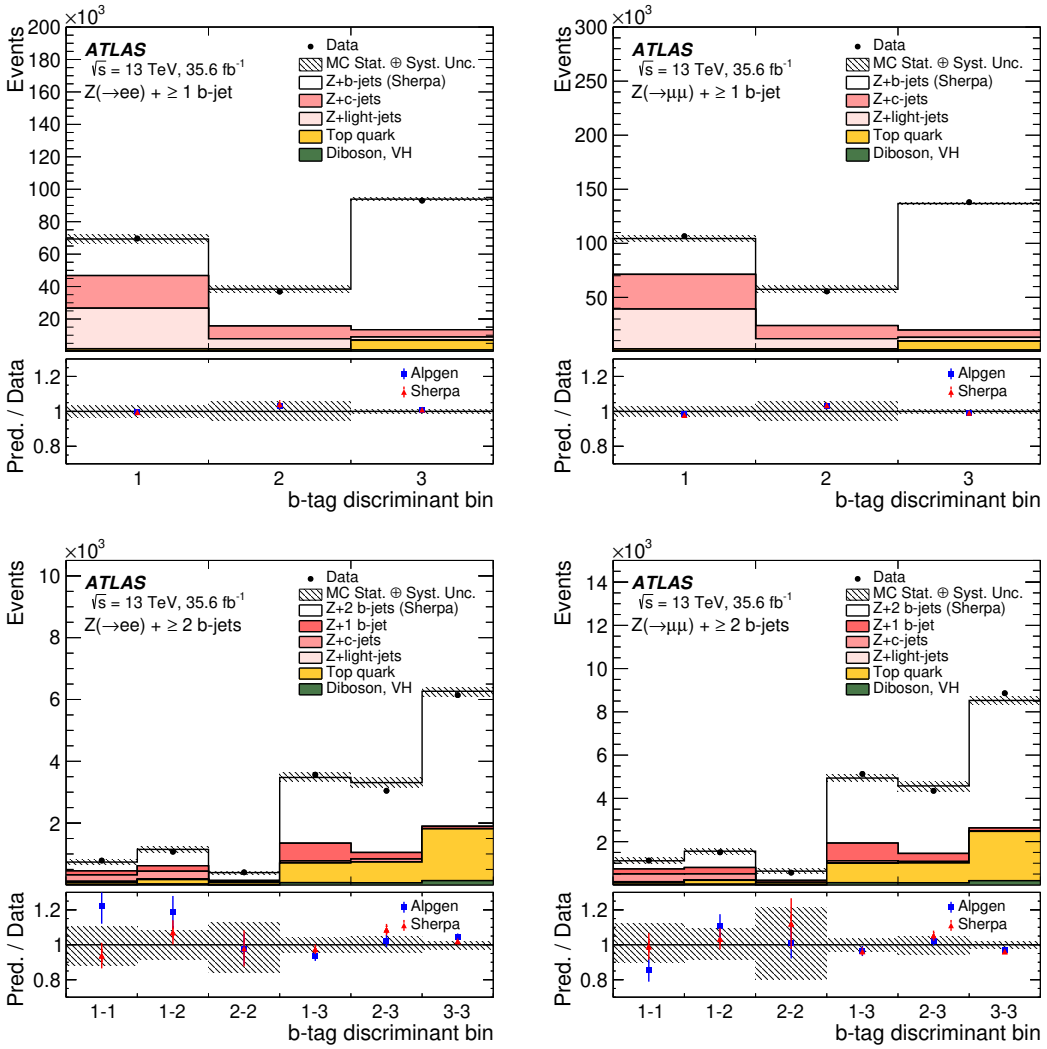

Figure 2. Post-fit b-tagging discriminant distributions for the electron (left) and muon (right) channels in the 1-tag (top) and 2-tag (bottom) signal regions. The lower panels display the ratios of the predictions to data using the signal and Z+jet background simulation either from SHERPA (red) or ALPGEN (blue). Systematic and statistical uncertainties for the predicted distributions are combined in the hatched band, and the statistical uncertainty, estimated with pseudo-experiments, is shown on the data points. The systematic uncertainties account for both the detector-level uncertainties and the theory uncertainty of the non-Z backgrounds.

and after separating the $Z + b$ from the $Z + c$ and $Z + l$ templates in the 2-tag region. An uncertainty affecting the shape and rate of the Z+jets background is derived by taking the difference between the post-fit Z+jets background evaluations using SHERPA and ALPGEN samples. Another uncertainty accounts for potential jet-jet correlations that are not covered by the *truth*-tagging procedure which mitigates the large statistical fluctuations in the 2-tag region for $Z + l$. A 20% uncertainty is derived by taking the largest difference between the double-tagged event yields obtained with or without the weighting procedure

JHEP07(2020)044

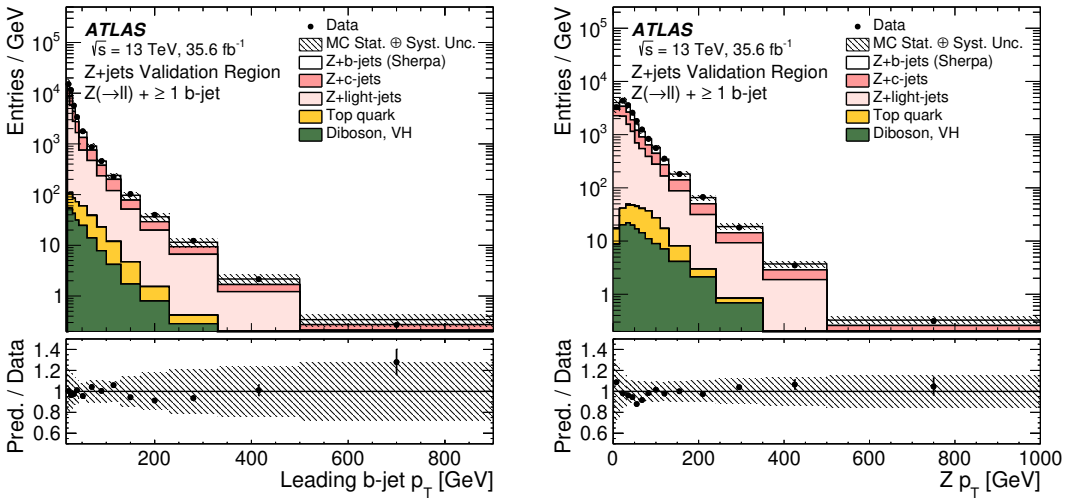

Figure 3. The p_{T} of the leading b-jet (left) and of the Z boson (right) for events with at least one b-jet in the Z+jets validation region defined in table 3. Post-fit distributions for signal and Z + jets backgrounds are shown. Systematic and statistical uncertainties for the predicted distributions are combined in the hatched band, and the statistical uncertainty is shown on the data points. The uncertainty in the predictions includes only the flavour-tagging efficiency uncertainty and flavour-fit uncertainty.

being applied to simulated samples of $Z + bb$, $Z + cc$, $W + bb$, and $W + cc$.[6] These samples suffer less from statistical limitations. The test is done with both the Sherpa and Alpgen samples.

The post-fit estimate of the Sherpa Z+jets background is validated in a region defined by applying the full signal event selection with the exception of b-tagging requirements. Events with at least one b-jet, with the b-tagging discriminant output in the b-jet efficiency range of 70%–77% and light-flavour jet (c-jet) misidentification rates of 0.51% (7.7%), are selected to provide a sample enriched in c-jets and light-flavour jets. As an example, figure 3 shows the p_{T} of the leading b-jet and the p_{T} of the Z boson in this region. The $Z + l$ and $Z + c$ backgrounds constitute 50% and 28% of the total prediction, respectively. Agreement between data and estimated backgrounds is observed within uncertainties. These include the uncertainties due to the flavour fit and b-tagging efficiency, and the statistical uncertainties of the predictions and data.

The normalisation factors of the signal samples, shown in tables 4 and 5, are applied in figures 2 and 3 in this section to demonstrate the robustness of this procedure, while in the following sections, post-fit normalisation factors are applied only to Z+jets background.

6 Kinematic distributions

After the signal selection criteria are applied, the measured and expected distributions are compared at the detector level. The Z+jets background is shown for the normalisation factors derived from the flavour fit. Pre-fit distributions are used for the signal samples.

[6]Simulated Z+jets events are categorised as $Z + cc$ ($W + cc$) if they belong to the $Z + c$ ($W + c$) category and have at least two c-jets.

JHEP07(2020)044

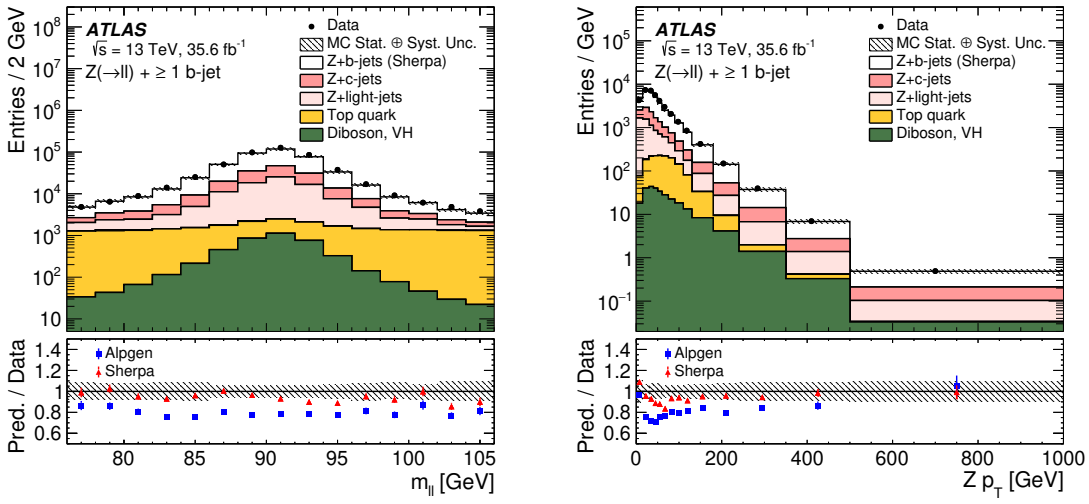

Figure 4. Distribution of events passing the signal selection as a function of $m_{\ell\ell}$ (left) and $p_{\mathrm{T},Z}$ (right) for events with at least one b-jet. The lower panels display the ratio of the predictions for signal plus background to data using either Sherpa (red) or Alpgen + Pythia6 (blue) as the signal simulation. The statistical uncertainty of the data is shown as black error bars and the total uncertainty of the prediction as a hatched band. The latter consists of the statistical uncertainty and all systematic uncertainties from the predictions.

Figure 4 shows, as an example, the distributions of the $m_{\ell\ell}$ and p_{T} of the Z boson for events in the 1-tag region. Figure 5 shows the p_{T} of the Z boson and the ΔR_{bb} distributions for events in the 2-tag region. The uncertainty bands include the statistical uncertainties of the simulated sample, the event-selection uncertainties described in section 4 (omitting the common luminosity uncertainty), and the background uncertainties described in section 5. Both generators do not describe precisely the data in the full range of the measurement, although the Sherpa generator provides the best agreement with data.

The total numbers of selected events in data and in predictions are presented in table 6, together with the prediction of each process, expressed as a fraction of the total number of predicted events.

7 Correction to particle level

The signal event yields are determined by subtracting the estimated background contributions from the data. The resulting distributions are corrected for detector-level effects to the fiducial phase space at particle level defined in table 7. The procedure, based on simulated samples, corrects for Z-boson, jet, and b-jet selection efficiencies, resolution effects, and small differences between the fiducial and detector-level phase spaces. The pre-fit distributions of the Sherpa signal samples are used to perform the unfolding procedure. The signal samples for the simulation of Z events with at least one or at least two b-jets are defined in section 4. Particle-level objects are selected with requirements close to the corresponding requirements for reconstructed signal candidate objects, in order to limit

JHEP07(2020)044

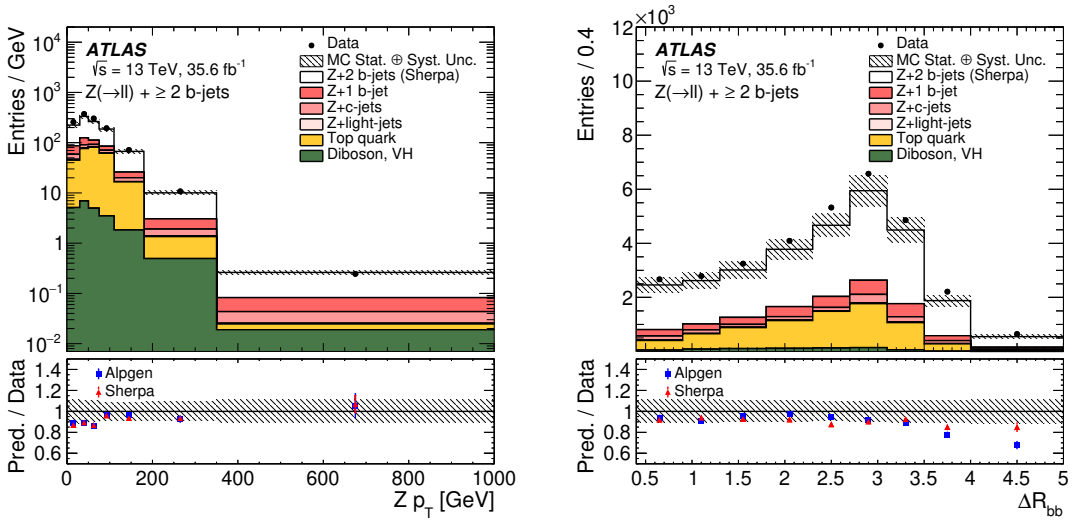

Figure 5. Distribution of events passing the signal selection as a function of $p_{\mathrm{T},Z}$ (left) and ΔR_{bb} (right) for events with at least two b-jets. The lower panels display the ratio of the predictions for signal plus background to data using either Sherpa (red) or Alpgen + Pythia6 (blue) as the signal simulation. The statistical uncertainty of the data is shown as black error bars and the total uncertainty of the prediction as the hatched band. The latter consists of the statistical uncertainty and all systematic uncertainties from the predictions.

1-tag region	
Signal	
$Z + b$, $Z + bb$	59%
Backgrounds	
$Z + c$	18%
$Z + l$	18%
Top	4%
Diboson, VH	1%
Others	$< 1\%$
Total predicted	470 000 ± 650
Data	499 645

2-tag region	
Signal	
$Z + bb$	60%
Backgrounds	
$Z + b$	9%
$Z + c$	5%
$Z + l$	$< 1\%$
Top	23%
Diboson, VH	2%
Others	1%
Total predicted	33 070 ± 180
Data	36 548

Table 6. The expected size of the signal and backgrounds, expressed as a fraction of the total number of predicted events for inclusive b-jet multiplicities for the signal selection. The signal and Z+jets background predictions are from the Sherpa generator, with the Z+jets background estimate obtained after applying the normalisation scale factors obtained from the flavour fit. The total numbers of predicted and observed events are also shown. The uncertainty in the total predicted number of events is statistical only.

the dependence of the measurement on theoretical predictions. In this definition, the lepton kinematic variables are computed using final-state leptons from the Z-boson decay. Photons radiated by the boson decay products within a cone of size $\Delta R = 0.1$ around the direction of a final-state lepton are added to the lepton, and the sum is referred to as the 'dressed' lepton. Particle-level jets are identified by applying the anti-k_t algorithm with

JHEP07(2020)044

Kinematic variable	Acceptance cut
Lepton p_{T}	$p_{\mathrm{T}} > 27$ GeV
Lepton η	$\lvert\eta\rvert < 2.5$
$m_{\ell\ell}$	$m_{\ell\ell} = 91 \pm 15$ GeV
b-jet p_{T}	$p_{\mathrm{T}} > 20$ GeV
b-jet rapidity	$\lvert y\rvert < 2.5$
b-jet-lepton angular distance	$\Delta R(b\text{-jet}, \ell) > 0.4$

Table 7. Kinematic criteria defining the fiducial phase space of the measurement at particle level.

$R = 0.4$ to all final-state particles with a lifetime longer than 30 ps, excluding the dressed Z-boson decay products. A jet is identified as b-tagged if it lies within $\Delta R = 0.3$ of one or more weakly decaying b-hadrons with $p_{\mathrm{T}} > 5$ GeV. If a b-hadron matches more than one jet, only the closest jet in ΔR is labelled as a b-jet.

The correction of differential distributions is implemented using an iterative Bayesian method of unfolding [103] with two iterations. Simulated events are used to generate a response matrix for each distribution to account for bin-to-bin migration effects between the detector-level and particle-level distributions. The matrix is filled with the events that pass both the detector-level and particle-level selections. The particle-level prediction is used as the initial prior to determine the first estimate of the unfolded data distribution. For the second iteration, the new estimate of unfolded data is obtained using the background-subtracted data and an unfolding matrix, which is derived on the basis of the Bayes' theorem from the response matrix and the current prior. The background-subtracted data are corrected for the expected fraction of events which pass the detector-level selection, but not the particle-level one (unmatched-events), before entering the iterative unfolding. For each bin of each differential distribution, the unfolded event yields are divided by the integrated luminosity of the data sample and by the bin width, to obtain the cross-section measurement. The differential cross-section measurement of a given observable in the i-th bin is given by:

$$\sigma_i = \frac{1}{\epsilon_i L} \sum U_{ij} f_j N_j^{\mathrm{bsD}},$$

where L is the integrated luminosity, ϵ_i is the reconstruction efficiency in i-th bin, N_j^{bsD} is the number of background-subtracted data events in the j-th bin, f_j is the factor that corrects for unmatched events in the j-th bin, and U_{ij} is the element (i, j) of the unfolding matrix calculated after two iterations, using the updated prior from the first iteration and the response matrix.

The measurement of the inclusive cross-section for Z-boson events with at least one or at least two b-jets is obtained by applying a particle-level correction to the number of events in data with at least one or at least two b-jets, after background subtraction. The correction, which is applied as a divisor of the background-subtracted data, is derived from the ratio of the total number of reconstructed events in the detector-level phase space to the number of particle-level events in the fiducial phase space. It is 0.399 ± 0.001 for Z-

JHEP07(2020)044

Source of uncertainty	$Z(\to \ell\ell) + \geq 1$ b-jet [%]	$Z(\to \ell\ell) + \geq 2$ b-jets [%]
b-jet tagging efficiency	7.0	14
b-jet mistag rate	2.4	1.1
Jet	2.4	5.0
Lepton	0.8	1.2
$E_{\mathrm{T}}^{\mathrm{miss}}$	0.6	1.3
$Z + c$ and $Z + l$ backgrounds	4.5	1.1
Top background	0.5	3.8
Other backgrounds	< 0.1	0.1
Pile-up	1.7	2.6
Unfolding	3.8	4.1
Luminosity	2.3	2.9
Total [%]	10	16

Table 8. Relative systematic uncertainties in the measured production cross-sections of $Z(\to \ell\ell) + \geq 1$ b-jet and $Z(\to \ell\ell) + \geq 2$ b-jets events. The "Jet" term includes the JES, JER and JVT uncertainties. The "Lepton" term includes the lepton trigger, efficiency, scale and resolution uncertainties. The "$Z + c$ and $Z + l$ backgrounds" term also includes the $Z + 1b$ background in the $Z + \geq 2$ b-jets measurement.

boson events with at least one b-jet and 0.258 ± 0.002 for Z-boson events with at least two b-jets, using Sherpa signal samples and quoting the statistical error.

Since the electron and muon decay channels are combined to increase the precision of the signal fits to data, the corrections and response matrices are made using electron and muon signal samples to obtain combined particle-level yields. To validate this procedure, the analysis is performed for each of the two lepton channels separately. The results obtained from the individual channels are compatible within 1.4σ and 1.6σ with the inclusive cross-section of Z-boson events with at least one b-jet and at least two b-jets, respectively. This comparison uses only the sum in quadrature of the statistical and uncorrelated systematic uncertainties. The differential cross-section measurements in the two channels also agree over the full range of each distribution.

8 Uncertainties in the cross-section measurements

Table 8 summarises the systematic uncertainties of the inclusive $Z + b$-jets cross-sections in the one- and two-b-tag regions. Figure 6 shows as an example the breakdown of the systematic uncertainties in the cross-section as a function of Z-boson p_{T} for events with at least one b-jet and as a function of ΔR_{bb} for events with at least two b-jets.

The systematic uncertainties in the cross-sections associated with the detector-level uncertainty sources described in section 4.1 are derived for each observable by propagating systematic shifts from each source through both the response matrices (unfolding factor) and the subtracted background contributions into the unfolded data for the differential (in-

JHEP07(2020)044

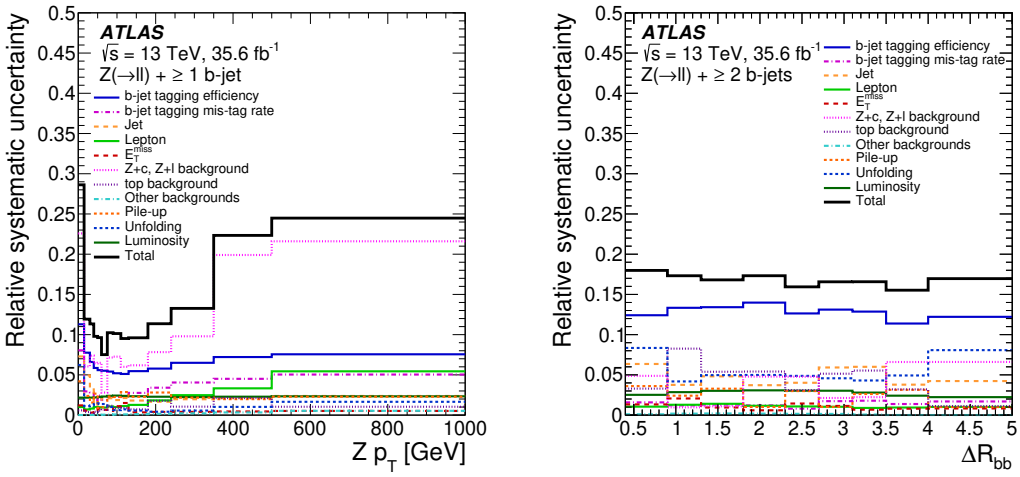

Figure 6. Relative systematic uncertainties in the fiducial cross-section as a function of the Z-boson p_{T} in events with at least one b-jet (left) and as a function of the ΔR between the two leading b-jets in events with at least two b-jets (right). The total uncertainty is shown in black while the different components listed in table 8 are shown in different colours.

clusive) cross-section measurements. The dominant source of uncertainty is the modelling of the b-tagging efficiency. Its impact on the inclusive cross-section ranges from 7.0% for Z-boson events with at least one b-jet to 14% for Z-boson events with at least two b-jets. Its effect on differential cross-section measurements ranges from 5% to 10% for Z-boson events with at least one b-jet and from 10% to 15% for Z-boson events with at least two b-jets. The impact of the mistag rate of c- and light-jets is smaller; it is 2.4% for Z-boson events with at least one b-jet and 1% for Z-boson events with at least two b-jets.

The uncertainty from each background source is determined by applying shifts to the subtracted background contributions and to the nominal response matrices or unfolding factors. The sources of uncertainty considered for $Z + l$ and $Z + c$ (and $Z + 1b$ in the $Z + \geq 2b$-jets measurement), $t\bar{t}$ and single-top, diboson and other minor backgrounds are described in section 5. The dominant uncertainty in the background to events with at least one b-jet originates from Z+jets events. This uncertainty contributes 4.5% to the uncertainty in the inclusive cross-section. An uncertainty of 3.7% derives from the difference between the modelling in Alpgen and Sherpa, while 2.6% is due to the flavour fit uncertainty. The impact of this uncertainty on the differential cross-sections ranges from a few per cent up to 25% in the extreme corners of the phase space. For a Z-boson p_{T} value of about 500 GeV, the difference between the modelling in Alpgen and Sherpa contributes 18% to this uncertainty, and the flavour fit uncertainty is 12%.

In contrast, the uncertainty in the estimation of background from $t\bar{t}$ events is the dominant source of uncertainty in the background to Z-boson events with at least two b-jets. It contributes 3.8% to the inclusive cross-section and ranges from 1% to 9% in the differential cross-sections.

The uncertainty due to modelling of the $Z + b$-jets signal samples in the events with at least one and at least two b-jets are also accounted for. This is evaluated for each observable

JHEP07(2020)044

by reweighting the generator-level distribution in the SHERPA samples to provide a better description of the data at detector level. The modified SHERPA samples are then used to emulate data and are unfolded with the nominal simulated sample. An additional source accounts for the possible mismodelling of an observable that is not one of the unfolded observables (i.e. a hidden variable). This uncertainty is evaluated by reweighting, in the SHERPA samples, the generator-level distribution of the leading lepton's p_{T}, which is one of the observables showing the largest mismodelling, to provide a better description of the data at detector level. The modified SHERPA samples are used to unfold the data. The effect of the hidden variable's mismodelling is negligible for all considered variables and all bins. A third uncertainty source accounts for the different hadronisation and parton-shower models used for the signal simulation. This uncertainty is evaluated by unfolding the ALPGEN signal samples, which emulate the background-subtracted data, with the SHERPA signal samples. The generator-level distributions from the ALPGEN samples are first reweighted to agree with SHERPA in order to remove effects related to shape differences. The difference between the generator-level distribution and the unfolded ALPGEN reweighted distribution is taken as the uncertainty. For the inclusive cross-section, the modelling uncertainty is estimated by replacing the unfolding factor computed with SHERPA with the one computed with ALPGEN. The dependence on the size of the simulated sample is derived using pseudo-experiments, and the spread of the results is taken as an uncertainty. The statistical term is typically less than a few per cent. It reaches 5% in the last bin of the ΔR_{bb} distribution and 15% only in the last bin of the Δy_{bb} distribution.

The total unfolding uncertainty in the inclusive cross-sections is at the level of 4% in each of the two signal regions. In the differential distributions it is less than 5% in the 1-tag region and at a level of 5%–10% in the 2-tag region, except in some bins of the angular variables and in the tail of the p_{T} and m_{bb} distributions, where it reaches 20%.

9 Results

The inclusive and differential cross-section measurements for $Z + \geq 1$ b-jet and $Z + \geq 2$ b-jets are shown in figures 7–15. The statistical uncertainty of the data is propagated through the unfolding by using 1000 pseudo-experiments, repeating the flavour fit for each of them. The statistical uncertainty in the inclusive cross-sections of $Z + \geq 1$ b-jet and $Z + \geq 2$ b-jets is 0.3% and 0.8% respectively. As mentioned in section 8, the systematic uncertainties are propagated through the unfolding via the response matrices or the unfolding factors and via the variation of the subtracted background. The measurements are compared with the predictions from SHERPA 5FNS (NLO), ALPGEN + PY6 4 FNS (LO), SHERPA FUSING 4FNS+5FNS (NLO), SHERPA ZBB 4FNS (NLO), MGAMC + PY8 5FNS (LO), MGAMC + PY8 ZBB 4FNS (NLO) and MGAMC + PY8 5FNS (NLO). Theoretical uncertainties of SHERPA 5FNS (NLO), computed as described in section 3, are shown in the comparison with data. In this section, all predictions are normalised to their own cross-section to allow an unbiased comparison among different generators.[7]

[7]The NNLO cross-section K-factor applied to the inclusive ALPGEN and SHERPA samples in previous sections is removed.

JHEP07(2020)044

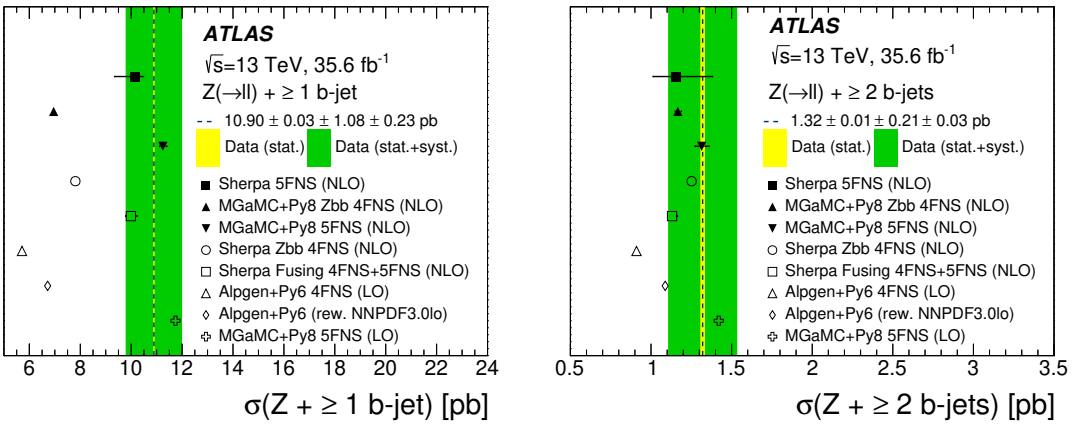

Figure 7. Measured cross-sections for $Z + \geq 1$ b-jet (left) and $Z + \geq 2$ b-jets (right). The data are compared with the predictions from Sherpa 5FNS (NLO), Alpgen + Py6 4 FNS (LO), Sherpa Fusing 4FNS+5FNS (NLO), Sherpa Zbb 4FNS (NLO), MGaMC + Py8 5FNS (LO), MGaMC + Py8 Zbb 4FNS (NLO) and MGaMC + Py8 5FNS (NLO). The yellow band corresponds to the statistical uncertainty of the data, and the green band to statistical and systematic uncertainties of the data, added in quadrature. The error bars on the Sherpa 5FNS (NLO) predictions correspond to the statistical and theoretical uncertainties added in quadrature. Only statistical uncertainties are shown for the other predictions.

9.1 Inclusive cross-sections

The measured inclusive cross-sections for $Z + \geq 1$ b-jet and $Z + \geq 2$ b-jets, shown in figure 7, are $10.90 \pm 0.03(\text{stat.}) \pm 1.08(\text{syst.}) \pm 0.25(\text{lumi.})$ pb and $1.32 \pm 0.01(\text{stat.}) \pm 0.21(\text{syst.}) \pm 0.04(\text{lumi.})$ pb, respectively. The 4FNS MC predictions are systematically lower than data in the inclusive one-b-jet case, both for MC generators with LO matrix elements, as implemented in Alpgen + Py6 4FNS (LO), and for Zbb predictions at NLO, as implemented in Sherpa Zbb 4FNS (NLO) and MGaMC + Py8 Zbb 4FNS (NLO). The 4FNS predictions agree well with data in the inclusive two-b-jet case. Even though the LO Alpgen + Py6 4FNS (LO) underestimates the data, the predictions and data agree within two standard deviations (2σ) of the experimental uncertainty. Use of the NNPDF3.0lo PDF set in Alpgen predictions gives better agreement with data because of a higher acceptance in the fiducial region. The 5FNS simulations, in general, adequately predict the inclusive cross-sections for both $Z + \geq 1$ b-jet and $Z + \geq 2$ b-jets. Overall, this is consistent with the results presented in the ATLAS measurement at $\sqrt{s} = 7$ TeV [11].

9.2 Differential cross-sections for $Z + \geq 1$ b-jet

The differential cross-section measurements for the $Z + \geq 1$ b-jet process are shown in figures 8–11. Each distribution is presented and discussed in detail in this section.

The distributions of the transverse momentum of the Z boson and of the jets probe pQCD over a wide range of scales and provide important input to the background prediction for other SM processes, including Higgs boson production and searches beyond the SM. The differential cross-section as a function of the Z-boson p_{T} for events with at least one b-jet is shown in figure 8 (left). In the low p_{T} region, up to 100 GeV, where soft radiative effects

JHEP07(2020)044

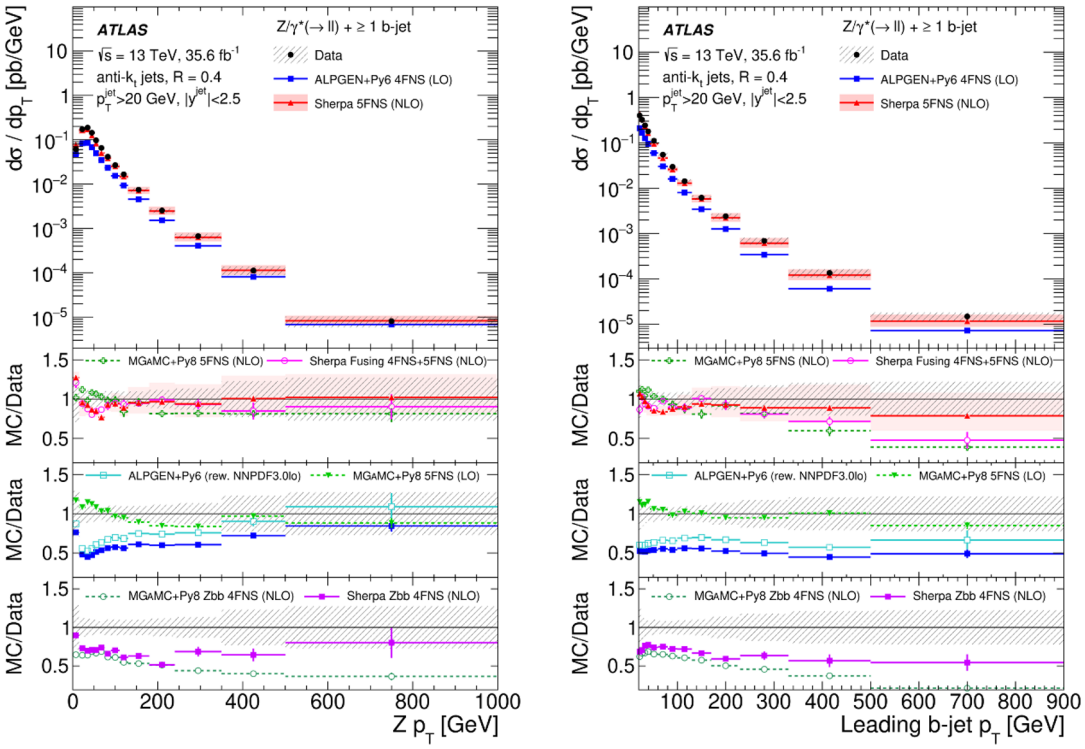

Figure 8. Measured cross-section as a function of Z-boson p_{T} (left) and leading b-jet p_{T} (right) in events with at least one b-jet. The data are compared with the predictions from Sherpa 5FNS (NLO), Alpgen + Py6 4 FNS (LO), Sherpa Fusing 4FNS+5FNS (NLO), Sherpa Zbb 4FNS (NLO), MGaMC + Py8 5FNS (LO), MGaMC + Py8 Zbb 4FNS (NLO) and MGaMC + Py8 5FNS (NLO). The error bars correspond to the statistical uncertainty, and the hatched bands to the data statistical and systematic uncertainties added in quadrature. The red band corresponds to the statistical and theoretical uncertainties of Sherpa 5FNS (NLO) added in quadrature. Only statistical uncertainties are shown for the other predictions.

play a role, all the predicted shapes except that of MGaMC + Py8 Zbb 4FNS (NLO) exhibit trends different from those in the data. Overall, the predictions from Sherpa 5FNS (NLO) and Sherpa Fusing 4FNS+5FNS (NLO) show the best agreement with data. Predictions from MGaMC + Py8 5FNS (LO) and MGaMC + Py8 5FNS (NLO) are within the experimental uncertainty band for most of the bins. The harder Z-boson p_{T} in Alpgen predictions than in data has already been reported by ATLAS for data collected at $\sqrt{s} = 7$ TeV [11]. Figure 8 (right) shows the leading b-jet p_{T}. MGaMC + Py8 5FNS (LO) provides a satisfactory description within the uncertainty of the data, while MGaMC + Py8 5FNS (NLO) underestimates the data in the high p_{T} region. This region is populated by additional hard radiation, which in MGaMC + Py8 5FNS (NLO) is simulated only via parton shower. Sherpa 5FNS (NLO) exhibits the best agreement with data. The contrasting behaviour of Sherpa Fusing 4FNS+5FNS (NLO), which underestimates the data at high p_{T}, may be interesting to investigate further in the future. The NLO 4FNS predictions of Zbb, as implemented in Sherpa and MGaMC, show a softer leading b-jet p_{T}, while the inclusive LO 4FNS prediction, as implemented in Alpgen, describes

JHEP07(2020)044

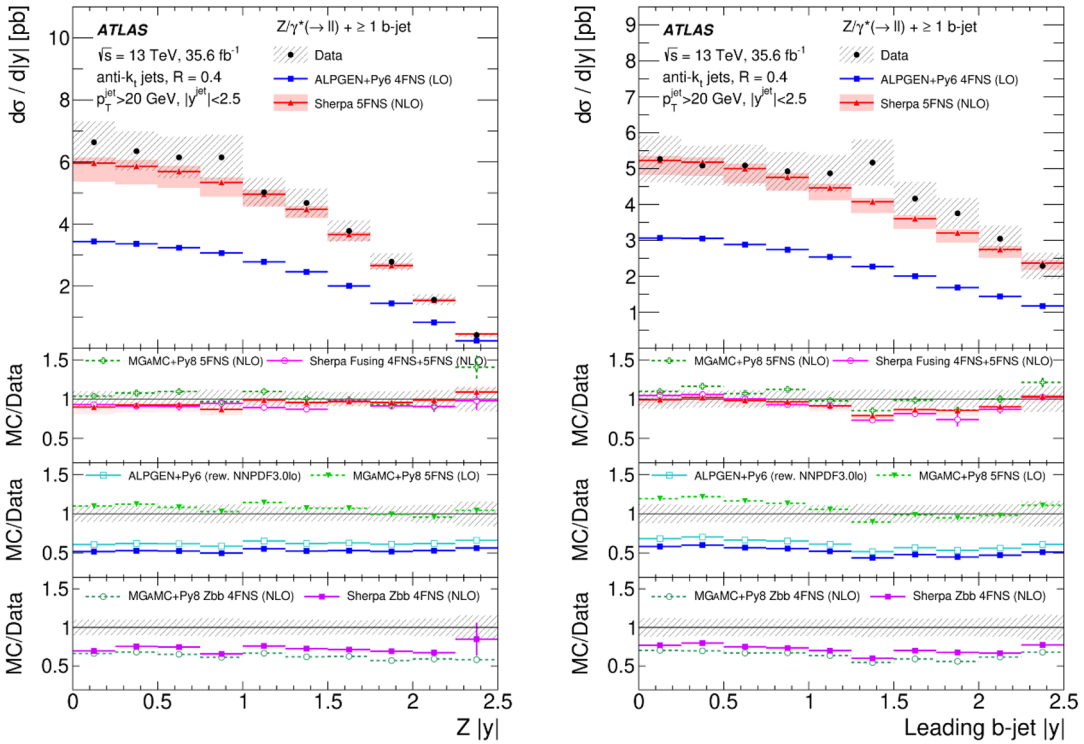

Figure 9. Measured cross-section as a function of Z-boson $|y|$ (left) and leading b-jet $|y|$ (right) in events with at least one b-jet. The data are compared with the predictions from Sherpa 5FNS (NLO), Alpgen + Py6 4 FNS (LO), Sherpa Fusing 4FNS+5FNS (NLO), Sherpa Zbb 4FNS (NLO), MGaMC + Py8 5FNS (LO), MGaMC + Py8 Zbb 4FNS (NLO) and MGaMC + Py8 5FNS (NLO). The error bars correspond to the statistical uncertainty, and the hatched bands to the data statistical and systematic uncertainties added in quadrature. The red band corresponds to the statistical and theoretical uncertainties of Sherpa 5FNS (NLO) added in quadrature. Only statistical uncertainties are shown for the other predictions.

the shape of the data quite well despite the large underestimation of the normalisation already discussed for figure 7.

The distributions of the Z-boson rapidity, the leading b-jet rapidity, and their separation, Δy_{Zb}, are directly sensitive to the b-quark PDFs and to higher-order diagram contributions, and they may show differences for different flavour schemes. The differential cross-sections as a function of the Z-boson rapidity and of the leading b-jet rapidity for events with at least one b-jet are shown in figure 9. All MC predictions provide a satisfactory description of the shape of the data. Some modulation relative to data is observed in the leading b-jet $|y|$ distribution, in some cases beyond the experimental uncertainty. Figure 10 (right) shows the differential cross-section as a function of Δy_{Zb}. Sherpa 5FNS (NLO) and Sherpa Fusing 4FNS+5FNS (NLO) describe the data quite well, while all other predictions exhibit a slightly smaller rapidity separation than data, even if within the uncertainty of the data. Use of a different PDF set as in Alpgen predictions leads to a change in the distribution, but the differences are small compared with the experimental uncertainties.

JHEP07(2020)044

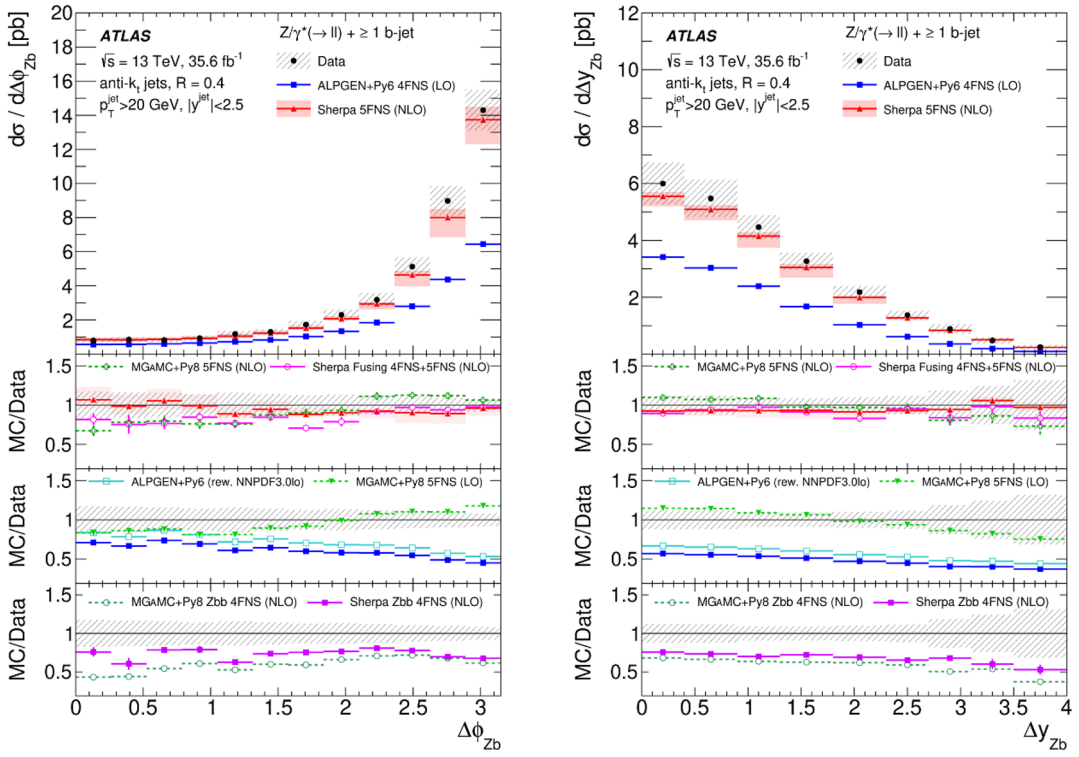

Figure 10. Measured cross-section as a function of $\Delta\phi$ (left) and Δy between the Z-boson candidate and the leading b-jet (right) in events with at least one b-jet. The data are compared with the predictions from Sherpa 5FNS (NLO), Alpgen + Py6 4 FNS (LO), Sherpa Fusing 4FNS+5FNS (NLO), Sherpa Zbb 4FNS (NLO), MGaMC + Py8 5FNS (LO), MGaMC + Py8 Zbb 4FNS (NLO) and MGaMC + Py8 5FNS (NLO). The error bars correspond to the statistical uncertainty, and the hatched bands to the data statistical and systematic uncertainties added in quadrature. The red band corresponds to the statistical and theoretical uncertainties of Sherpa 5FNS (NLO) added in quadrature. Only statistical uncertainties are shown for the other predictions.

The distribution of $\Delta\phi_{Zb}$ is sensitive to the presence of additional radiation in the event. In fixed order calculations of the $Z + 1b$ process, the LO matrix element provides contributions only for $\Delta\phi_{Zb} = \pi$, while the NLO matrix element is the first order which populates the region of $\Delta\phi_{Zb} < \pi$. In MC simulations the region below π is populated via parton shower and via merging of parton shower with multi-parton matrix elements. Therefore the region of small azimuthal separation between the Z boson and the leading b-jet is the most sensitive to additional QCD radiation and soft corrections. It is also sensitive to the presence of boosted particles decaying into a Z boson and b-quarks. The differential cross-section as a function of $\Delta\phi_{Zb}$ for events with at least one b-jet is shown in figure 10 (left). The Sherpa 5FNS (NLO) generator provides the best agreement with data. Sherpa Fusing 4FNS+5FNS (NLO) is still consistent with data within the experimental uncertainty in most of the bins, but a small difference between the two simulations is observed for small values. This result is highly correlated with the difference observed in the leading b-jet p_{T} distribution. It confirms that the current performance

JHEP07(2020)044

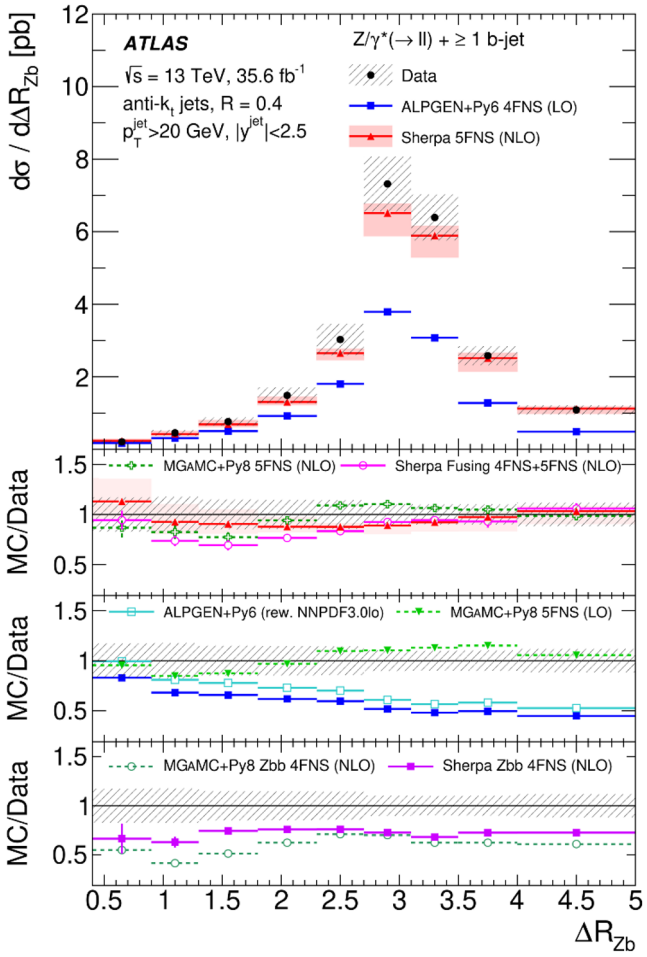

Figure 11. Measured cross-section as a function of the ΔR between the Z-boson candidate and the leading b-jet in events with at least one b-jet. The data are compared with the predictions from Sherpa 5FNS (NLO), Alpgen + Py6 4 FNS (LO), Sherpa Fusing 4FNS+5FNS (NLO), Sherpa Zbb 4FNS (NLO), MGaMC + Py8 5FNS (LO), MGaMC + Py8 Zbb 4FNS (NLO) and MGaMC + Py8 5FNS (NLO). The error bars correspond to the statistical uncertainty, and the hatched bands to the statistical and systematic uncertainties of the data, added in quadrature. The red band corresponds to the statistical and theoretical uncertainties of Sherpa 5FNS (NLO) added in quadrature. Only statistical uncertainties are shown for the other predictions.

of Sherpa Fusing 4FNS+5FNS (NLO) in the regime of high-p_{T} jets with a Z boson emitted collinearly is slightly worse than the Sherpa 5FNS (NLO) configuration. All MGaMC simulations predict too many large azimuthal separations, with a consequent deficit at small angles. Also, in this case the modelling in MGaMC + Py8 5FNS (NLO) is slightly worse than in MGaMC + Py8 5FNS (LO). The differential cross-section as a function of ΔR_{Zb}, as shown in figure 11, contains the convolution of effects discussed for the Δy_{Zb} and $\Delta\phi_{Zb}$ distributions.

JHEP07(2020)044

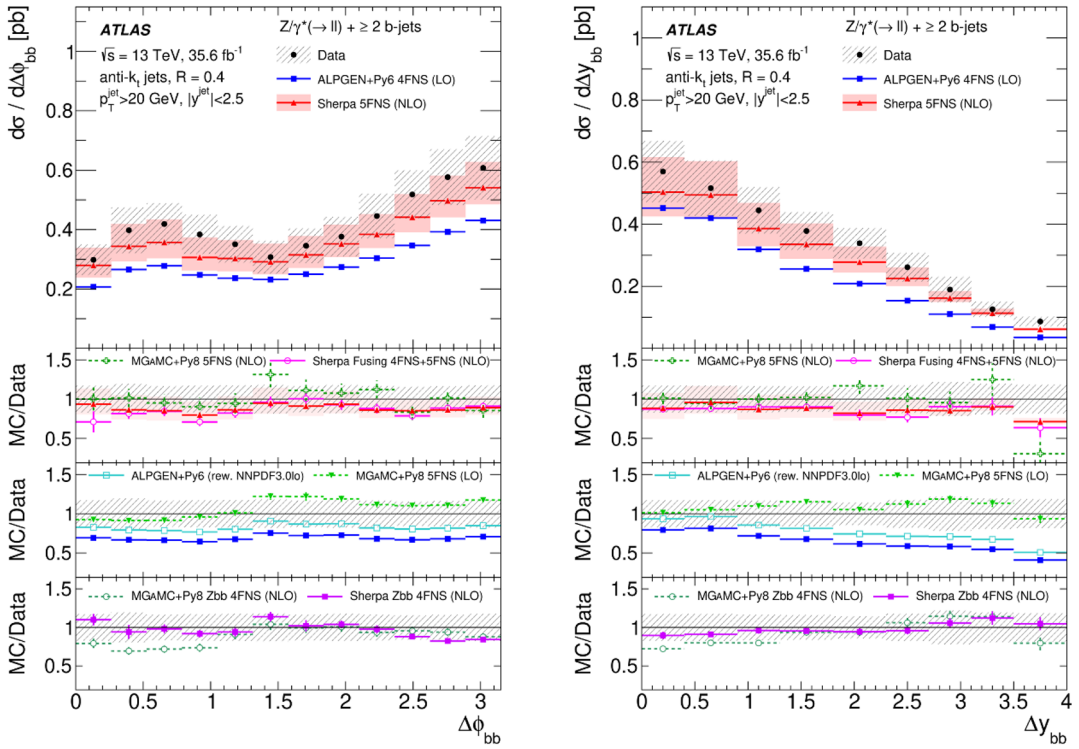

Figure 12. Measured cross-section as a function of $\Delta\phi$ (left) and Δy between the two leading b-jets (right) in events with at least two b-jets. The data are compared with the predictions from Sherpa 5FNS (NLO), Alpgen + Py6 4 FNS (LO), Sherpa Fusing 4FNS+5FNS (NLO), Sherpa Zbb 4FNS (NLO), MGaMC + Py8 5FNS (LO), MGaMC + Py8 Zbb 4FNS (NLO) and MGaMC + Py8 5FNS (NLO). The error bars correspond to the statistical uncertainty, and the hatched bands to the data statistical and systematic uncertainties added in quadrature. The red band corresponds to the statistical and theoretical uncertainties of Sherpa 5FNS (NLO) added in quadrature. Only statistical uncertainties are shown for the other predictions.

9.3 Differential cross-sections for $Z + \geq 2$ b-jets

Events with a Z boson produced in association with two b-jets constitute an important background to other SM and beyond-SM processes. Furthermore, they probe the mechanism of a gluon splitting into heavy quarks. The differential cross-section measurements for $Z + \geq 2$ b-jet are shown in figures 12–15. Each distribution is presented and discussed in detail in this section.

The distributions of angular separation between the two leading b-jets allow characterisation of the hard radiation at large angles and the soft radiation for collinear emissions. The differential cross-sections as a function of $\Delta\phi_{bb}$ and of Δy_{bb} are shown in figure 12. Most of the predictions provide satisfactory descriptions of the data within the large experimental uncertainties. Disagreement between data and MGaMC + Py8 Zbb 4FNS (NLO) is observed at low values of $\Delta\phi_{bb}$. Mismodelling of Δy_{bb} is observed for Alpgen. This observable has some sensitivity to PDFs, but that is below the experimental uncertainties. The ΔR_{bb} observable is sensitive to the various production mechanisms of the Zbb

JHEP07(2020)044

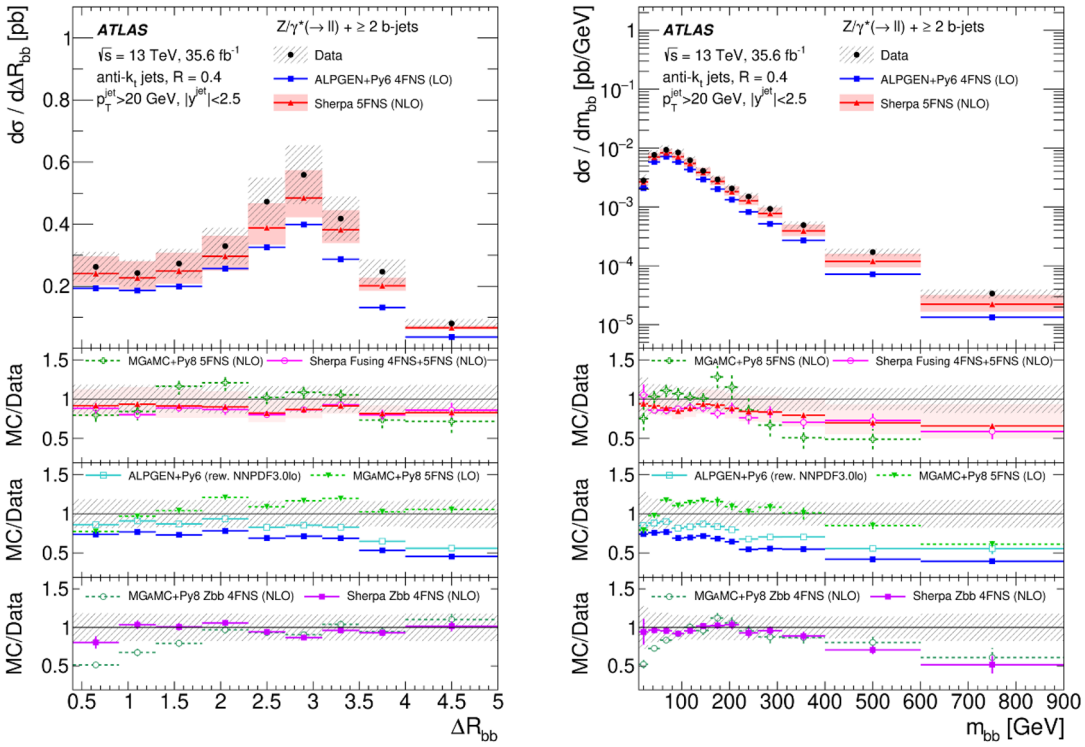

Figure 13. Measured cross-section as a function of ΔR between the two leading b-jets (left) and invariant mass of the two leading b-jets (right) in events with at least two b-jets. The data are compared with the predictions from Sherpa 5FNS (NLO), Alpgen + Py6 4 FNS (LO), Sherpa Fusing 4FNS+5FNS (NLO), Sherpa Zbb 4FNS (NLO), MGaMC + Py8 5FNS (LO), MGaMC + Py8 Zbb 4FNS (NLO) and MGaMC + Py8 5FNS (NLO). The error bars correspond to the statistical uncertainty, and the hatched bands to the data statistical and systematic uncertainties added in quadrature. The red band corresponds to the statistical and theoretical uncertainties of Sherpa 5FNS (NLO) added in quadrature. Only statistical uncertainties are shown for the other predictions.

final state. The region at low ΔR_{bb} is dominated by the production of two b-jets from gluon splitting. Probing this region requires two b-jets in the final state, so it is not sensitive to very small angles of the splitting. The interplay of the modelling of $\Delta\phi_{bb}$ and Δy_{bb} in Alpgen + Py6 4 FNS (LO) influences the prediction of the ΔR_{bb} distribution shown in figure 13 (left). All Sherpa predictions describe the shape of this observable quite well, featuring a substantial improvement at low ΔR_{bb} relative to the LO version reported by ATLAS using data at $\sqrt{s} = 7$ TeV. Overall, this is consistent with the results presented in the ATLAS measurement of gluon-splitting properties at $\sqrt{s} = 13$ TeV [11]. MGaMC + Py8 Zbb 4FNS (NLO) presents a large mismodelling at low ΔR_{bb}, which is the part of the phase space dominated by gluon splitting.

The invariant mass of the two leading b-jets is an important observable in the measurement of associated ZH production with Higgs boson decays into $b\bar{b}$, and in searches for physics beyond the SM in the same final state. The differential cross-section as a function of m_{bb} for events with at least two b-jets is shown in figure 13 (right). All Sherpa

JHEP07(2020)044

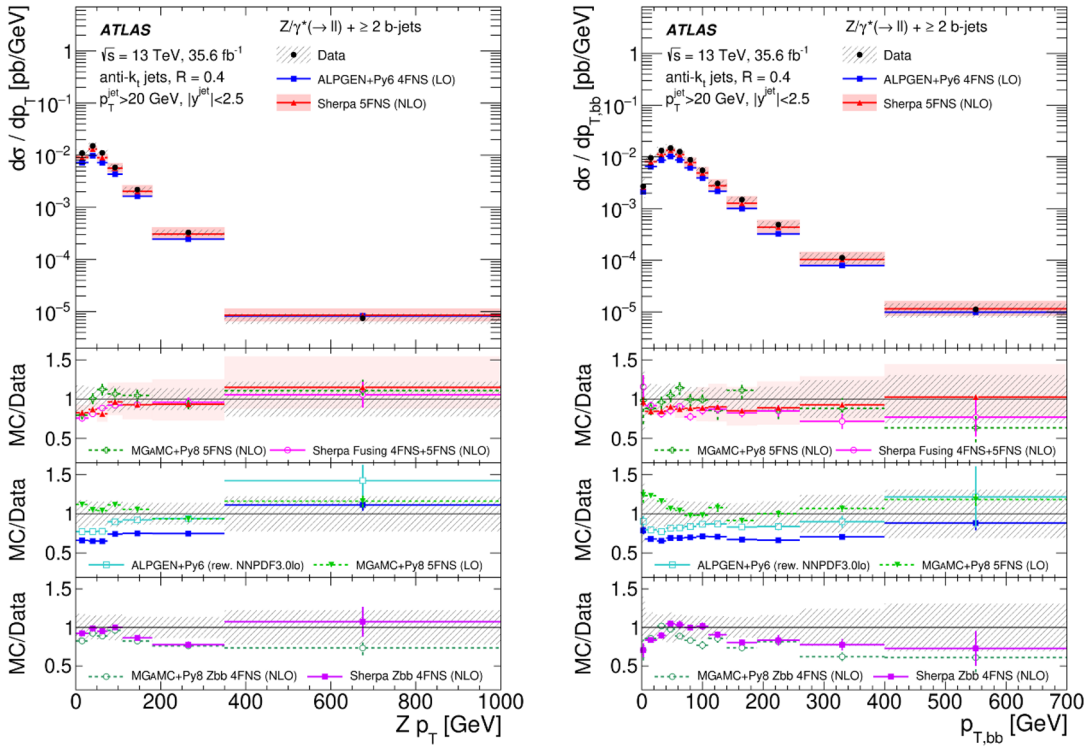

Figure 14. Measured cross-section as a function of p_{T} of the Z boson (left) and of the di-b-jet system ($p_{\mathrm{T},bb}$) (right) in events with at least two b-jets. The data are compared with the predictions from Sherpa 5FNS (NLO), Alpgen + Py6 4 FNS (LO), Sherpa Fusing 4FNS+5FNS (NLO), Sherpa Zbb 4FNS (NLO), MGaMC + Py8 5FNS (LO), MGaMC + Py8 Zbb 4FNS (NLO) and MGaMC + Py8 5FNS (NLO). The error bars correspond to the statistical uncertainty, and the hatched bands to the data statistical and systematic uncertainties added in quadrature. The red band corresponds to the statistical and theoretical uncertainties of Sherpa 5FNS (NLO) added in quadrature. Only statistical uncertainties are shown for the other predictions.

predictions provide a quite good model of the shape of this observable's distribution up to about 300 GeV, while the other predictions show various discrepancies in this region. This is particularly evident for MGaMC + Py8 Zbb 4FNS (NLO), and it is consistent with the mismodelling observed at low ΔR_{bb}, the region dominated by gluon splitting. In the high mass range all predictions underestimate the data, resulting in a sizeable mismodelling. Hence the use of these predictions for the background estimate in searches for physics beyond the SM in this final state could be problematic.

The differential cross-sections as a function of the Z-boson p_{T} and of the p_{T} of the di-b-jet system ($p_{\mathrm{T},bb}$) for events with at least two b-jets are shown in figure 14. Most of the predictions agree with data within the large experimental uncertainties, which are about 25% in most of the bins, and large statistical uncertainties of the predictions, which for some MC samples reach 25% in the highest bins. Alpgen shows a harder Z-boson p_{T} spectrum than data, as was observed in the distribution of events with at least one b-jet. The Zbb simulation at NLO with 4FNS, as implemented in MGaMC + Py8 Zbb 4FNS (NLO) and Sherpa Zbb 4FNS (NLO), shows better agreement with data with respect

JHEP07(2020)044

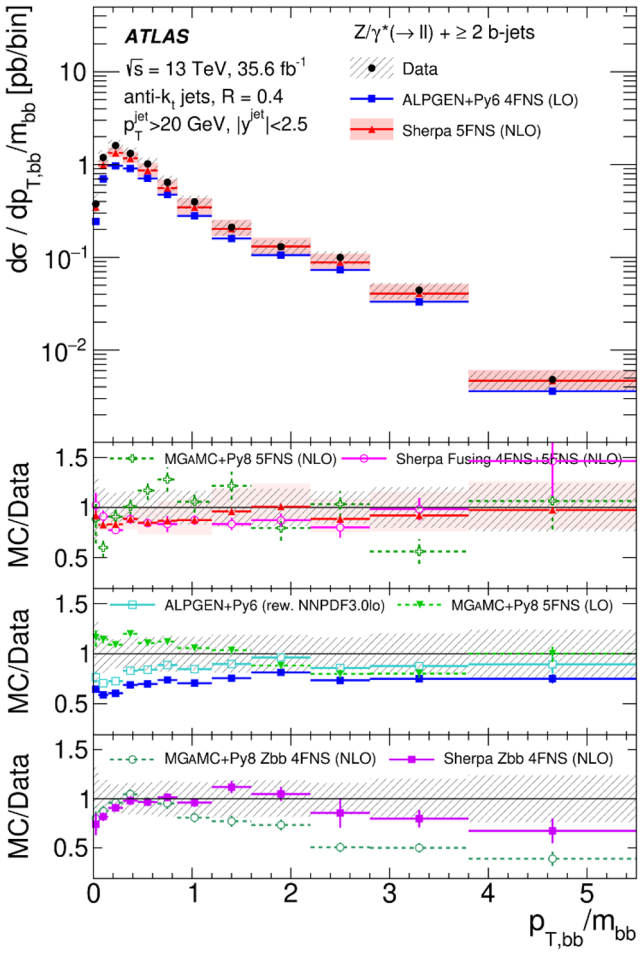

Figure 15. Measured cross-section as a function of the p_{T} of the di-b-jet system divided by its invariant mass ($p_{\mathrm{T},bb}/m_{bb}$) in events with at least two b-jets. The data are compared with the predictions from Sherpa 5FNS (NLO), Alpgen + Py6 4 FNS (LO), Sherpa Fusing 4FNS+5FNS (NLO), Sherpa Zbb 4FNS (NLO), MGaMC + Py8 5FNS (LO), MGaMC + Py8 Zbb 4FNS (NLO) and MGaMC + Py8 5FNS (NLO). The error bars correspond to the statistical uncertainty, and the hatched bands to the statistical and systematic uncertainties of the data, added in quadrature. The red band corresponds to the statistical and theoretical uncertainties of Sherpa 5FNS (NLO) added in quadrature. Only statistical uncertainties are shown for the other predictions.

to the p_{T} distributions for events with at least one b-jet, but significant disagreement is still observed.

Finally, the ratio of the p_{T} of the di-b-jet system to its invariant mass ($p_{\mathrm{T},bb}/m_{bb}$) is sensitive to gluon splitting: a small value indicates a hard splitting and a large value is a consequence of soft splitting. The differential cross-section as a function of $p_{\mathrm{T},bb}/m_{bb}$ is shown in figure 15. Sherpa 5FNS (NLO) and Sherpa Fusing 4FNS+5FNS (NLO) show quite good agreement with data, while MGaMC + Py8 Zbb 4FNS (NLO) agrees less well.

JHEP07(2020)044

10 Conclusion

This paper presents a measurement of the cross-sections for Z-boson production in association with one or more b-jets in pp collisions at $\sqrt{s} = 13$ TeV. The analysed data correspond to an integrated luminosity of $35.6\,\text{fb}^{-1}$ recorded by the ATLAS detector at the LHC.

The cross-sections are measured using the electron and muon decay modes of the Z boson in a fiducial phase space. In addition to the inclusive cross-sections, differential cross-sections of several kinematic observables are measured, extending the range of jet transverse momenta to higher values than reported in previous ATLAS publications, which used data at lower centre-of-mass energies.

The measurements are compared with predictions from a variety of Monte Carlo generators. In general, 5-flavour number scheme (5FNS) calculations at NLO accuracy predict the inclusive cross-sections well, while inclusive 4-flavour number scheme (4FNS) LO calculations largely underestimate the data. Predictions of Zbb at NLO accuracy agree with data only in the two-b-jets case, and underestimate the data in the case of events with at least one b-jet. Overall, Sherpa 5FNS (NLO), a 5FNS generator with matrix elements at NLO for up to two partons and matrix elements at LO for up to four partons, describes the various differential distributions within the experimental uncertainties. A significant discrepancy, common to all generators, is found for large values of m_{bb}. The Sherpa Fusing 4FNS+5FNS (NLO) simulation, which combines 4FNS with 5FNS at NLO accuracy using a novel technique, agrees with Sherpa 5FNS (NLO), showing that in general at the scales tested by this measurement the effects of this merging are minor. A disagreement of about 20 30% is observed for large values of the leading b-jet transverse momentum, and for small angular separations between the Z boson and the leading b-jet.

The 5FNS simulation with matrix elements for up to four partons at LO, as implemented in MGaMC + Py8 (LO), describes the data within the experimental uncertainties in most cases. In some cases this simulation is even better than predictions from MGaMC + Py8 5FNS (NLO), which has matrix elements with only one parton at NLO. This indicates the importance of simulations with several partons in the matrix element for a fair description of the data. The pure Zbb simulation at NLO in the 4FNS, as generated by Sherpa and MGaMC, shows significant deviations from the data even in the two-b-jets configuration, and this is more pronounced in MGaMC.

This measurement provides essential input for the improvement of theoretical predictions and Monte Carlo generators of Z-boson production in association with b-jets, allowing a better quantitative understanding of perturbative QCD.

Acknowledgments

We thank CERN for the very successful operation of the LHC, as well as the support staff from our institutions without whom ATLAS could not be operated efficiently.

We acknowledge the support of ANPCyT, Argentina; YerPhI, Armenia; ARC, Australia; BMWFW and FWF, Austria; ANAS, Azerbaijan; SSTC, Belarus; CNPq and FAPESP, Brazil; NSERC, NRC and CFI, Canada; CERN; CONICYT, Chile; CAS, MOST

JHEP07(2020)044

and NSFC, China; COLCIENCIAS, Colombia; MSMT CR, MPO CR and VSC CR, Czech Republic; DNRF and DNSRC, Denmark; IN2P3-CNRS and CEA-DRF/IRFU, France; SRNSFG, Georgia; BMBF, HGF and MPG, Germany; GSRT, Greece; RGC and Hong Kong SAR, China; ISF and Benoziyo Center, Israel; INFN, Italy; MEXT and JSPS, Japan; CNRST, Morocco; NWO, Netherlands; RCN, Norway; MNiSW and NCN, Poland; FCT, Portugal; MNE/IFA, Romania; MES of Russia and NRC KI, Russia Federation; JINR; MESTD, Serbia; MSSR, Slovakia; ARRS and MIZŠ, Slovenia; DST/NRF, South Africa; MINECO, Spain; SRC and Wallenberg Foundation, Sweden; SERI, SNSF and Cantons of Bern and Geneva, Switzerland; MOST, Taiwan; TAEK, Turkey; STFC, United Kingdom; DOE and NSF, United States of America. In addition, individual groups and members have received support from BCKDF, CANARIE, Compute Canada and CRC, Canada; ERC, ERDF, Horizon 2020, Marie Skłodowska-Curie Actions and COST, European Union; Investissements d'Avenir Labex, Investissements d'Avenir Idex and ANR, France; DFG and AvH Foundation, Germany; Herakleitos, Thales and Aristeia programmes co-financed by EU-ESF and the Greek NSRF, Greece; BSF-NSF and GIF, Israel; CERCA Programme Generalitat de Catalunya and PROMETEO Programme Generalitat Valenciana, Spain; Göran Gustafssons Stiftelse, Sweden; The Royal Society and Leverhulme Trust, United Kingdom.

The crucial computing support from all WLCG partners is acknowledged gratefully, in particular from CERN, the ATLAS Tier-1 facilities at TRIUMF (Canada), NDGF (Denmark, Norway, Sweden), CC-IN2P3 (France), KIT/GridKA (Germany), INFN-CNAF (Italy), NL-T1 (Netherlands), PIC (Spain), ASGC (Taiwan), RAL (U.K.) and BNL (U.S.A.), the Tier-2 facilities worldwide and large non-WLCG resource providers. Major contributors of computing resources are listed in ref. [104].

References

[1] F. Febres Cordero, L. Reina and D. Wackeroth, *W- and Z-boson production with a massive bottom-quark pair at the Large Hadron Collider*, *Phys. Rev. D* **80** (2009) 034015 [arXiv:0906.1923] [INSPIRE].

[2] J.M. Campbell, R. Ellis, F. Maltoni and S. Willenbrock, *Associated production of a Z boson and a single heavy quark jet*, *Phys. Rev. D* **69** (2004) 074021 [hep-ph/0312024] [INSPIRE].

[3] F. Maltoni, G. Ridolfi and M. Ubiali, *b-initiated processes at the LHC: a reappraisal*, *JHEP* **07** (2012) 022 [*Erratum ibid.* **04** (2013) 095] [arXiv:1203.6393] [INSPIRE].

[4] G. Ridolfi, M. Ubiali and M. Zaro, *A fragmentation-based study of heavy quark production*, *JHEP* **01** (2020) 196 [arXiv:1911.01975] [INSPIRE].

[5] CDF collaboration, *Measurement of cross sections for b jet production in events with a Z boson in $p\bar{p}$ collisions at $\sqrt{s} = 1.96$ TeV*, *Phys. Rev. D* **79** (2009) 052008 [arXiv:0812.4458] [INSPIRE].

JHEP07(2020)044

[6] D0 collaboration, *Measurement of the ratio of differential cross sections $\sigma(p\bar{p} \to Z + bjet)/\sigma(p\bar{p} \to Z + jet)$ in $p\bar{p}$ collisions at $\sqrt{s} = 1.96$ TeV*, *Phys. Rev. D* **87** (2013) 092010 [arXiv:1301.2233] [INSPIRE].

[7] CDF collaboration, *First measurement of the b-jet cross section in events with a W boson in $p\bar{p}$ collisions at $\sqrt{s} = 1.96$ TeV*, *Phys. Rev. Lett.* **104** (2010) 131801 [arXiv:0909.1505] [INSPIRE].

[8] D0 collaboration, *Measurement of the $p\bar{p} \to W + b + X$ production cross section at $\sqrt{s} = 1.96$ TeV*, *Phys. Lett. B* **718** (2013) 1314 [arXiv:1210.0627] [INSPIRE].

[9] *LHC Machine*, 2008 *JINST* **3** S08001 [INSPIRE].

[10] ATLAS collaboration, *Measurement of the cross-section for W boson production in association with b-jets in pp collisions at $\sqrt{s} = 7$ TeV with the ATLAS detector*, *JHEP* **06** (2013) 084 [arXiv:1302.2929] [INSPIRE].

[11] ATLAS collaboration, *Measurement of differential production cross-sections for a Z boson in association with b-jets in 7 TeV proton-proton collisions with the ATLAS detector*, *JHEP* **10** (2014) 141 [arXiv:1407.3643] [INSPIRE].

[12] CMS collaboration, *Measurement of the production cross sections for a Z boson and one or more b jets in pp collisions at $\sqrt{s} = 7$ TeV*, *JHEP* **06** (2014) 120 [arXiv:1402.1521] [INSPIRE].

[13] CMS collaboration, *Measurement of the cross section and angular correlations for associated production of a Z Boson with b hadrons in pp collisions at $\sqrt{s} = 7$ TeV*, *JHEP* **12** (2013) 039 [arXiv:1310.1349] [INSPIRE].

[14] CMS collaboration, *Measurement of the production cross section for a W boson and two b jets in pp collisions at $\sqrt{s} = 7$ TeV*, *Phys. Lett. B* **735** (2014) 204 [arXiv:1312.6608] [INSPIRE].

[15] CMS collaboration, *Measurement of the Z/γ^*+b-jet cross section in pp collisions at $\sqrt{s} = 7$ TeV*, *JHEP* **06** (2012) 126 [arXiv:1204.1643] [INSPIRE].

[16] CMS collaboration, *Measurement of the production cross section of a W boson in association with two b jets in pp collisions at $\sqrt{s} = 8$ TeV*, *Eur. Phys. J. C* **77** (2017) 92 [arXiv:1608.07561] [INSPIRE].

[17] CMS collaboration, *Measurements of the associated production of a Z boson and b jets in pp collisions at $\sqrt{s} = 8$ TeV*, *Eur. Phys. J. C* **77** (2017) 751 [arXiv:1611.06507] [INSPIRE].

[18] CMS collaboration, *Measurement of the associated production of a Z boson with charm or bottom quark jets in proton-proton collisions at $\sqrt{s} = 13$ TeV*, arXiv:2001.06899 [INSPIRE].

[19] ATLAS collaboration, *The ATLAS experiment at the CERN Large Hadron Collider*, 2008 *JINST* **3** S08003 [INSPIRE].

[20] ATLAS collaboration, *ATLAS Insertable B-layer technical design report*, ATLAS-TDR-19 (2010).

[21] ATLAS IBL collaboration, *Production and integration of the ATLAS insertable B-layer*, 2018 *JINST* **13** T05008 [arXiv:1803.00844] [INSPIRE].

[22] ATLAS collaboration, *Performance of the ATLAS trigger system in 2015*, *Eur. Phys. J. C* **77** (2017) 317 [arXiv:1611.09661] [INSPIRE].

JHEP07(2020)044

[23] ATLAS collaboration, *Luminosity determination in pp collisions at $\sqrt{s} = 13$ TeV using the ATLAS detector at the LHC*, ATLAS-CONF-2019-021 (2019).

[24] G. Avoni et al., *The new LUCID-2 detector for luminosity measurement and monitoring in ATLAS*, 2018 *JINST* **13** P07017 [INSPIRE].

[25] SHERPA collaboration, *Event generation with Sherpa 2.2*, *SciPost Phys.* **7** (2019) 034 [arXiv:1905.09127] [INSPIRE].

[26] T. Gleisberg and S. Hoeche, *Comix, a new matrix element generator*, *JHEP* **12** (2008) 039 [arXiv:0808.3674] [INSPIRE].

[27] F. Cascioli, P. Maierhofer and S. Pozzorini, *Scattering amplitudes with open loops*, *Phys. Rev. Lett.* **108** (2012) 111601 [arXiv:1111.5206] [INSPIRE].

[28] A. Denner, S. Dittmaier and L. Hofer, *Collier: a Fortran-based Complex One-Loop LIbrary in Extended Regularizations*, *Comput. Phys. Commun.* **212** (2017) 220 [arXiv:1604.06792] [INSPIRE].

[29] S. Schumann and F. Krauss, *A parton shower algorithm based on Catani-Seymour dipole factorisation*, *JHEP* **03** (2008) 038 [arXiv:0709.1027] [INSPIRE].

[30] S. Hoeche, F. Krauss, M. Schonherr and F. Siegert, *A critical appraisal of NLO+PS matching methods*, *JHEP* **09** (2012) 049 [arXiv:1111.1220] [INSPIRE].

[31] S. Hoeche, F. Krauss, M. Schonherr and F. Siegert, *QCD matrix elements + parton showers: the NLO case*, *JHEP* **04** (2013) 027 [arXiv:1207.5030] [INSPIRE].

[32] S. Catani, F. Krauss, R. Kuhn and B.R. Webber, *QCD matrix elements + parton showers*, *JHEP* **11** (2001) 063 [hep-ph/0109231] [INSPIRE].

[33] S. Hoeche, F. Krauss, S. Schumann and F. Siegert, *QCD matrix elements and truncated showers*, *JHEP* **05** (2009) 053 [arXiv:0903.1219] [INSPIRE].

[34] NNPDF collaboration, *Parton distributions for the LHC Run II*, *JHEP* **04** (2015) 040 [arXiv:1410.8849] [INSPIRE].

[35] E. Bothmann, M. Schönherr and S. Schumann, *Reweighting QCD matrix-element and parton-shower calculations*, *Eur. Phys. J. C* **76** (2016) 590 [arXiv:1606.08753] [INSPIRE].

[36] M.L. Mangano et al., *ALPGEN, a generator for hard multiparton processes in hadronic collisions*, *JHEP* **07** (2003) 001 [hep-ph/0206293] [INSPIRE].

[37] T. Sjöstrand, S. Mrenna and P.Z. Skands, *PYTHIA 6.4 physics and manual*, *JHEP* **05** (2006) 026 [hep-ph/0603175] [INSPIRE].

[38] P.Z. Skands, *Tuning Monte Carlo generators: the Perugia tunes*, *Phys. Rev. D* **82** (2010) 074018 [arXiv:1005.3457] [INSPIRE].

[39] J. Pumplin et al., *New generation of parton distributions with uncertainties from global QCD analysis*, *JHEP* **07** (2002) 012 [hep-ph/0201195] [INSPIRE].

[40] J. Alwall et al., *Comparative study of various algorithms for the merging of parton showers and matrix elements in hadronic collisions*, *Eur. Phys. J. C* **53** (2008) 473 [arXiv:0706.2569] [INSPIRE].

[41] D.J. Lange, *The EvtGen particle decay simulation package*, *Nucl. Instrum. Meth. A* **462** (2001) 152 [INSPIRE].

JHEP07(2020)044

[42] P. Golonka and Z. Was, *PHOTOS Monte Carlo: a precision tool for QED corrections in Z and W decays*, *Eur. Phys. J. C* **45** (2006) 97 [hep-ph/0506026] [INSPIRE].

[43] N. Davidson, T. Przedzinski and Z. Was, *PHOTOS interface in C++: technical and physics documentation*, *Comput. Phys. Commun.* **199** (2016) 86 [arXiv:1011.0937] [INSPIRE].

[44] C. Anastasiou, L.J. Dixon, K. Melnikov and F. Petriello, *High precision QCD at hadron colliders: electroweak gauge boson rapidity distributions at NNLO*, *Phys. Rev. D* **69** (2004) 094008 [hep-ph/0312266] [INSPIRE].

[45] R. Gavin, Y. Li, F. Petriello and S. Quackenbush, *FEWZ 2.0: a code for hadronic Z production at next-to-next-to-leading order*, *Comput. Phys. Commun.* **182** (2011) 2388 [arXiv:1011.3540] [INSPIRE].

[46] R. Gavin, Y. Li, F. Petriello and S. Quackenbush, *W physics at the LHC with FEWZ 2.1*, *Comput. Phys. Commun.* **184** (2013) 208 [arXiv:1201.5896] [INSPIRE].

[47] Y. Li and F. Petriello, *Combining QCD and electroweak corrections to dilepton production in FEWZ*, *Phys. Rev. D* **86** (2012) 094034 [arXiv:1208.5967] [INSPIRE].

[48] S. Frixione, P. Nason and G. Ridolfi, *A positive-weight next-to-leading-order Monte Carlo for heavy flavour hadroproduction*, *JHEP* **09** (2007) 126 [arXiv:0707.3088] [INSPIRE].

[49] P. Nason, *A new method for combining NLO QCD with shower Monte Carlo algorithms*, *JHEP* **11** (2004) 040 [hep-ph/0409146] [INSPIRE].

[50] S. Frixione, P. Nason and C. Oleari, *Matching NLO QCD computations with parton shower simulations: the POWHEG method*, *JHEP* **11** (2007) 070 [arXiv:0709.2092] [INSPIRE].

[51] S. Alioli, P. Nason, C. Oleari and E. Re, *A general framework for implementing NLO calculations in shower Monte Carlo programs: the POWHEG BOX*, *JHEP* **06** (2010) 043 [arXiv:1002.2581] [INSPIRE].

[52] ATLAS collaboration, *Studies on top-quark Monte Carlo modelling for Top2016*, ATL-PHYS-PUB-2016-020 (2016).

[53] T. Sjöstrand et al., *An introduction to PYTHIA 8.2*, *Comput. Phys. Commun.* **191** (2015) 159 [arXiv:1410.3012] [INSPIRE].

[54] ATLAS collaboration, *ATLAS PYTHIA 8 tunes to 7 TeV datas*, ATL-PHYS-PUB-2014-021 (2014).

[55] M. Beneke, P. Falgari, S. Klein and C. Schwinn, *Hadronic top-quark pair production with NNLL threshold resummation*, *Nucl. Phys. B* **855** (2012) 695 [arXiv:1109.1536] [INSPIRE].

[56] M. Cacciari, M. Czakon, M. Mangano, A. Mitov and P. Nason, *Top-pair production at hadron colliders with next-to-next-to-leading logarithmic soft-gluon resummation*, *Phys. Lett. B* **710** (2012) 612 [arXiv:1111.5869] [INSPIRE].

[57] P. Bärnreuther, M. Czakon and A. Mitov, *Percent level precision physics at the Tevatron: first genuine NNLO QCD corrections to $q\bar{q} \to t\bar{t} + X$*, *Phys. Rev. Lett.* **109** (2012) 132001 [arXiv:1204.5201] [INSPIRE].

[58] M. Czakon and A. Mitov, *NNLO corrections to top-pair production at hadron colliders: the all-fermionic scattering channels*, *JHEP* **12** (2012) 054 [arXiv:1207.0236] [INSPIRE].

[59] M. Czakon and A. Mitov, *NNLO corrections to top pair production at hadron colliders: the quark-gluon reaction*, *JHEP* **01** (2013) 080 [arXiv:1210.6832] [INSPIRE].

JHEP07(2020)044

[60] M. Czakon, P. Fiedler and A. Mitov, *Total top-quark pair-production cross section at hadron colliders through $O(\alpha_S^4)$*, *Phys. Rev. Lett.* **110** (2013) 252004 [arXiv:1303.6254] [INSPIRE].

[61] M. Czakon and A. Mitov, *Top++: a program for the calculation of the top-pair cross-section at hadron colliders*, *Comput. Phys. Commun.* **185** (2014) 2930 [arXiv:1112.5675] [INSPIRE].

[62] J. Alwall et al., *The automated computation of tree-level and next-to-leading order differential cross sections and their matching to parton shower simulations*, *JHEP* **07** (2014) 079 [arXiv:1405.0301] [INSPIRE].

[63] M. Bahr et al., *HERWIG++ physics and manual*, *Eur. Phys. J. C* **58** (2008) 639 [arXiv:0803.0883] [INSPIRE].

[64] J. Bellm et al., *HERWIG 7.0/HERWIG++ 3.0 release note*, *Eur. Phys. J. C* **76** (2016) 196 [arXiv:1512.01178] [INSPIRE].

[65] H.-L. Lai et al., *New parton distributions for collider physics*, *Phys. Rev. D* **82** (2010) 074024 [arXiv:1007.2241] [INSPIRE].

[66] M. Aliev et al., *HATHOR: HAdronic Top and Heavy quarks crOss section calculatoR*, *Comput. Phys. Commun.* **182** (2011) 1034 [arXiv:1007.1327] [INSPIRE].

[67] P. Kant et al., *HatHor for single top-quark production: Updated predictions and uncertainty estimates for single top-quark production in hadronic collisions*, *Comput. Phys. Commun.* **191** (2015) 74 [arXiv:1406.4403] [INSPIRE].

[68] N. Kidonakis, *Two-loop soft anomalous dimensions for single top quark associated production with a W- or H-*, *Phys. Rev. D* **82** (2010) 054018 [arXiv:1005.4451] [INSPIRE].

[69] T. Gleisberg et al., *Event generation with SHERPA 1.1*, *JHEP* **02** (2009) 007 [arXiv:0811.4622] [INSPIRE].

[70] G. Cullen et al., *Automated one-loop calculations with GoSam*, *Eur. Phys. J. C* **72** (2012) 1889 [arXiv:1111.2034] [INSPIRE].

[71] K. Hamilton, P. Nason and G. Zanderighi, *MINLO: Multi-scale Improved NLO*, *JHEP* **10** (2012) 155 [arXiv:1206.3572] [INSPIRE].

[72] G. Luisoni, P. Nason, C. Oleari and F. Tramontano, *$HW^{\pm}/HZ + 0$ and 1 jet at NLO with the POWHEG BOX interfaced to GoSam and their merging within MiNLO*, *JHEP* **10** (2013) 083 [arXiv:1306.2542] [INSPIRE].

[73] O. Brein, A. Djouadi and R. Harlander, *NNLO QCD corrections to the Higgs-strahlung processes at hadron colliders*, *Phys. Lett. B* **579** (2004) 149 [hep-ph/0307206] [INSPIRE].

[74] A. Denner, S. Dittmaier, S. Kallweit and A. Mück, *Electroweak corrections to Higgs-strahlung off W/Z bosons at the Tevatron and the LHC with HAWK*, *JHEP* **03** (2012) 075 [arXiv:1112.5142] [INSPIRE].

[75] L. Altenkamp et al., *Gluon-induced Higgs-strahlung at next-to-leading order QCD*, *JHEP* **02** (2013) 078 [arXiv:1211.5015] [INSPIRE].

[76] ATLAS collaboration, *The ATLAS simulation infrastructure*, *Eur. Phys. J. C* **70** (2010) 823 [arXiv:1005.4568] [INSPIRE].

[77] GEANT4 collaboration, *GEANT4 — a simulation toolkit*, *Nucl. Instrum. Meth. A* **506** (2003) 250 [INSPIRE].

JHEP07(2020)044

[78] ATLAS collaboration, *Summary of ATLAS Pythia 8 tunes*, ATLAS-PHYS-PUB-2012-003 (2012).

[79] A.D. Martin, W.J. Stirling, R.S. Thorne and G. Watt, *Parton distributions for the LHC*, *Eur. Phys. J. C* **63** (2009) 189 [arXiv:0901.0002] [INSPIRE].

[80] https://sherpa.hepforge.org/doc/SHERPA-MC-2.2.6.html

[81] S. Höche, J. Krause and F. Siegert, *Multijet merging in a variable flavor number scheme*, *Phys. Rev. D* **100** (2019) 014011 [arXiv:1904.09382] [INSPIRE].

[82] ATLAS collaboration, *Monte Carlo generators for the production of a W or Z/γ^* boson in association with jets at ATLAS in Run 2*, ATL-PHYS-PUB-2016-003 (2016).

[83] R. Frederix and S. Frixione, *Merging meets matching in MC@NLO*, *JHEP* **12** (2012) 061 [arXiv:1209.6215] [INSPIRE].

[84] J. Butterworth et al., *PDF4LHC recommendations for LHC Run II*, *J. Phys. G* **43** (2016) 023001 [arXiv:1510.03865] [INSPIRE].

[85] ATLAS collaboration, *Electron reconstruction and identification in the ATLAS experiment using the 2015 and 2016 LHC proton-proton collision data at $\sqrt{s} = 13$ TeV*, *Eur. Phys. J. C* **79** (2019) 639 [arXiv:1902.04655] [INSPIRE].

[86] ATLAS collaboration, *Muon reconstruction performance of the ATLAS detector in proton–proton collision data at $\sqrt{s} = 13$ TeV*, *Eur. Phys. J. C* **76** (2016) 292 [arXiv:1603.05598] [INSPIRE].

[87] M. Cacciari, G.P. Salam and G. Soyez, *The anti-k_t jet clustering algorithm*, *JHEP* **04** (2008) 063 [arXiv:0802.1189] [INSPIRE].

[88] M. Cacciari, G.P. Salam and G. Soyez, *FastJet user manual*, *Eur. Phys. J. C* **72** (2012) 1896 [arXiv:1111.6097] [INSPIRE].

[89] ATLAS collaboration, *Topological cell clustering in the ATLAS calorimeters and its performance in LHC Run 1*, *Eur. Phys. J. C* **77** (2017) 490 [arXiv:1603.02934] [INSPIRE].

[90] ATLAS collaboration, *Jet energy scale measurements and their systematic uncertainties in proton-proton collisions at $\sqrt{s} = 13$ TeV with the ATLAS detector*, *Phys. Rev. D* **96** (2017) 072002 [arXiv:1703.09665] [INSPIRE].

[91] ATLAS collaboration, *Selection of jets produced in 13TeV proton-proton collisions with the ATLAS detector*, ATLAS-CONF-2015-029 (2015).

[92] ATLAS collaboration, *Performance of pile-up mitigation techniques for jets in pp collisions at $\sqrt{s} = 8$ TeV using the ATLAS detector*, *Eur. Phys. J. C* **76** (2016) 581 [arXiv:1510.03823] [INSPIRE].

[93] ATLAS collaboration, *Performance of b-jet identification in the ATLAS experiment*, 2016 *JINST* **11** P04008 [arXiv:1512.01094] [INSPIRE].

[94] ATLAS collaboration, *Optimisation of the ATLAS b-tagging performance for the 2016 LHC Run*, ATL-PHYS-PUB-2016-012 (2016).

[95] ATLAS collaboration, *Performance of missing transverse momentum reconstruction with the ATLAS detector using proton-proton collisions at $\sqrt{s} = 13$ TeV*, *Eur. Phys. J. C* **78** (2018) 903 [arXiv:1802.08168] [INSPIRE].

JHEP07(2020)044

[96] ATLAS collaboration, *Jet energy resolution in proton-proton collisions at $\sqrt{s} = 7$ TeV recorded in 2010 with the ATLAS detector*, *Eur. Phys. J. C* **73** (2013) 2306 [arXiv:1210.6210] [INSPIRE].

[97] ATLAS collaboration, *Identification and rejection of pile-up jets at high pseudorapidity with the ATLAS detector*, *Eur. Phys. J. C* **77** (2017) 580 [*Erratum ibid.* **77** (2017) 712] [arXiv:1705.02211] [INSPIRE].

[98] ATLAS collaboration, *Measurements of b-jet tagging efficiency with the ATLAS detector using $t\bar{t}$ events at $\sqrt{s} = 13$ TeV*, *JHEP* **08** (2018) 089 [arXiv:1805.01845] [INSPIRE].

[99] ATLAS collaboration, *Measurement of b-tagging efficiency of c-jets in $t\bar{t}$ events using a likelihood approach with the ATLAS detector*, ATLAS-CONF-2018-001 (2018).

[100] ATLAS collaboration, *Calibration of light-flavour b-jet mistagging rates using ATLAS proton-proton collision data at $\sqrt{s} = 13$ TeV*, ATLAS-CONF-2018-006 (2018).

[101] ATLAS collaboration, *Measurement of the inelastic proton-proton cross section at $\sqrt{s} = 13$ TeV with the ATLAS detector at the LHC*, *Phys. Rev. Lett.* **117** (2016) 182002 [arXiv:1606.02625] [INSPIRE].

[102] ATLAS collaboration, *Evidence for the $H \to b\bar{b}$ decay with the ATLAS detector*, *JHEP* **12** (2017) 024 [arXiv:1708.03299] [INSPIRE].

[103] G. D'Agostini, *A multidimensional unfolding method based on Bayes' theorem*, *Nucl. Instrum. Meth. A* **362** (1995) 487 [INSPIRE].

[104] ATLAS collaboration, *ATLAS computing acknowledgements*, ATL-GEN-PUB-2016-002 (2016).

JHEP07(2020)044

The ATLAS collaboration

G. Aad[102], B. Abbott[128], D.C. Abbott[103], A. Abed Abud[36], K. Abeling[53], D.K. Abhayasinghe[94], S.H. Abidi[166], O.S. AbouZeid[40], N.L. Abraham[155], H. Abramowicz[160], H. Abreu[159], Y. Abulaiti[6], B.S. Acharya[67a,67b,n], B. Achkar[53], L. Adam[100], C. Adam Bourdarios[5], L. Adamczyk[84a], L. Adamek[166], J. Adelman[121], M. Adersberger[114], A. Adiguzel[12c], S. Adorni[54], T. Adye[143], A.A. Affolder[145], Y. Afik[159], C. Agapopoulou[65], M.N. Agaras[38], A. Aggarwal[119], C. Agheorghiesei[27c], J.A. Aguilar-Saavedra[139f,139a,ae], A. Ahmad[36], F. Ahmadov[80], W.S. Ahmed[104], X. Ai[18], G. Aielli[74a,74b], S. Akatsuka[86], T.P.A. Åkesson[97], E. Akilli[54], A.V. Akimov[111], K. Al Khoury[65], G.L. Alberghi[23b,23a], J. Albert[175], M.J. Alconada Verzini[160], S. Alderweireldt[36], M. Aleksa[36], I.N. Aleksandrov[80], C. Alexa[27b], T. Alexopoulos[10], A. Alfonsi[120], F. Alfonsi[23b,23a], M. Alhroob[128], B. Ali[141], S. Ali[157], M. Aliev[165], G. Alimonti[69a], C. Allaire[36], B.M.M. Allbrooke[155], B.W. Allen[131], P.P. Allport[21], A. Aloisio[70a,70b], F. Alonso[89], C. Alpigiani[147], A.A. Alshehri[57], E. Alunno Camelia[74a,74b], M. Alvarez Estevez[99], M.G. Alviggi[70a,70b], Y. Amaral Coutinho[81b], A. Ambler[104], L. Ambroz[134], C. Amelung[26], D. Amidei[106], S.P. Amor Dos Santos[139a], S. Amoroso[46], C.S. Amrouche[54], F. An[79], C. Anastopoulos[148], N. Andari[144], T. Andeen[11], C.F. Anders[61b], J.K. Anders[20], S.Y. Andrean[45a,45b], A. Andreazza[69a,69b], V. Andrei[61a], C.R. Anelli[175], S. Angelidakis[38], A. Angerami[39], A.V. Anisenkov[122b,122a], A. Annovi[72a], C. Antel[54], M.T. Anthony[148], E. Antipov[129], M. Antonelli[51], D.J.A. Antrim[170], F. Anulli[73a], M. Aoki[82], J.A. Aparisi Pozo[173], M.A. Aparo[155], L. Aperio Bella[15a], V. Araujo Ferraz[81b], R. Araujo Pereira[81b], C. Arcangeletti[51], A.T.H. Arce[49], F.A. Arduh[89], J-F. Arguin[110], S. Argyropoulos[52], J.-H. Arling[46], A.J. Armbruster[36], A. Armstrong[170], O. Arnaez[166], H. Arnold[120], Z.P. Arrubarrena Tame[114], G. Artoni[134], S. Artz[100], S. Asai[162], T. Asawatavonvanich[164], N. Asbah[59], E.M. Asimakopoulou[171], L. Asquith[155], J. Assahsah[35d], K. Assamagan[29], R. Astalos[28a], R.J. Atkin[33a], M. Atkinson[172], N.B. Atlay[19], H. Atmani[65], K. Augsten[141], G. Avolio[36], M.K. Ayoub[15a], G. Azuelos[110,am], H. Bachacou[144], K. Bachas[161], M. Backes[134], F. Backman[45a,45b], P. Bagnaia[73a,73b], M. Bahmani[85], H. Bahrasemani[151], A.J. Bailey[173], V.R. Bailey[172], J.T. Baines[143], C. Bakalis[10], O.K. Baker[182], P.J. Bakker[120], D. Bakshi Gupta[8], S. Balaji[156], E.M. Baldin[122b,122a], P. Balek[179], F. Balli[144], W.K. Balunas[134], J. Balz[100], E. Banas[85], M. Bandieramonte[138], A. Bandyopadhyay[24], Sw. Banerjee[180,i], L. Barak[160], W.M. Barbe[38], E.L. Barberio[105], D. Barberis[55b,55a], M. Barbero[102], G. Barbour[95], T. Barillari[115], M-S. Barisits[36], J. Barkeloo[131], T. Barklow[152], R. Barnea[159], B.M. Barnett[143], R.M. Barnett[18], Z. Barnovska-Blenessy[60a], A. Baroncelli[60a], G. Barone[29], A.J. Barr[134], L. Barranco Navarro[45a,45b], F. Barreiro[99], J. Barreiro Guimarães da Costa[15a], U. Barron[160], S. Barsov[137], F. Bartels[61a], R. Bartoldus[152], G. Bartolini[102], A.E. Barton[90], P. Bartos[28a], A. Basalaev[46], A. Basan[100], A. Bassalat[65,aj], M.J. Basso[166], R.L. Bates[57], S. Batlamous[35e], J.R. Batley[32], B. Batool[150], M. Battaglia[145], M. Bauce[73a,73b], F. Bauer[144], K.T. Bauer[170], H.S. Bawa[31], J.B. Beacham[49], T. Beau[135], P.H. Beauchemin[169], F. Becherer[52], P. Bechtle[24], H.C. Beck[53], H.P. Beck[20,q], K. Becker[177], C. Becot[46], A. Beddall[12d], A.J. Beddall[12a], V.A. Bednyakov[80], M. Bedognetti[120], C.P. Bee[154], T.A. Beermann[181], M. Begalli[81b], M. Begel[29], A. Behera[154], J.K. Behr[46], F. Beisiegel[24], M. Belfkir[5], A.S. Bell[95], G. Bella[160], L. Bellagamba[23b], A. Bellerive[34], P. Bellos[9], K. Beloborodov[122b,122a], K. Belotskiy[112], N.L. Belyaev[112], D. Benchekroun[35a], N. Benekos[10], Y. Benhammou[160], D.P. Benjamin[6], M. Benoit[54], J.R. Bensinger[26], S. Bentvelsen[120], L. Beresford[134], M. Beretta[51], D. Berge[19], E. Bergeaas Kuutmann[171], N. Berger[5], B. Bergmann[141], L.J. Bergsten[26], J. Beringer[18], S. Berlendis[7], G. Bernardi[135], C. Bernius[152], F.U. Bernlochner[24], T. Berry[94], P. Berta[100], C. Bertella[15a], A. Berthold[48], I.A. Bertram[90], O. Bessidskaia Bylund[181], N. Besson[144],

JHEP07(2020)044

A. Bethani[101], S. Bethke[115], A. Betti[42], A.J. Bevan[93], J. Beyer[115], D.S. Bhattacharya[176], P. Bhattarai[26], R. Bi[138], R.M. Bianchi[138], O. Biebel[114], D. Biedermann[19], R. Bielski[36], K. Bierwagen[100], N.V. Biesuz[72a,72b], M. Biglietti[75a], T.R.V. Billoud[110], M. Bindi[53], A. Bingul[12d], C. Bini[73a,73b], S. Biondi[23b,23a], M. Birman[179], T. Bisanz[53], J.P. Biswal[3], D. Biswas[180,i], A. Bitadze[101], C. Bittrich[48], K. Bjørke[133], T. Blazek[28a], I. Bloch[46], C. Blocker[26], A. Blue[57], U. Blumenschein[93], G.J. Bobbink[120], V.S. Bobrovnikov[122b,122a], S.S. Bocchetta[97], A. Bocci[49], D. Boerner[46], D. Bogavac[14], A.G. Bogdanchikov[122b,122a], C. Bohm[45a], V. Boisvert[94], P. Bokan[53,171], T. Bold[84a], A.E. Bolz[61b], M. Bomben[135], M. Bona[93], J.S. Bonilla[131], M. Boonekamp[144], C.D. Booth[94], H.M. Borecka-Bielska[91], L.S. Borgna[95], A. Borisov[123], G. Borissov[90], J. Bortfeldt[36], D. Bortoletto[134], D. Boscherini[23b], M. Bosman[14], J.D. Bossio Sola[104], K. Bouaouda[35a], J. Boudreau[138], E.V. Bouhova-Thacker[90], D. Boumediene[38], S.K. Boutle[57], A. Boveia[127], J. Boyd[36], D. Boye[33c], I.R. Boyko[80], A.J. Bozson[94], J. Bracinik[21], N. Brahimi[102], G. Brandt[181], O. Brandt[32], F. Braren[46], B. Brau[103], J.E. Brau[131], W.D. Breaden Madden[57], K. Brendlinger[46], L. Brenner[46], R. Brenner[171], S. Bressler[179], B. Brickwedde[100], D.L. Briglin[21], D. Britton[57], D. Britzger[115], I. Brock[24], R. Brock[107], G. Brooijmans[39], W.K. Brooks[146d], E. Brost[29], P.A. Bruckman de Renstrom[85], D. Bruncko[28b], A. Bruni[23b], G. Bruni[23b], L.S. Bruni[120], S. Bruno[74a,74b], M. Bruschi[23b], N. Bruscino[73a,73b], L. Bryngemark[97], T. Buanes[17], Q. Buat[36], P. Buchholz[150], A.G. Buckley[57], I.A. Budagov[80], M.K. Bugge[133], F. Bührer[52], O. Bulekov[112], B.A. Bullard[59], T.J. Burch[121], S. Burdin[91], C.D. Burgard[120], A.M. Burger[129], B. Burghgrave[8], J.T.P. Burr[46], C.D. Burton[11], J.C. Burzynski[103], V. Büscher[100], E. Buschmann[53], P.J. Bussey[57], J.M. Butler[25], C.M. Buttar[57], J.M. Butterworth[95], P. Butti[36], W. Buttinger[36], C.J. Buxo Vazquez[107], A. Buzatu[157], A.R. Buzykaev[122b,122a], G. Cabras[23b,23a], S. Cabrera Urbán[173], D. Caforio[56], H. Cai[172], V.M.M. Cairo[152], O. Cakir[4a], N. Calace[36], P. Calafiura[18], G. Calderini[135], P. Calfayan[66], G. Callea[57], L.P. Caloba[81b], A. Caltabiano[74a,74b], S. Calvente Lopez[99], D. Calvet[38], S. Calvet[38], T.P. Calvet[154], M. Calvetti[72a,72b], R. Camacho Toro[135], S. Camarda[36], D. Camarero Munoz[99], P. Camarri[74a,74b], M.T. Camerlingo[75a,75b], D. Cameron[133], C. Camincher[36], S. Campana[36], M. Campanelli[95], A. Camplani[40], A. Campoverde[150], V. Canale[70a,70b], A. Canesse[104], M. Cano Bret[78], J. Cantero[129], T. Cao[160], Y. Cao[172], M.D.M. Capeans Garrido[36], M. Capua[41b,41a], R. Cardarelli[74a], F. Cardillo[148], G. Carducci[41b,41a], I. Carli[142], T. Carli[36], G. Carlino[70a], B.T. Carlson[138], E.M. Carlson[175,167a], L. Carminati[69a,69b], R.M.D. Carney[152], S. Caron[119], E. Carquin[146d], S. Carrá[46], J.W.S. Carter[166], T.M. Carter[50], M.P. Casado[14,e], A.F. Casha[166], F.L. Castillo[173], L. Castillo Garcia[14], V. Castillo Gimenez[173], N.F. Castro[139a,139e], A. Catinaccio[36], J.R. Catmore[133], A. Cattai[36], V. Cavaliere[29], E. Cavallaro[14], V. Cavasinni[72a,72b], E. Celebi[12b], F. Celli[134], L. Cerda Alberich[173], K. Cerny[130], A.S. Cerqueira[81a], A. Cerri[155], L. Cerrito[74a,74b], F. Cerutti[18], A. Cervelli[23b,23a], S.A. Cetin[12b], Z. Chadi[35a], D. Chakraborty[121], J. Chan[180], W.S. Chan[120], W.Y. Chan[91], J.D. Chapman[32], B. Chargeishvili[158b], D.G. Charlton[21], T.P. Charman[93], C.C. Chau[34], S. Che[127], S. Chekanov[6], S.V. Chekulaev[167a], G.A. Chelkov[80,ah], B. Chen[79], C. Chen[60a], C.H. Chen[79], H. Chen[29], J. Chen[60a], J. Chen[39], J. Chen[26], S. Chen[136], S.J. Chen[15c], X. Chen[15b], Y. Chen[60a], Y-H. Chen[46], H.C. Cheng[63a], H.J. Cheng[15a], A. Cheplakov[80], E. Cheremushkina[123], R. Cherkaoui El Moursli[35e], E. Cheu[7], K. Cheung[64], T.J.A. Chevalérias[144], L. Chevalier[144], V. Chiarella[51], G. Chiarelli[72a], G. Chiodini[68a], A.S. Chisholm[21], A. Chitan[27b], I. Chiu[162], Y.H. Chiu[175], M.V. Chizhov[80], K. Choi[11], A.R. Chomont[73a,73b], S. Chouridou[161], Y.S. Chow[120], L.D. Christopher[33e], M.C. Chu[63a], X. Chu[15a,15d], J. Chudoba[140], J.J. Chwastowski[85], L. Chytka[130], D. Cieri[115], K.M. Ciesla[85], D. Cinca[47], V. Cindro[92], I.A. Cioară[27b], A. Ciocio[18], F. Cirotto[70a,70b], Z.H. Citron[179,j], M. Citterio[69a], D.A. Ciubotaru[27b], B.M. Ciungu[166], A. Clark[54], M.R. Clark[39], P.J. Clark[50], S.E. Clawson[101], C. Clement[45a,45b], Y. Coadou[102], M. Cobal[67a,67c], A. Coccaro[55b], J. Cochran[79],

JHEP07(2020)044

R. Coelho Lopes De Sa[103], H. Cohen[160], A.E.C. Coimbra[36], B. Cole[39], A.P. Colijn[120], J. Collot[58], P. Conde Muiño[139a,139h], S.H. Connell[33c], I.A. Connelly[57], S. Constantinescu[27b], F. Conventi[70a,an], A.M. Cooper-Sarkar[134], F. Cormier[174], K.J.R. Cormier[166], L.D. Corpe[95], M. Corradi[73a,73b], E.E. Corrigan[97], F. Corriveau[104,ac], M.J. Costa[173], F. Costanza[5], D. Costanzo[148], G. Cowan[94], J.W. Cowley[32], J. Crane[101], K. Cranmer[125], S.J. Crawley[57], R.A. Creager[136], S. Crépé-Renaudin[58], F. Crescioli[135], M. Cristinziani[24], V. Croft[169], G. Crosetti[41b,41a], A. Cueto[5], T. Cuhadar Donszelmann[170], A.R. Cukierman[152], W.R. Cunningham[57], S. Czekierda[85], P. Czodrowski[36], M.M. Czurylo[61b], M.J. Da Cunha Sargedas De Sousa[60b], J.V. Da Fonseca Pinto[81b], C. Da Via[101], W. Dabrowski[84a], F. Dachs[36], T. Dado[28a], S. Dahbi[33e], T. Dai[106], C. Dallapiccola[103], M. Dam[40], G. D'amen[29], V. D'Amico[75a,75b], J. Damp[100], J.R. Dandoy[136], M.F. Daneri[30], N.S. Dann[101], M. Danninger[151], V. Dao[36], G. Darbo[55b], O. Dartsi[5], A. Dattagupta[131], T. Daubney[46], S. D'Auria[69a,69b], C. David[167b], T. Davidek[142], D.R. Davis[49], I. Dawson[148], K. De[8], R. De Asmundis[70a], M. De Beurs[120], S. De Castro[23b,23a], S. De Cecco[73a,73b], N. De Groot[119], P. de Jong[120], H. De la Torre[107], A. De Maria[15c], D. De Pedis[73a], A. De Salvo[73a], U. De Sanctis[74a,74b], M. De Santis[74a,74b], A. De Santo[155], K. De Vasconcelos Corga[102], J.B. De Vivie De Regie[65], C. Debenedetti[145], D.V. Dedovich[80], A.M. Deiana[42], J. Del Peso[99], Y. Delabat Diaz[46], D. Delgove[65], F. Deliot[144,p], C.M. Delitzsch[7], M. Della Pietra[70a,70b], D. Della Volpe[54], A. Dell'Acqua[36], L. Dell'Asta[74a,74b], M. Delmastro[5], C. Delporte[65], P.A. Delsart[58], D.A. DeMarco[166], S. Demers[182], M. Demichev[80], G. Demontigny[110], S.P. Denisov[123], L. D'Eramo[121], D. Derendarz[85], J.E. Derkaoui[35d], F. Derue[135], P. Dervan[91], K. Desch[24], C. Deterre[46], K. Dette[166], C. Deutsch[24], M.R. Devesa[30], P.O. Deviveiros[36], F.A. Di Bello[73a,73b], A. Di Ciaccio[74a,74b], L. Di Ciaccio[5], W.K. Di Clemente[136], C. Di Donato[70a,70b], A. Di Girolamo[36], G. Di Gregorio[72a,72b], B. Di Micco[75a,75b], R. Di Nardo[75a,75b], K.F. Di Petrillo[59], R. Di Sipio[166], C. Diaconu[102], F.A. Dias[40], T. Dias Do Vale[139a], M.A. Diaz[146a], F.G. Diaz Capriles[24], J. Dickinson[18], E.B. Diehl[106], J. Dietrich[19], S. Díez Cornell[46], A. Dimitrievska[18], W. Ding[15b], J. Dingfelder[24], F. Dittus[36], F. Djama[102], T. Djobava[158b], J.I. Djuvsland[17], M.A.B. Do Vale[81c], M. Dobre[27b], D. Dodsworth[26], C. Doglioni[97], J. Dolejsi[142], Z. Dolezal[142], M. Donadelli[81d], B. Dong[60c], J. Donini[38], A. D'onofrio[15c], M. D'Onofrio[91], J. Dopke[143], A. Doria[70a], M.T. Dova[89], A.T. Doyle[57], E. Drechsler[151], E. Dreyer[151], T. Dreyer[53], A.S. Drobac[169], D. Du[60b], T.A. du Pree[120], Y. Duan[60b], F. Dubinin[111], M. Dubovsky[28a], A. Dubreuil[54], E. Duchovni[179], G. Duckeck[114], O.A. Ducu[110], D. Duda[115], A. Dudarev[36], A.C. Dudder[100], E.M. Duffield[18], L. Duflot[65], M. Dührssen[36], C. Dülsen[181], M. Dumancic[179], A.E. Dumitriu[27b], A.K. Duncan[57], M. Dunford[61a], A. Duperrin[102], H. Duran Yildiz[4a], M. Düren[56], A. Durglishvili[158b], D. Duschinger[48], B. Dutta[46], D. Duvnjak[1], G.I. Dyckes[136], M. Dyndal[36], S. Dysch[101], B.S. Dziedzic[85], K.M. Ecker[115], M.G. Eggleston[49], T. Eifert[8], G. Eigen[17], K. Einsweiler[18], T. Ekelof[171], H. El Jarrari[35e], R. El Kosseifi[102], V. Ellajosyula[171], M. Ellert[171], F. Ellinghaus[181], A.A. Elliot[93], N. Ellis[36], J. Elmsheuser[29], M. Elsing[36], D. Emeliyanov[143], A. Emerman[39], Y. Enari[162], M.B. Epland[49], J. Erdmann[47], A. Ereditato[20], P.A. Erland[85], M. Errenst[36], M. Escalier[65], C. Escobar[173], O. Estrada Pastor[173], E. Etzion[160], H. Evans[66], M.O. Evans[155], A. Ezhilov[137], F. Fabbri[57], L. Fabbri[23b,23a], V. Fabiani[119], G. Facini[177], R.M. Faisca Rodrigues Pereira[139a], R.M. Fakhrutdinov[123], S. Falciano[73a], P.J. Falke[24], S. Falke[36], J. Faltova[142], Y. Fang[15a], Y. Fang[15a], G. Fanourakis[44], M. Fanti[69a,69b], M. Faraj[67a,67c,r], A. Farbin[8], A. Farilla[75a], E.M. Farina[71a,71b], T. Farooque[107], S.M. Farrington[50], P. Farthouat[36], F. Fassi[35e], P. Fassnacht[36], D. Fassouliotis[9], M. Faucci Giannelli[50], W.J. Fawcett[32], L. Fayard[65], O.L. Fedin[137,o], W. Fedorko[174], A. Fehr[20], M. Feickert[172], L. Feligioni[102], A. Fell[148], C. Feng[60b], M. Feng[49], M.J. Fenton[170], A.B. Fenyuk[123], S.W. Ferguson[43], J. Ferrando[46], A. Ferrante[172], A. Ferrari[171], P. Ferrari[120], R. Ferrari[71a], D.E. Ferreira de Lima[61b], A. Ferrer[173], D. Ferrere[54],

JHEP07(2020)044

C. Ferretti[106], F. Fiedler[100], A. Filipčič[92], F. Filthaut[119], K.D. Finelli[25], M.C.N. Fiolhais[139a,139c,a], L. Fiorini[173], F. Fischer[114], W.C. Fisher[107], I. Fleck[150], P. Fleischmann[106], T. Flick[181], B.M. Flierl[114], L. Flores[136], L.R. Flores Castillo[63a], F.M. Follega[76a,76b], N. Fomin[17], J.H. Foo[166], G.T. Forcolin[76a,76b], A. Formica[144], F.A. Förster[14], A.C. Forti[101], E. Fortin[102], M.G. Foti[134], D. Fournier[65], H. Fox[90], P. Francavilla[72a,72b], S. Francescato[73a,73b], M. Franchini[23b,23a], S. Franchino[61a], D. Francis[36], L. Franco[5], L. Franconi[20], M. Franklin[59], A.N. Fray[93], P.M. Freeman[21], B. Freund[110], W.S. Freund[81b], E.M. Freundlich[47], D.C. Frizzell[128], D. Froidevaux[36], J.A. Frost[134], M. Fujimoto[126], C. Fukunaga[163], E. Fullana Torregrosa[173], T. Fusayasu[116], J. Fuster[173], A. Gabrielli[23b,23a], A. Gabrielli[18], S. Gadatsch[54], P. Gadow[115], G. Gagliardi[55b,55a], L.G. Gagnon[110], B. Galhardo[139a], G.E. Gallardo[134], E.J. Gallas[134], B.J. Gallop[143], G. Galster[40], R. Gamboa Goni[93], K.K. Gan[127], S. Ganguly[179], J. Gao[60a], Y. Gao[50], Y.S. Gao[31,l], C. García[173], J.E. García Navarro[173], J.A. García Pascual[15a], C. Garcia-Argos[52], M. Garcia-Sciveres[18], R.W. Gardner[37], N. Garelli[152], S. Gargiulo[52], C.A. Garner[166], V. Garonne[133], S.J. Gasiorowski[147], P. Gaspar[81b], A. Gaudiello[55b,55a], G. Gaudio[71a], I.L. Gavrilenko[111], A. Gavrilyuk[124], C. Gay[174], G. Gaycken[46], E.N. Gazis[10], A.A. Geanta[27b], C.M. Gee[145], C.N.P. Gee[143], J. Geisen[97], M. Geisen[100], C. Gemme[55b], M.H. Genest[58], C. Geng[106], S. Gentile[73a,73b], S. George[94], T. Geralis[44], L.O. Gerlach[53], P. Gessinger-Befurt[100], G. Gessner[47], S. Ghasemi[150], M. Ghasemi Bostanabad[175], M. Ghneimat[150], A. Ghosh[65], A. Ghosh[78], B. Giacobbe[23b], S. Giagu[73a,73b], N. Giangiacomi[23b,23a], P. Giannetti[72a], A. Giannini[70a,70b], G. Giannini[14], S.M. Gibson[94], M. Gignac[145], D. Gillberg[34], G. Gilles[181], D.M. Gingrich[3,am], M.P. Giordani[67a,67c], P.F. Giraud[144], G. Giugliarelli[67a,67c], D. Giugni[69a], F. Giuli[74a,74b], S. Gkaitatzis[161], I. Gkialas[9,g], E.L. Gkougkousis[14], P. Gkountoumis[10], L.K. Gladilin[113], C. Glasman[99], J. Glatzer[14], P.C.F. Glaysher[46], A. Glazov[46], G.R. Gledhill[131], I. Gnesi[41b], M. Goblirsch-Kolb[26], D. Godin[110], S. Goldfarb[105], T. Golling[54], D. Golubkov[123], A. Gomes[139a,139b], R. Goncalves Gama[53], R. Gonçalo[139a], G. Gonella[131], L. Gonella[21], A. Gongadze[80], F. Gonnella[21], J.L. Gonski[39], S. González de la Hoz[173], S. Gonzalez Fernandez[14], C. Gonzalez Renteria[18], R. Gonzalez Suarez[171], S. Gonzalez-Sevilla[54], G.R. Gonzalvo Rodriguez[173], L. Goossens[36], N.A. Gorasia[21], P.A. Gorbounov[124], H.A. Gordon[29], B. Gorini[36], E. Gorini[68a,68b], A. Gorišek[92], A.T. Goshaw[49], M.I. Gostkin[80], C.A. Gottardo[119], M. Gouighri[35b], A.G. Goussiou[147], N. Govender[33c], C. Goy[5], E. Gozani[159], I. Grabowska-Bold[84a], E.C. Graham[91], J. Gramling[170], E. Gramstad[133], S. Grancagnolo[19], M. Grandi[155], V. Gratchev[137], P.M. Gravila[27f], F.G. Gravili[68a,68b], C. Gray[57], H.M. Gray[18], C. Grefe[24], K. Gregersen[97], I.M. Gregor[46], P. Grenier[152], K. Grevtsov[46], C. Grieco[14], N.A. Grieser[128], A.A. Grillo[145], K. Grimm[31,k], S. Grinstein[14,x], J.-F. Grivaz[65], S. Groh[100], E. Gross[179], J. Grosse-Knetter[53], Z.J. Grout[95], C. Grud[106], A. Grummer[118], J.C. Grundy[134], L. Guan[106], W. Guan[180], C. Gubbels[174], J. Guenther[36], A. Guerguichon[65], J.G.R. Guerrero Rojas[173], F. Guescini[115], D. Guest[170], R. Gugel[52], T. Guillemin[5], S. Guindon[36], U. Gul[57], J. Guo[60c], W. Guo[106], Y. Guo[60a], Z. Guo[102], R. Gupta[46], S. Gurbuz[12c], G. Gustavino[128], M. Guth[52], P. Gutierrez[128], C. Gutschow[95], C. Guyot[144], C. Gwenlan[134], C.B. Gwilliam[91], A. Haas[125], C. Haber[18], H.K. Hadavand[8], A. Hadef[60a], M. Haleem[176], J. Haley[129], J.J. Hall[148], G. Halladjian[107], G.D. Hallewell[102], K. Hamacher[181], P. Hamal[130], K. Hamano[175], H. Hamdaoui[35e], M. Hamer[24], G.N. Hamity[50], K. Han[60a,w], L. Han[60a], S. Han[15a], Y.F. Han[166], K. Hanagaki[82,u], M. Hance[145], D.M. Handl[114], B. Haney[136], M.D. Hank[37], R. Hankache[135], E. Hansen[97], J.B. Hansen[40], J.D. Hansen[40], M.C. Hansen[24], P.H. Hansen[40], E.C. Hanson[101], K. Hara[168], T. Harenberg[181], S. Harkusha[108], P.F. Harrison[177], N.M. Hartman[152], N.M. Hartmann[114], Y. Hasegawa[149], A. Hasib[50], S. Hassani[144], S. Haug[20], R. Hauser[107], L.B. Havener[39], M. Havranek[141], C.M. Hawkes[21], R.J. Hawkings[36], S. Hayashida[117], D. Hayden[107], C. Hayes[106], R.L. Hayes[174], C.P. Hays[134], J.M. Hays[93], H.S. Hayward[91],

JHEP07(2020)044

S.J. Haywood[143], F. He[60a], M.P. Heath[50], V. Hedberg[97], S. Heer[24], A.L. Heggelund[133], K.K. Heidegger[52], W.D. Heidorn[79], J. Heilman[34], S. Heim[46], T. Heim[18], B. Heinemann[46,ak], J.J. Heinrich[131], L. Heinrich[36], J. Hejbal[140], L. Helary[61b], A. Held[125], S. Hellesund[133], C.M. Helling[145], S. Hellman[45a,45b], C. Helsens[36], R.C.W. Henderson[90], Y. Heng[180], L. Henkelmann[32], A.M. Henriques Correia[36], H. Herde[26], Y. Hernández Jiménez[33e], H. Herr[100], M.G. Herrmann[114], T. Herrmann[48], G. Herten[52], R. Hertenberger[114], L. Hervas[36], T.C. Herwig[136], G.G. Hesketh[95], N.P. Hessey[167a], H. Hibi[83], A. Higashida[162], S. Higashino[82], E. Higón-Rodriguez[173], K. Hildebrand[37], J.C. Hill[32], K.K. Hill[29], K.H. Hiller[46], S.J. Hillier[21], M. Hils[48], I. Hinchliffe[18], F. Hinterkeuser[24], M. Hirose[132], S. Hirose[52], D. Hirschbuehl[181], B. Hiti[92], O. Hladik[140], D.R. Hlaluku[33e], J. Hobbs[154], N. Hod[179], M.C. Hodgkinson[148], A. Hoecker[36], D. Hohn[52], D. Hohov[65], T. Holm[24], T.R. Holmes[37], M. Holzbock[114], L.B.A.H. Hommels[32], T.M. Hong[138], J.C. Honig[52], A. Hönle[115], B.H. Hooberman[172], W.H. Hopkins[6], Y. Horii[117], P. Horn[48], L.A. Horyn[37], S. Hou[157], A. Hoummada[35a], J. Howarth[57], J. Hoya[89], M. Hrabovsky[130], J. Hrdinka[77], I. Hristova[19], J. Hrivnac[65], A. Hrynevich[109], T. Hryn'ova[5], P.J. Hsu[64], S.-C. Hsu[147], Q. Hu[29], S. Hu[60c], Y.F. Hu[15a,15d], D.P. Huang[95], Y. Huang[60a], Y. Huang[15a], Z. Hubacek[141], F. Hubaut[102], M. Huebner[24], F. Huegging[24], T.B. Huffman[134], M. Huhtinen[36], R.F.H. Hunter[34], P. Huo[154], N. Huseynov[80,ad], J. Huston[107], J. Huth[59], R. Hyneman[106], S. Hyrych[28a], G. Iacobucci[54], G. Iakovidis[29], I. Ibragimov[150], L. Iconomidou-Fayard[65], P. Iengo[36], R. Ignazzi[40], O. Igonkina[120,z,*], R. Iguchi[162], T. Iizawa[54], Y. Ikegami[82], M. Ikeno[82], D. Iliadis[161], N. Ilic[119,166,ac], F. Iltzsche[48], H. Imam[35a], G. Introzzi[71a,71b], M. Iodice[75a], K. Iordanidou[167a], V. Ippolito[73a,73b], M.F. Isacson[171], M. Ishino[162], W. Islam[129], C. Issever[19,46], S. Istin[159], F. Ito[168], J.M. Iturbe Ponce[63a], R. Iuppa[76a,76b], A. Ivina[179], H. Iwasaki[82], J.M. Izen[43], V. Izzo[70a], P. Jacka[140], P. Jackson[1], R.M. Jacobs[46], B.P. Jaeger[151], V. Jain[2], G. Jäkel[181], K.B. Jakobi[100], K. Jakobs[52], T. Jakoubek[140], J. Jamieson[57], K.W. Janas[84a], R. Jansky[54], M. Janus[53], P.A. Janus[84a], G. Jarlskog[97], A.E. Jaspan[91], N. Javadov[80,ad], T. Javůrek[36], M. Javurkova[103], F. Jeanneau[144], L. Jeanty[131], J. Jejelava[158a], A. Jelinskas[177], P. Jenni[52,b], N. Jeong[46], S. Jézéquel[5], H. Ji[180], J. Jia[154], H. Jiang[79], Y. Jiang[60a], Z. Jiang[152], S. Jiggins[52], F.A. Jimenez Morales[38], J. Jimenez Pena[115], S. Jin[15c], A. Jinaru[27b], O. Jinnouchi[164], H. Jivan[33e], P. Johansson[148], K.A. Johns[7], C.A. Johnson[66], R.W.L. Jones[90], S.D. Jones[155], S. Jones[7], T.J. Jones[91], J. Jongmanns[61a], P.M. Jorge[139a], J. Jovicevic[36], X. Ju[18], J.J. Junggeburth[115], A. Juste Rozas[14,x], A. Kaczmarska[85], M. Kado[73a,73b], H. Kagan[127], M. Kagan[152], A. Kahn[39], C. Kahra[100], T. Kaji[178], E. Kajomovitz[159], C.W. Kalderon[29], A. Kaluza[100], A. Kamenshchikov[123], M. Kaneda[162], N.J. Kang[145], S. Kang[79], Y. Kano[117], J. Kanzaki[82], L.S. Kaplan[180], D. Kar[33e], K. Karava[134], M.J. Kareem[167b], I. Karkanias[161], S.N. Karpov[80], Z.M. Karpova[80], V. Kartvelishvili[90], A.N. Karyukhin[123], A. Kastanas[45a,45b], C. Kato[60d,60c], J. Katzy[46], K. Kawade[149], K. Kawagoe[88], T. Kawaguchi[117], T. Kawamoto[144], G. Kawamura[53], E.F. Kay[175], S. Kazakos[14], V.F. Kazanin[122b,122a], R. Keeler[175], R. Kehoe[42], J.S. Keller[34], E. Kellermann[97], D. Kelsey[155], J.J. Kempster[21], J. Kendrick[21], K.E. Kennedy[39], O. Kepka[140], S. Kersten[181], B.P. Kerševan[92], S. Ketabchi Haghighat[166], M. Khader[172], F. Khalil-Zada[13], M. Khandoga[144], A. Khanov[129], A.G. Kharlamov[122b,122a], T. Kharlamova[122b,122a], E.E. Khoda[174], A. Khodinov[165], T.J. Khoo[54], G. Khoriauli[176], E. Khramov[80], J. Khubua[158b], S. Kido[83], M. Kiehn[54], C.R. Kilby[94], E. Kim[164], Y.K. Kim[37], N. Kimura[95], O.M. Kind[19], B.T. King[91,*], D. Kirchmeier[48], J. Kirk[143], A.E. Kiryunin[115], T. Kishimoto[162], D.P. Kisliuk[166], V. Kitali[46], C. Kitsaki[10], O. Kivernyk[24], T. Klapdor-Kleingrothaus[52], M. Klassen[61a], C. Klein[34], M.H. Klein[106], M. Klein[91], U. Klein[91], K. Kleinknecht[100], P. Klimek[121], A. Klimentov[29], T. Klingl[24], T. Klioutchnikova[36], F.F. Klitzner[114], P. Kluit[120], S. Kluth[115], E. Kneringer[77], E.B.F.G. Knoops[102], A. Knue[52], D. Kobayashi[88], T. Kobayashi[162], M. Kobel[48], M. Kocian[152], T. Kodama[162], P. Kodys[142],

JHEP07(2020)044

D.M. Koeck[155], P.T. Koenig[24], T. Koffas[34], N.M. Köhler[36], M. Kolb[144], I. Koletsou[5], T. Komarek[130], T. Kondo[82], K. Köneke[52], A.X.Y. Kong[1], A.C. König[119], T. Kono[126], V. Konstantinides[95], N. Konstantinidis[95], B. Konya[97], R. Kopeliansky[66], S. Koperny[84a], K. Korcyl[85], K. Kordas[161], G. Koren[160], A. Korn[95], I. Korolkov[14], E.V. Korolkova[148], N. Korotkova[113], O. Kortner[115], S. Kortner[115], V.V. Kostyukhin[148,165], A. Kotsokechagia[65], A. Kotwal[49], A. Koulouris[10], A. Kourkoumeli-Charalampidi[71a,71b], C. Kourkoumelis[9], E. Kourlitis[148], V. Kouskoura[29], A.B. Kowalewska[85], R. Kowalewski[175], W. Kozanecki[101], A.S. Kozhin[123], V.A. Kramarenko[113], G. Kramberger[92], D. Krasnopevtsev[60a], M.W. Krasny[135], A. Krasznahorkay[36], D. Krauss[115], J.A. Kremer[100], J. Kretzschmar[91], P. Krieger[166], F. Krieter[114], A. Krishnan[61b], K. Krizka[18], K. Kroeninger[47], H. Kroha[115], J. Kroll[140], J. Kroll[136], K.S. Krowpman[107], U. Kruchonak[80], H. Krüger[24], N. Krumnack[79], M.C. Kruse[49], J.A. Krzysiak[85], T. Kubota[105], O. Kuchinskaia[165], S. Kuday[4b], J.T. Kuechler[46], S. Kuehn[36], A. Kugel[61a], T. Kuhl[46], V. Kukhtin[80], Y. Kulchitsky[108,af], S. Kuleshov[146b], Y.P. Kulinich[172], M. Kuna[58], T. Kunigo[86], A. Kupco[140], T. Kupfer[47], O. Kuprash[52], H. Kurashige[83], L.L. Kurchaninov[167a], Y.A. Kurochkin[108], A. Kurova[112], M.G. Kurth[15a,15d], E.S. Kuwertz[36], M. Kuze[164], A.K. Kvam[147], J. Kvita[130], T. Kwan[104], L. La Rotonda[41b,41a], F. La Ruffa[41b,41a], C. Lacasta[173], F. Lacava[73a,73b], D.P.J. Lack[101], H. Lacker[19], D. Lacour[135], E. Ladygin[80], R. Lafaye[5], B. Laforge[135], T. Lagouri[146b], S. Lai[53], I.K. Lakomiec[84a], S. Lammers[66], W. Lampl[7], C. Lampoudis[161], E. Lançon[29], U. Landgraf[52], M.P.J. Landon[93], M.C. Lanfermann[54], V.S. Lang[52], J.C. Lange[53], R.J. Langenberg[103], A.J. Lankford[170], F. Lanni[29], K. Lantzsch[24], A. Lanza[71a], A. Lapertosa[55b,55a], S. Laplace[135], J.F. Laporte[144], T. Lari[69a], F. Lasagni Manghi[23b,23a], M. Lassnig[36], T.S. Lau[63a], A. Laudrain[65], A. Laurier[34], M. Lavorgna[70a,70b], S.D. Lawlor[94], M. Lazzaroni[69a,69b], B. Le[101], E. Le Guirriec[102], A. Lebedev[79], M. LeBlanc[7], T. LeCompte[6], F. Ledroit-Guillon[58], A.C.A. Lee[95], C.A. Lee[29], G.R. Lee[17], L. Lee[59], S.C. Lee[157], S. Lee[79], B. Lefebvre[167a], H.P. Lefebvre[94], M. Lefebvre[175], C. Leggett[18], K. Lehmann[151], N. Lehmann[20], G. Lehmann Miotto[36], W.A. Leight[46], A. Leisos[161,v], M.A.L. Leite[81d], C.E. Leitgeb[114], R. Leitner[142], D. Lellouch[179,*], K.J.C. Leney[42], T. Lenz[24], R. Leone[7], S. Leone[72a], C. Leonidopoulos[50], A. Leopold[135], C. Leroy[110], R. Les[166], C.G. Lester[32], M. Levchenko[137], J. Levêque[5], D. Levin[106], L.J. Levinson[179], D.J. Lewis[21], B. Li[15b], B. Li[106], C-Q. Li[60a], F. Li[60c], H. Li[60a], H. Li[60b], J. Li[60c], K. Li[147], L. Li[60c], M. Li[15a,15d], Q. Li[15a,15d], Q.Y. Li[60a], S. Li[60d,60c], X. Li[46], Y. Li[46], Z. Li[60b], Z. Li[104], Z. Liang[15a], M. Liberatore[46], B. Liberti[74a], A. Liblong[166], K. Lie[63c], S. Lim[29], C.Y. Lin[32], K. Lin[107], T.H. Lin[100], R.A. Linck[66], R.E. Lindley[7], J.H. Lindon[21], A. Linss[46], A.L. Lionti[54], E. Lipeles[136], A. Lipniacka[17], T.M. Liss[172,al], A. Lister[174], J.D. Little[8], B. Liu[79], B.L. Liu[6], H.B. Liu[29], H. Liu[106], J.B. Liu[60a], J.K.K. Liu[37], K. Liu[60d], M. Liu[60a], P. Liu[15a], Y. Liu[46], Y. Liu[15a,15d], Y.L. Liu[106], Y.W. Liu[60a], M. Livan[71a,71b], A. Lleres[58], J. Llorente Merino[151], S.L. Lloyd[93], C.Y. Lo[63b], E.M. Lobodzinska[46], P. Loch[7], S. Loffredo[74a,74b], T. Lohse[19], K. Lohwasser[148], M. Lokajicek[140], J.D. Long[172], R.E. Long[90], L. Longo[36], K.A. Looper[127], I. Lopez Paz[101], A. Lopez Solis[148], J. Lorenz[114], N. Lorenzo Martinez[5], A.M. Lory[114], P.J. Lösel[114], A. Lösle[52], X. Lou[46], X. Lou[15a], A. Lounis[65], J. Love[6], P.A. Love[90], J.J. Lozano Bahilo[173], M. Lu[60a], Y.J. Lu[64], H.J. Lubatti[147], C. Luci[73a,73b], A. Lucotte[58], C. Luedtke[52], F. Luehring[66], I. Luise[135], L. Luminari[73a], B. Lund-Jensen[153], M.S. Lutz[160], D. Lynn[29], H. Lyons[91], R. Lysak[140], E. Lytken[97], F. Lyu[15a], V. Lyubushkin[80], T. Lyubushkina[80], H. Ma[29], L.L. Ma[60b], Y. Ma[95], G. Maccarrone[51], A. Macchiolo[115], C.M. Macdonald[148], J. Machado Miguens[136], D. Madaffari[173], R. Madar[38], W.F. Mader[48], M. Madugoda Ralalage Don[129], N. Madysa[48], J. Maeda[83], T. Maeno[29], M. Maerker[48], V. Magerl[52], N. Magini[79], J. Magro[67a,67c,r], D.J. Mahon[39], C. Maidantchik[81b], T. Maier[114], A. Maio[139a,139b,139d], K. Maj[84a], O. Majersky[28a], S. Majewski[131], Y. Makida[82], N. Makovec[65], B. Malaescu[135], Pa. Malecki[85], V.P. Maleev[137], F. Malek[58], U. Mallik[78], D. Malon[6], C. Malone[32],

JHEP07(2020)044

S. Maltezos[10], S. Malyukov[80], J. Mamuzic[173], G. Mancini[51], I. Mandić[92], L. Manhaes de Andrade Filho[81a], I.M. Maniatis[161], J. Manjarres Ramos[48], K.H. Mankinen[97], A. Mann[114], A. Manousos[77], B. Mansoulie[144], I. Manthos[161], S. Manzoni[120], A. Marantis[161], G. Marceca[30], L. Marchese[134], G. Marchiori[135], M. Marcisovsky[140], L. Marcoccia[74a,74b], C. Marcon[97], C.A. Marin Tobon[36], M. Marjanovic[128], Z. Marshall[18], M.U.F. Martensson[171], S. Marti-Garcia[173], C.B. Martin[127], T.A. Martin[177], V.J. Martin[50], B. Martin dit Latour[17], L. Martinelli[75a,75b], M. Martinez[14,x], P. Martinez Agullo[173], V.I. Martinez Outschoorn[103], S. Martin-Haugh[143], V.S. Martoiu[27b], A.C. Martyniuk[95], A. Marzin[36], S.R. Maschek[115], L. Masetti[100], T. Mashimo[162], R. Mashinistov[111], J. Masik[101], A.L. Maslennikov[122b,122a], L. Massa[23b,23a], P. Massarotti[70a,70b], P. Mastrandrea[72a,72b], A. Mastroberardino[41b,41a], T. Masubuchi[162], D. Matakias[29], A. Matic[114], N. Matsuzawa[162], P. Mättig[24], J. Maurer[27b], B. Maček[92], D.A. Maximov[122b,122a], R. Mazini[157], I. Maznas[161], S.M. Mazza[145], J.P. Mc Gowan[104], S.P. Mc Kee[106], T.G. McCarthy[115], W.P. McCormack[18], E.F. McDonald[105], J.A. Mcfayden[36], G. Mchedlidze[158b], M.A. McKay[42], K.D. McLean[175], S.J. McMahon[143], P.C. McNamara[105], C.J. McNicol[177], R.A. McPherson[175,ac], J.E. Mdhluli[33e], Z.A. Meadows[103], S. Meehan[36], T. Megy[38], S. Mehlhase[114], A. Mehta[91], B. Meirose[43], D. Melini[159], B.R. Mellado Garcia[33e], J.D. Mellenthin[53], M. Melo[28a], F. Meloni[46], A. Melzer[24], S.B. Menary[101], E.D. Mendes Gouveia[139a,139e], L. Meng[36], X.T. Meng[106], S. Menke[115], E. Meoni[41b,41a], S. Mergelmeyer[19], S.A.M. Merkt[138], C. Merlassino[134], P. Mermod[54], L. Merola[70a,70b], C. Meroni[69a], G. Merz[106], O. Meshkov[113,111], J.K.R. Meshreki[150], A. Messina[73a,73b], J. Metcalfe[6], A.S. Mete[6], C. Meyer[66], J-P. Meyer[144], H. Meyer Zu Theenhausen[61a], F. Miano[155], M. Michetti[19], R.P. Middleton[143], L. Mijović[50], G. Mikenberg[179], M. Mikestikova[140], M. Mikuž[92], H. Mildner[148], M. Milesi[105], A. Milic[166], C.D. Milke[42], D.W. Miller[37], A. Milov[179], D.A. Milstead[45a,45b], R.A. Mina[152], A.A. Minaenko[123], M. Miñano Moya[173], I.A. Minashvili[158b], A.I. Mincer[125], B. Mindur[84a], M. Mineev[80], Y. Minegishi[162], L.M. Mir[14], M. Mironova[134], A. Mirto[68a,68b], K.P. Mistry[136], T. Mitani[178], J. Mitrevski[114], V.A. Mitsou[173], M. Mittal[60c], O. Miu[166], A. Miucci[20], P.S. Miyagawa[148], A. Mizukami[82], J.U. Mjörnmark[97], T. Mkrtchyan[61a], M. Mlynarikova[142], T. Moa[45a,45b], S. Mobius[53], K. Mochizuki[110], P. Mogg[114], S. Mohapatra[39], R. Moles-Valls[24], M.C. Mondragon[107], K. Mönig[46], E. Monnier[102], A. Montalbano[151], J. Montejo Berlingen[36], M. Montella[95], F. Monticelli[89], S. Monzani[69a], N. Morange[65], D. Moreno[22a], M. Moreno Llácer[173], C. Moreno Martinez[14], P. Morettini[55b], M. Morgenstern[159], S. Morgenstern[48], D. Mori[151], M. Morii[59], M. Morinaga[178], V. Morisbak[133], A.K. Morley[36], G. Mornacchi[36], A.P. Morris[95], L. Morvaj[154], P. Moschovakos[36], B. Moser[120], M. Mosidze[158b], T. Moskalets[144], H.J. Moss[148], J. Moss[31,m], E.J.W. Moyse[103], S. Muanza[102], J. Mueller[138], R.S.P. Mueller[114], D. Muenstermann[90], G.A. Mullier[97], D.P. Mungo[69a,69b], J.L. Munoz Martinez[14], F.J. Munoz Sanchez[101], P. Murin[28b], W.J. Murray[177,143], A. Murrone[69a,69b], M. Muškinja[18], C. Mwewa[33a], A.G. Myagkov[123,ah], A.A. Myers[138], J. Myers[131], M. Myska[141], B.P. Nachman[18], O. Nackenhorst[47], A.Nag Nag[48], K. Nagai[134], K. Nagano[82], Y. Nagasaka[62], J.L. Nagle[29], E. Nagy[102], A.M. Nairz[36], Y. Nakahama[117], K. Nakamura[82], T. Nakamura[162], H. Nanjo[132], F. Napolitano[61a], R.F. Naranjo Garcia[46], R. Narayan[42], I. Naryshkin[137], T. Naumann[46], G. Navarro[22a], P.Y. Nechaeva[111], F. Nechansky[46], T.J. Neep[21], A. Negri[71a,71b], M. Negrini[23b], C. Nellist[119], M.E. Nelson[45a,45b], S. Nemecek[140], M. Nessi[36,d], M.S. Neubauer[172], F. Neuhaus[100], M. Neumann[181], R. Newhouse[174], P.R. Newman[21], C.W. Ng[138], Y.S. Ng[19], Y.W.Y. Ng[170], B. Ngair[35e], H.D.N. Nguyen[102], T. Nguyen Manh[110], E. Nibigira[38], R.B. Nickerson[134], R. Nicolaidou[144], D.S. Nielsen[40], J. Nielsen[145], N. Nikiforou[11], V. Nikolaenko[123,ah], I. Nikolic-Audit[135], K. Nikolopoulos[21], P. Nilsson[29], H.R. Nindhito[54], Y. Ninomiya[82], A. Nisati[73a], N. Nishu[60c], R. Nisius[115], I. Nitsche[47], T. Nitta[178], T. Nobe[162], D.L. Noel[32], Y. Noguchi[86], I. Nomidis[135], M.A. Nomura[29],

JHEP07(2020)044

M. Nordberg[36], J. Novak[92], T. Novak[92], O. Novgorodova[48], R. Novotny[141], L. Nozka[130], K. Ntekas[170], E. Nurse[95], F.G. Oakham[34,am], H. Oberlack[115], J. Ocariz[135], A. Ochi[83], I. Ochoa[39], J.P. Ochoa-Ricoux[146a], K. O'Connor[26], S. Oda[88], S. Odaka[82], S. Oerdek[53], A. Ogrodnik[84a], A. Oh[101], S.H. Oh[49], C.C. Ohm[153], H. Oide[164], M.L. Ojeda[166], H. Okawa[168], Y. Okazaki[86], M.W. O'Keefe[91], Y. Okumura[162], T. Okuyama[82], A. Olariu[27b], L.F. Oleiro Seabra[139a], S.A. Olivares Pino[146a], D. Oliveira Damazio[29], J.L. Oliver[1], M.J.R. Olsson[170], A. Olszewski[85], J. Olszowska[85], D.C. O'Neil[151], A.P. O'neill[134], A. Onofre[139a,139e], P.U.E. Onyisi[11], H. Oppen[133], R.G. Oreamuno Madriz[121], M.J. Oreglia[37], G.E. Orellana[89], D. Orestano[75a,75b], N. Orlando[14], R.S. Orr[166], V. O'Shea[57], R. Ospanov[60a], G. Otero y Garzon[30], H. Otono[88], P.S. Ott[61a], G.J. Ottino[18], M. Ouchrif[35d], J. Ouellette[29], F. Ould-Saada[133], A. Ouraou[144], Q. Ouyang[15a], M. Owen[57], R.E. Owen[21], V.E. Ozcan[12c], N. Ozturk[8], J. Pacalt[130], H.A. Pacey[32], K. Pachal[49], A. Pacheco Pages[14], C. Padilla Aranda[14], S. Pagan Griso[18], M. Paganini[182], G. Palacino[66], S. Palazzo[50], S. Palestini[36], M. Palka[84b], D. Pallin[38], P. Palni[84a], I. Panagoulias[10], C.E. Pandini[36], J.G. Panduro Vazquez[94], P. Pani[46], G. Panizzo[67a,67c], L. Paolozzi[54], C. Papadatos[110], K. Papageorgiou[9,g], S. Parajuli[42], A. Paramonov[6], C. Paraskevopoulos[10], D. Paredes Hernandez[63b], S.R. Paredes Saenz[134], B. Parida[165], T.H. Park[166], A.J. Parker[31], M.A. Parker[32], F. Parodi[55b,55a], E.W. Parrish[121], J.A. Parsons[39], U. Parzefall[52], L. Pascual Dominguez[135], V.R. Pascuzzi[18], J.M.P. Pasner[145], F. Pasquali[120], E. Pasqualucci[73a], S. Passaggio[55b], F. Pastore[94], P. Pasuwan[45a,45b], S. Pataraia[100], J.R. Pater[101], A. Pathak[180,i], J. Patton[91], T. Pauly[36], J. Pearkes[152], B. Pearson[115], M. Pedersen[133], L. Pedraza Diaz[119], R. Pedro[139a], T. Peiffer[53], S.V. Peleganchuk[122b,122a], O. Penc[140], H. Peng[60a], B.S. Peralva[81a], M.M. Perego[65], A.P. Pereira Peixoto[139a], L. Pereira Sanchez[45a,45b], D.V. Perepelitsa[29], F. Peri[19], L. Perini[69a,69b], H. Pernegger[36], S. Perrella[139a], A. Perrevoort[120], K. Peters[46], R.F.Y. Peters[101], B.A. Petersen[36], T.C. Petersen[40], E. Petit[102], A. Petridis[1], C. Petridou[161], P. Petroff[65], F. Petrucci[75a,75b], M. Pettee[182], N.E. Pettersson[103], K. Petukhova[142], A. Peyaud[144], R. Pezoa[146d], L. Pezzotti[71a,71b], T. Pham[105], F.H. Phillips[107], P.W. Phillips[143], M.W. Phipps[172], G. Piacquadio[154], E. Pianori[18], A. Picazio[103], R.H. Pickles[101], R. Piegaia[30], D. Pietreanu[27b], J.E. Pilcher[37], A.D. Pilkington[101], M. Pinamonti[67a,67c], J.L. Pinfold[3], C. Pitman Donaldson[95], M. Pitt[160], L. Pizzimento[74a,74b], M.-A. Pleier[29], V. Pleskot[142], E. Plotnikova[80], P. Podberezko[122b,122a], R. Poettgen[97], R. Poggi[54], L. Poggioli[135], I. Pogrebnyak[107], D. Pohl[24], I. Pokharel[53], G. Polesello[71a], A. Poley[18], A. Policicchio[73a,73b], R. Polifka[142], A. Polini[23b], C.S. Pollard[46], V. Polychronakos[29], D. Ponomarenko[112], L. Pontecorvo[36], S. Popa[27a], G.A. Popeneciu[27d], L. Portales[5], D.M. Portillo Quintero[58], S. Pospisil[141], K. Potamianos[46], I.N. Potrap[80], C.J. Potter[32], H. Potti[11], T. Poulsen[97], J. Poveda[173], T.D. Powell[148], G. Pownall[46], M.E. Pozo Astigarraga[36], P. Pralavorio[102], S. Prell[79], D. Price[101], M. Primavera[68a], S. Prince[104], M.L. Proffitt[147], N. Proklova[112], K. Prokofiev[63c], F. Prokoshin[80], S. Protopopescu[29], J. Proudfoot[6], M. Przybycien[84a], D. Pudzha[137], A. Puri[172], P. Puzo[65], J. Qian[106], Y. Qin[101], A. Quadt[53], M. Queitsch-Maitland[36], A. Qureshi[1], M. Racko[28a], F. Ragusa[69a,69b], G. Rahal[98], J.A. Raine[54], S. Rajagopalan[29], A. Ramirez Morales[93], K. Ran[15a,15d], T. Rashid[65], D.M. Rauch[46], F. Rauscher[114], S. Rave[100], B. Ravina[148], I. Ravinovich[179], J.H. Rawling[101], M. Raymond[36], A.L. Read[133], N.P. Readioff[58], M. Reale[68a,68b], D.M. Rebuzzi[71a,71b], G. Redlinger[29], K. Reeves[43], L. Rehnisch[19], J. Reichert[136], D. Reikher[160], A. Reiss[100], A. Rej[150], C. Rembser[36], A. Renardi[46], M. Renda[27b], M. Rescigno[73a], S. Resconi[69a], E.D. Resseguie[18], S. Rettie[95], B. Reynolds[127], E. Reynolds[21], O.L. Rezanova[122b,122a], P. Reznicek[142], E. Ricci[76a,76b], R. Richter[115], S. Richter[46], E. Richter-Was[84b], O. Ricken[24], M. Ridel[135], P. Rieck[115], O. Rifki[46], M. Rijssenbeek[154], A. Rimoldi[71a,71b], M. Rimoldi[46], L. Rinaldi[23b], G. Ripellino[153], I. Riu[14], P. Rivadeneira[46], J.C. Rivera Vergara[175], F. Rizatdinova[129], E. Rizvi[93], C. Rizzi[36], R.T. Roberts[101], S.H. Robertson[104,ac], M. Robin[46], D. Robinson[32], C.M. Robles Gajardo[146d],

JHEP07(2020)044

M. Robles Manzano[100], A. Robson[57], A. Rocchi[74a,74b], E. Rocco[100], C. Roda[72a,72b], S. Rodriguez Bosca[173], D. Rodriguez Rodriguez[173], A.M. Rodríguez Vera[167b], S. Roe[36], O. Røhne[133], R. Röhrig[115], R.A. Rojas[146d], B. Roland[52], C.P.A. Roland[66], J. Roloff[29], A. Romaniouk[112], M. Romano[23b,23a], N. Rompotis[91], M. Ronzani[125], L. Roos[135], S. Rosati[73a], G. Rosin[103], B.J. Rosser[136], E. Rossi[46], E. Rossi[75a,75b], E. Rossi[70a,70b], L.P. Rossi[55b], L. Rossini[69a,69b], R. Rosten[14], M. Rotaru[27b], B. Rottler[52], D. Rousseau[65], G. Rovelli[71a,71b], A. Roy[11], D. Roy[33e], A. Rozanov[102], Y. Rozen[159], X. Ruan[33e], F. Rühr[52], A. Ruiz-Martinez[173], A. Rummler[36], Z. Rurikova[52], N.A. Rusakovich[80], H.L. Russell[104], L. Rustige[38,47], J.P. Rutherfoord[7], E.M. Rüttinger[148], M. Rybar[39], G. Rybkin[65], E.B. Rye[133], A. Ryzhov[123], J.A. Sabater Iglesias[46], P. Sabatini[53], S. Sacerdoti[65], H.F-W. Sadrozinski[145], R. Sadykov[80], F. Safai Tehrani[73a], B. Safarzadeh Samani[155], M. Safdari[152], P. Saha[121], S. Saha[104], M. Sahinsoy[61a], A. Sahu[181], M. Saimpert[36], M. Saito[162], T. Saito[162], H. Sakamoto[162], D. Salamani[54], G. Salamanna[75a,75b], J.E. Salazar Loyola[146d], A. Salnikov[152], J. Salt[173], A. Salvador Salas[14], D. Salvatore[41b,41a], F. Salvatore[155], A. Salvucci[63a,63b,63c], A. Salzburger[36], J. Samarati[36], D. Sammel[52], D. Sampsonidis[161], D. Sampsonidou[161], J. Sánchez[173], A. Sanchez Pineda[67a,36,67c], H. Sandaker[133], C.O. Sander[46], I.G. Sanderswood[90], M. Sandhoff[181], C. Sandoval[22a], D.P.C. Sankey[143], M. Sannino[55b,55a], Y. Sano[117], A. Sansoni[51], C. Santoni[38], H. Santos[139a,139b], S.N. Santpur[18], A. Santra[173], A. Sapronov[80], J.G. Saraiva[139a,139d], O. Sasaki[82], K. Sato[168], F. Sauerburger[52], E. Sauvan[5], P. Savard[166,am], R. Sawada[162], C. Sawyer[143], L. Sawyer[96,ag], C. Sbarra[23b], A. Sbrizzi[23a], T. Scanlon[95], J. Schaarschmidt[147], P. Schacht[115], B.M. Schachtner[114], D. Schaefer[37], L. Schaefer[136], J. Schaeffer[100], S. Schaepe[36], U. Schäfer[100], A.C. Schaffer[65], D. Schaile[114], R.D. Schamberger[154], E. Schanet[114], N. Scharmberg[101], V.A. Schegelsky[137], D. Scheirich[142], F. Schenck[19], M. Schernau[170], C. Schiavi[55b,55a], L.K. Schildgen[24], Z.M. Schillaci[26], E.J. Schioppa[68a,68b], M. Schioppa[41b,41a], K.E. Schleicher[52], S. Schlenker[36], K.R. Schmidt-Sommerfeld[115], K. Schmieden[36], C. Schmitt[100], S. Schmitt[46], S. Schmitz[100], J.C. Schmoeckel[46], L. Schoeffel[144], A. Schoening[61b], P.G. Scholer[52], E. Schopf[134], M. Schott[100], J.F.P. Schouwenberg[119], J. Schovancova[36], S. Schramm[54], F. Schroeder[181], A. Schulte[100], H-C. Schultz-Coulon[61a], M. Schumacher[52], B.A. Schumm[145], Ph. Schune[144], A. Schwartzman[152], T.A. Schwarz[106], Ph. Schwemling[144], R. Schwienhorst[107], A. Sciandra[145], G. Sciolla[26], M. Scodeggio[46], M. Scornajenghi[41b,41a], F. Scuri[72a], F. Scutti[105], L.M. Scyboz[115], C.D. Sebastiani[73a,73b], P. Seema[19], S.C. Seidel[118], A. Seiden[145], B.D. Seidlitz[29], T. Seiss[37], C. Seitz[46], J.M. Seixas[81b], G. Sekhniaidze[70a], S.J. Sekula[42], N. Semprini-Cesari[23b,23a], S. Sen[49], C. Serfon[29], L. Serin[65], L. Serkin[67a,67b], M. Sessa[60a], H. Severini[128], S. Sevova[152], F. Sforza[55b,55a], A. Sfyrla[54], E. Shabalina[53], J.D. Shahinian[145], N.W. Shaikh[45a,45b], D. Shaked Renous[179], L.Y. Shan[15a], M. Shapiro[18], A. Sharma[134], A.S. Sharma[1], P.B. Shatalov[124], K. Shaw[155], S.M. Shaw[101], M. Shehade[179], Y. Shen[128], A.D. Sherman[25], P. Sherwood[95], L. Shi[157], S. Shimizu[82], C.O. Shimmin[182], Y. Shimogama[178], M. Shimojima[116], I.P.J. Shipsey[134], S. Shirabe[164], M. Shiyakova[80,aa], J. Shlomi[179], A. Shmeleva[111], M.J. Shochet[37], J. Shojaii[105], D.R. Shope[128], S. Shrestha[127], E.M. Shrif[33e], E. Shulga[179], P. Sicho[140], A.M. Sickles[172], E. Sideras Haddad[33e], O. Sidiropoulou[36], A. Sidoti[23b,23a], F. Siegert[48], Dj. Sijacki[16], M.Jr. Silva[180], M.V. Silva Oliveira[81a], S.B. Silverstein[45a], S. Simion[65], R. Simoniello[100], C.J. Simpson-allsop[21], S. Simsek[12b], P. Sinervo[166], V. Sinetckii[113], S. Singh[151], M. Sioli[23b,23a], I. Siral[131], S.Yu. Sivoklokov[113], J. Sjölin[45a,45b], A. Skaf[53], E. Skorda[97], P. Skubic[128], M. Slawinska[85], K. Sliwa[169], R. Slovak[142], V. Smakhtin[179], B.H. Smart[143], J. Smiesko[28b], N. Smirnov[112], S.Yu. Smirnov[112], Y. Smirnov[112], L.N. Smirnova[113,s], O. Smirnova[97], J.W. Smith[53], M. Smizanska[90], K. Smolek[141], A. Smykiewicz[85], A.A. Snesarev[111], H.L. Snoek[120], I.M. Snyder[131], S. Snyder[29], R. Sobie[175,ac], A. Soffer[160], A. Søgaard[50], F. Sohns[53], C.A. Solans Sanchez[36], E.Yu. Soldatov[112], U. Soldevila[173], A.A. Solodkov[123], A. Soloshenko[80],

JHEP07(2020)044

O.V. Solovyanov[123], V. Solovyev[137], P. Sommer[148], H. Son[169], W. Song[143], W.Y. Song[167b], A. Sopczak[141], A.L. Sopio[95], F. Sopkova[28b], C.L. Sotiropoulou[72a,72b], S. Sottocornola[71a,71b], R. Soualah[67a,67c,f], A.M. Soukharev[122b,122a], D. South[46], S. Spagnolo[68a,68b], M. Spalla[115], M. Spangenberg[177], F. Spanò[94], D. Sperlich[52], T.M. Spieker[61a], G. Spigo[36], M. Spina[155], D.P. Spiteri[57], M. Spousta[142], A. Stabile[69a,69b], B.L. Stamas[121], R. Stamen[61a], M. Stamenkovic[120], E. Stanecka[85], B. Stanislaus[134], M.M. Stanitzki[46], M. Stankaityte[134], B. Stapf[120], E.A. Starchenko[123], G.H. Stark[145], J. Stark[58], P. Staroba[140], P. Starovoitov[61a], S. Stärz[104], R. Staszewski[85], G. Stavropoulos[44], M. Stegler[46], P. Steinberg[29], A.L. Steinhebel[131], B. Stelzer[151], H.J. Stelzer[138], O. Stelzer-Chilton[167a], H. Stenzel[56], T.J. Stevenson[155], G.A. Stewart[36], M.C. Stockton[36], G. Stoicea[27b], M. Stolarski[139a], S. Stonjek[115], A. Straessner[48], J. Strandberg[153], S. Strandberg[45a,45b], M. Strauss[128], T. Strebler[102], P. Strizenec[28b], R. Ströhmer[176], D.M. Strom[131], R. Stroynowski[42], A. Strubig[50], S.A. Stucci[29], B. Stugu[17], J. Stupak[128], N.A. Styles[46], D. Su[152], W. Su[60c], S. Suchek[61a], V.V. Sulin[111], M.J. Sullivan[91], D.M.S. Sultan[54], S. Sultansoy[4c], T. Sumida[86], S. Sun[106], X. Sun[101], K. Suruliz[155], C.J.E. Suster[156], M.R. Sutton[155], S. Suzuki[82], M. Svatos[140], M. Swiatlowski[167a], S.P. Swift[2], T. Swirski[176], A. Sydorenko[100], I. Sykora[28a], M. Sykora[142], T. Sykora[142], D. Ta[100], K. Tackmann[46,y], J. Taenzer[160], A. Taffard[170], R. Tafirout[167a], R. Takashima[87], K. Takeda[83], T. Takeshita[149], E.P. Takeva[50], Y. Takubo[82], M. Talby[102], A.A. Talyshev[122b,122a], K.C. Tam[63b], N.M. Tamir[160], J. Tanaka[162], R. Tanaka[65], S. Tapia Araya[172], S. Tapprogge[100], A. Tarek Abouelfadl Mohamed[107], S. Tarem[159], K. Tariq[60b], G. Tarna[27b,c], G.F. Tartarelli[69a], P. Tas[142], M. Tasevsky[140], T. Tashiro[86], E. Tassi[41b,41a], A. Tavares Delgado[139a], Y. Tayalati[35e], A.J. Taylor[50], G.N. Taylor[105], W. Taylor[167b], H. Teagle[91], A.S. Tee[90], R. Teixeira De Lima[152], P. Teixeira-Dias[94], H. Ten Kate[36], J.J. Teoh[120], S. Terada[82], K. Terashi[162], J. Terron[99], S. Terzo[14], M. Testa[51], R.J. Teuscher[166,ac], S.J. Thais[182], N. Themistokleous[50], T. Theveneaux-Pelzer[46], F. Thiele[40], D.W. Thomas[94], J.O. Thomas[42], J.P. Thomas[21], E.A. Thompson[46], P.D. Thompson[21], E. Thomson[136], E.J. Thorpe[93], R.E. Ticse Torres[53], V.O. Tikhomirov[111,ai], Yu.A. Tikhonov[122b,122a], S. Timoshenko[112], P. Tipton[182], S. Tisserant[102], K. Todome[23b,23a], S. Todorova-Nova[142], S. Todt[48], J. Tojo[88], S. Tokár[28a], K. Tokushuku[82], E. Tolley[127], R. Tombs[32], K.G. Tomiwa[33e], M. Tomoto[117], L. Tompkins[152], P. Tornambe[103], E. Torrence[131], H. Torres[48], E. Torró Pastor[147], C. Tosciri[134], J. Toth[102,ab], D.R. Tovey[148], A. Traeet[17], C.J. Treado[125], T. Trefzger[176], F. Tresoldi[155], A. Tricoli[29], I.M. Trigger[167a], S. Trincaz-Duvoid[135], D.A. Trischuk[174], W. Trischuk[166], B. Trocmé[58], A. Trofymov[65], C. Troncon[69a], F. Trovato[155], L. Truong[33c], M. Trzebinski[85], A. Trzupek[85], F. Tsai[46], J.C-L. Tseng[134], P.V. Tsiareshka[108,af], A. Tsirigotis[161,v], V. Tsiskaridze[154], E.G. Tskhadadze[158a], M. Tsopoulou[161], I.I. Tsukerman[124], V. Tsulaia[18], S. Tsuno[82], D. Tsybychev[154], Y. Tu[63b], A. Tudorache[27b], V. Tudorache[27b], T.T. Tulbure[27a], A.N. Tuna[59], S. Turchikhin[80], D. Turgeman[179], I. Turk Cakir[4b,t], R.J. Turner[21], R.T. Turra[69a], P.M. Tuts[39], S. Tzamarias[161], E. Tzovara[100], G. Ucchielli[47], K. Uchida[162], F. Ukegawa[168], G. Unal[36], A. Undrus[29], G. Unel[170], F.C. Ungaro[105], Y. Unno[82], K. Uno[162], J. Urban[28b], P. Urquijo[105], G. Usai[8], Z. Uysal[12d], V. Vacek[141], B. Vachon[104], K.O.H. Vadla[133], A. Vaidya[95], C. Valderanis[114], E. Valdes Santurio[45a,45b], M. Valente[54], S. Valentinetti[23b,23a], A. Valero[173], L. Valéry[46], R.A. Vallance[21], A. Vallier[36], J.A. Valls Ferrer[173], T.R. Van Daalen[14], P. Van Gemmeren[6], I. Van Vulpen[120], M. Vanadia[74a,74b], W. Vandelli[36], M. Vandenbroucke[144], E.R. Vandewall[129], A. Vaniachine[165], D. Vannicola[73a,73b], R. Vari[73a], E.W. Varnes[7], C. Varni[55b,55a], T. Varol[157], D. Varouchas[65], K.E. Varvell[156], M.E. Vasile[27b], G.A. Vasquez[175], F. Vazeille[38], D. Vazquez Furelos[14], T. Vazquez Schroeder[36], J. Veatch[53], V. Vecchio[101], M.J. Veen[120], L.M. Veloce[166], F. Veloso[139a,139c], S. Veneziano[73a], A. Ventura[68a,68b], N. Venturi[36], A. Verbytskyi[115], V. Vercesi[71a], M. Verducci[72a,72b], C.M. Vergel Infante[79], C. Vergis[24],

JHEP07(2020)044

W. Verkerke[120], A.T. Vermeulen[120], J.C. Vermeulen[120], C. Vernieri[152], M.C. Vetterli[151,am], N. Viaux Maira[146d], T. Vickey[148], O.E. Vickey Boeriu[148], G.H.A. Viehhauser[134], L. Vigani[61b], M. Villa[23b,23a], M. Villaplana Perez[3], E.M. Villhauer[50], E. Vilucchi[51], M.G. Vincter[34], G.S. Virdee[21], A. Vishwakarma[46], C. Vittori[23b,23a], I. Vivarelli[155], M. Vogel[181], P. Vokac[141], S.E. von Buddenbrock[33e], E. Von Toerne[24], V. Vorobel[142], K. Vorobev[112], M. Vos[173], J.H. Vossebeld[91], M. Vozak[101], N. Vranjes[16], M. Vranjes Milosavljevic[16], V. Vrba[141], M. Vreeswijk[120], R. Vuillermet[36], I. Vukotic[37], S. Wada[168], P. Wagner[24], W. Wagner[181], J. Wagner-Kuhr[114], S. Wahdan[181], H. Wahlberg[89], R. Wakasa[168], V.M. Walbrecht[115], J. Walder[90], R. Walker[114], S.D. Walker[94], W. Walkowiak[150], V. Wallangen[45a,45b], A.M. Wang[59], A.Z. Wang[180], C. Wang[60c], F. Wang[180], H. Wang[18], H. Wang[3], J. Wang[63a], J. Wang[61b], P. Wang[42], Q. Wang[128], R.-J. Wang[100], R. Wang[60a], R. Wang[6], S.M. Wang[157], W.T. Wang[60a], W. Wang[15c], W.X. Wang[60a], Y. Wang[60a], Z. Wang[60c], C. Wanotayaroj[46], A. Warburton[104], C.P. Ward[32], D.R. Wardrope[95], N. Warrack[57], A. Washbrook[50], A.T. Watson[21], M.F. Watson[21], G. Watts[147], B.M. Waugh[95], A.F. Webb[11], C. Weber[29], M.S. Weber[20], S.A. Weber[34], S.M. Weber[61a], A.R. Weidberg[134], J. Weingarten[47], M. Weirich[100], C. Weiser[52], P.S. Wells[36], T. Wenaus[29], T. Wengler[36], S. Wenig[36], N. Wermes[24], M.D. Werner[79], M. Wessels[61a], T.D. Weston[20], K. Whalen[131], N.L. Whallon[147], A.M. Wharton[90], A.S. White[106], A. White[8], M.J. White[1], D. Whiteson[170], B.W. Whitmore[90], W. Wiedenmann[180], C. Wiel[48], M. Wielers[143], N. Wieseotte[100], C. Wiglesworth[40], L.A.M. Wiik-Fuchs[52], H.G. Wilkens[36], L.J. Wilkins[94], H.H. Williams[136], S. Williams[32], C. Willis[107], S. Willocq[103], P.J. Windischhofer[134], I. Wingerter-Seez[5], E. Winkels[155], F. Winklmeier[131], B.T. Winter[52], M. Wittgen[152], M. Wobisch[96], A. Wolf[100], T.M.H. Wolf[120], R. Wolff[102], R. Wölker[134], J. Wollrath[52], M.W. Wolter[85], H. Wolters[139a,139c], V.W.S. Wong[174], N.L. Woods[145], S.D. Worm[46], B.K. Wosiek[85], K.W. Woźniak[85], K. Wraight[57], S.L. Wu[180], X. Wu[54], Y. Wu[60a], T.R. Wyatt[101], B.M. Wynne[50], S. Xella[40], Z. Xi[106], L. Xia[177], X. Xiao[106], X. Xie[60a], I. Xiotidis[155], D. Xu[15a], H. Xu[60a], H. Xu[60a], L. Xu[29], T. Xu[144], W. Xu[106], Z. Xu[60b], Z. Xu[152], B. Yabsley[156], S. Yacoob[33a], K. Yajima[132], D.P. Yallup[95], N. Yamaguchi[88], Y. Yamaguchi[164], A. Yamamoto[82], M. Yamatani[162], T. Yamazaki[162], Y. Yamazaki[83], J. Yan[60c], Z. Yan[25], H.J. Yang[60c,60d], H.T. Yang[18], S. Yang[60a], T. Yang[63c], X. Yang[60b,58], Y. Yang[162], Z. Yang[60a], W-M. Yao[18], Y.C. Yap[46], Y. Yasu[82], E. Yatsenko[60c,60d], H. Ye[15c], J. Ye[42], S. Ye[29], I. Yeletskikh[80], M.R. Yexley[90], E. Yigitbasi[25], P. Yin[39], K. Yorita[178], K. Yoshihara[79], C.J.S. Young[36], C. Young[152], J. Yu[79], R. Yuan[60b,h], X. Yue[61a], M. Zaazoua[35e], B. Zabinski[85], G. Zacharis[10], E. Zaffaroni[54], J. Zahreddine[135], A.M. Zaitsev[123,ah], T. Zakareishvili[158b], N. Zakharchuk[34], S. Zambito[59], D. Zanzi[36], D.R. Zaripovas[57], S.V. Zeißner[47], C. Zeitnitz[181], G. Zemaityte[134], J.C. Zeng[172], O. Zenin[123], T. Ženiš[28a], D. Zerwas[65], M. Zgubič[134], B. Zhang[15c], D.F. Zhang[15b], G. Zhang[15b], J. Zhang[6], Kaili. Zhang[15a], L. Zhang[15c], L. Zhang[60a], M. Zhang[172], R. Zhang[180], S. Zhang[106], X. Zhang[60c], X. Zhang[60b], Y. Zhang[15a,15d], Z. Zhang[63a], Z. Zhang[65], P. Zhao[49], Z. Zhao[60a], A. Zhemchugov[80], Z. Zheng[106], D. Zhong[172], B. Zhou[106], C. Zhou[180], H. Zhou[7], M.S. Zhou[15a,15d], M. Zhou[154], N. Zhou[60c], Y. Zhou[7], C.G. Zhu[60b], C. Zhu[15a,15d], H.L. Zhu[60a], H. Zhu[15a], J. Zhu[106], Y. Zhu[60a], X. Zhuang[15a], K. Zhukov[111], V. Zhulanov[122b,122a], D. Zieminska[66], N.I. Zimine[80], S. Zimmermann[52], Z. Zinonos[115], M. Ziolkowski[150], L. Živković[16], G. Zobernig[180], A. Zoccoli[23b,23a], K. Zoch[53], T.G. Zorbas[148], R. Zou[37], L. Zwalinski[36]

[1] *Department of Physics, University of Adelaide, Adelaide; Australia*

[2] *Physics Department, SUNY Albany, Albany NY; United States of America*

[3] *Department of Physics, University of Alberta, Edmonton AB; Canada*

[4] *Department of Physics[(a)], Ankara University, Ankara; Istanbul Aydin University[(b)], Application and Research Center for Advanced Studies, Istanbul; Division of Physics[(c)], TOBB University of Economics and Technology, Ankara; Turkey*

JHEP07(2020)044

[5] LAPP, Université Grenoble Alpes, Université Savoie Mont Blanc, CNRS/IN2P3, Annecy; France
[6] High Energy Physics Division, Argonne National Laboratory, Argonne IL; United States of America
[7] Department of Physics, University of Arizona, Tucson AZ; United States of America
[8] Department of Physics, University of Texas at Arlington, Arlington TX; United States of America
[9] Physics Department, National and Kapodistrian University of Athens, Athens; Greece
[10] Physics Department, National Technical University of Athens, Zografou; Greece
[11] Department of Physics, University of Texas at Austin, Austin TX; United States of America
[12] Bahcesehir University[(a)], Faculty of Engineering and Natural Sciences, Istanbul; Istanbul Bilgi University[(b)], Faculty of Engineering and Natural Sciences, Istanbul; Department of Physics[(c)], Bogazici University, Istanbul; Department of Physics Engineering[(d)], Gaziantep University, Gaziantep; Turkey
[13] Institute of Physics, Azerbaijan Academy of Sciences, Baku; Azerbaijan
[14] Institut de Física d'Altes Energies (IFAE), Barcelona Institute of Science and Technology, Barcelona; Spain
[15] Institute of High Energy Physics[(a)], Chinese Academy of Sciences, Beijing; Physics Department[(b)], Tsinghua University, Beijing; Department of Physics[(c)], Nanjing University, Nanjing; University of Chinese Academy of Science (UCAS)[(d)], Beijing; China
[16] Institute of Physics, University of Belgrade, Belgrade; Serbia
[17] Department for Physics and Technology, University of Bergen, Bergen; Norway
[18] Physics Division, Lawrence Berkeley National Laboratory and University of California, Berkeley CA; United States of America
[19] Institut für Physik, Humboldt Universität zu Berlin, Berlin; Germany
[20] Albert Einstein Center for Fundamental Physics and Laboratory for High Energy Physics, University of Bern, Bern; Switzerland
[21] School of Physics and Astronomy, University of Birmingham, Birmingham; United Kingdom
[22] Facultad de Ciencias y Centro de Investigaciónes[(a)], Universidad Antonio Nariño, Bogotá; Departamento de Física[(b)], Universidad Nacional de Colombia, Bogotá, Colombia; Colombia
[23] INFN Bologna and Università di Bologna[(a)], Dipartimento di Fisica; INFN Sezione di Bologna[(b)]; Italy
[24] Physikalisches Institut, Universität Bonn, Bonn; Germany
[25] Department of Physics, Boston University, Boston MA; United States of America
[26] Department of Physics, Brandeis University, Waltham MA; United States of America
[27] Transilvania University of Brasov[(a)], Brasov; Horia Hulubei National Institute of Physics and Nuclear Engineering[(b)], Bucharest; Department of Physics[(c)], Alexandru Ioan Cuza University of Iasi, Iasi; National Institute for Research and Development of Isotopic and Molecular Technologies[(d)], Physics Department, Cluj-Napoca; University Politehnica Bucharest[(e)], Bucharest; West University in Timisoara[(f)], Timisoara; Romania
[28] Faculty of Mathematics[(a)], Physics and Informatics, Comenius University, Bratislava; Department of Subnuclear Physics[(b)], Institute of Experimental Physics of the Slovak Academy of Sciences, Kosice; Slovak Republic
[29] Physics Department, Brookhaven National Laboratory, Upton NY; United States of America
[30] Departamento de Física, Universidad de Buenos Aires, Buenos Aires; Argentina
[31] California State University, CA; United States of America
[32] Cavendish Laboratory, University of Cambridge, Cambridge; United Kingdom
[33] Department of Physics[(a)], University of Cape Town, Cape Town; [(b)]iThemba Labs, Western Cape; Department of Mechanical Engineering Science[(c)], University of Johannesburg, Johannesburg; University of South Africa[(d)], Department of Physics, Pretoria; School of Physics[(e)], University of the Witwatersrand, Johannesburg; South Africa
[34] Department of Physics, Carleton University, Ottawa ON; Canada
[35] Faculté des Sciences Ain Chock[(a)], Réseau Universitaire de Physique des Hautes Energies - Université Hassan II, Casablanca; Faculté des Sciences[(b)], Université Ibn-Tofail, Kénitra; Faculté des Sciences Semlalia[(c)], Université Cadi Ayyad, LPHEA-Marrakech; Faculté des Sciences[(d)], Université Mohamed Premier and LPTPM, Oujda; Faculté des sciences[(e)], Université Mohammed V, Rabat; Morocco

JHEP07(2020)044

[36] CERN, Geneva; Switzerland
[37] Enrico Fermi Institute, University of Chicago, Chicago IL; United States of America
[38] LPC, Université Clermont Auvergne, CNRS/IN2P3, Clermont-Ferrand; France
[39] Nevis Laboratory, Columbia University, Irvington NY; United States of America
[40] Niels Bohr Institute, University of Copenhagen, Copenhagen; Denmark
[41] Dipartimento di Fisica[(a)], Università della Calabria, Rende; INFN Gruppo Collegato di Cosenza[(b)], Laboratori Nazionali di Frascati; Italy
[42] Physics Department, Southern Methodist University, Dallas TX; United States of America
[43] Physics Department, University of Texas at Dallas, Richardson TX; United States of America
[44] National Centre for Scientific Research "Demokritos", Agia Paraskevi; Greece
[45] Department of Physics[(a)], Stockholm University; Oskar Klein Centre[(b)], Stockholm; Sweden
[46] Deutsches Elektronen-Synchrotron DESY, Hamburg and Zeuthen; Germany
[47] Lehrstuhl für Experimentelle Physik IV, Technische Universität Dortmund, Dortmund; Germany
[48] Institut für Kern- und Teilchenphysik, Technische Universität Dresden, Dresden; Germany
[49] Department of Physics, Duke University, Durham NC; United States of America
[50] SUPA - School of Physics and Astronomy, University of Edinburgh, Edinburgh; United Kingdom
[51] INFN e Laboratori Nazionali di Frascati, Frascati; Italy
[52] Physikalisches Institut, Albert-Ludwigs-Universität Freiburg, Freiburg; Germany
[53] II. Physikalisches Institut, Georg-August-Universität Göttingen, Göttingen; Germany
[54] Département de Physique Nucléaire et Corpusculaire, Université de Genève, Genève; Switzerland
[55] Dipartimento di Fisica[(a)], Università di Genova, Genova; INFN Sezione di Genova[(b)]; Italy
[56] II. Physikalisches Institut, Justus-Liebig-Universität Giessen, Giessen; Germany
[57] SUPA - School of Physics and Astronomy, University of Glasgow, Glasgow; United Kingdom
[58] LPSC, Université Grenoble Alpes, CNRS/IN2P3, Grenoble INP, Grenoble; France
[59] Laboratory for Particle Physics and Cosmology, Harvard University, Cambridge MA; United States of America
[60] Department of Modern Physics and State Key Laboratory of Particle Detection and Electronics[(a)], University of Science and Technology of China, Hefei; Institute of Frontier and Interdisciplinary Science and Key Laboratory of Particle Physics and Particle Irradiation (MOE)[(b)], Shandong University, Qingdao; School of Physics and Astronomy[(c)], Shanghai Jiao Tong University, KLPPAC-MoE, SKLPPC, Shanghai; Tsung-Dao Lee Institute[(d)], Shanghai; China
[61] Kirchhoff-Institut für Physik[(a)], Ruprecht-Karls-Universität Heidelberg, Heidelberg; Physikalisches Institut[(b)], Ruprecht-Karls-Universität Heidelberg, Heidelberg; Germany
[62] Faculty of Applied Information Science, Hiroshima Institute of Technology, Hiroshima; Japan
[63] Department of Physics[(a)], Chinese University of Hong Kong, Shatin, N.T., Hong Kong; Department of Physics[(b)], University of Hong Kong, Hong Kong; Department of Physics and Institute for Advanced Study[(c)], Hong Kong University of Science and Technology, Clear Water Bay, Kowloon, Hong Kong; China
[64] Department of Physics, National Tsing Hua University, Hsinchu; Taiwan
[65] IJCLab, Université Paris-Saclay, CNRS/IN2P3, 91405, Orsay; France
[66] Department of Physics, Indiana University, Bloomington IN; United States of America
[67] INFN Gruppo Collegato di Udine[(a)], Sezione di Trieste, Udine; ICTP[(b)], Trieste; Dipartimento Politecnico di Ingegneria e Architettura[(c)], Università di Udine, Udine; Italy
[68] INFN Sezione di Lecce[(a)]; Dipartimento di Matematica e Fisica[(b)], Università del Salento, Lecce; Italy
[69] INFN Sezione di Milano[(a)]; Dipartimento di Fisica[(b)], Università di Milano, Milano; Italy
[70] INFN Sezione di Napoli[(a)]; Dipartimento di Fisica[(b)], Università di Napoli, Napoli; Italy
[71] INFN Sezione di Pavia[(a)]; Dipartimento di Fisica[(b)], Università di Pavia, Pavia; Italy
[72] INFN Sezione di Pisa[(a)]; Dipartimento di Fisica E. Fermi[(b)], Università di Pisa, Pisa; Italy
[73] INFN Sezione di Roma[(a)]; Dipartimento di Fisica[(b)], Sapienza Università di Roma, Roma; Italy
[74] INFN Sezione di Roma Tor Vergata[(a)]; Dipartimento di Fisica[(b)], Università di Roma Tor Vergata, Roma; Italy

JHEP07(2020)044

[75] *INFN Sezione di Roma Tre[(a)]; Dipartimento di Matematica e Fisica[(b)], Università Roma Tre, Roma; Italy*
[76] *INFN-TIFPA[(a)]; Università degli Studi di Trento[(b)], Trento; Italy*
[77] *Institut für Astro- und Teilchenphysik, Leopold-Franzens-Universität, Innsbruck; Austria*
[78] *University of Iowa, Iowa City IA; United States of America*
[79] *Department of Physics and Astronomy, Iowa State University, Ames IA; United States of America*
[80] *Joint Institute for Nuclear Research, Dubna; Russia*
[81] *Departamento de Engenharia Elétrica[(a)], Universidade Federal de Juiz de Fora (UFJF), Juiz de Fora; Universidade Federal do Rio De Janeiro COPPE/EE/IF[(b)], Rio de Janeiro; Universidade Federal de São João del Rei (UFSJ)[(c)], São João del Rei; Instituto de Física[(d)], Universidade de São Paulo, São Paulo; Brazil*
[82] *KEK, High Energy Accelerator Research Organization, Tsukuba; Japan*
[83] *Graduate School of Science, Kobe University, Kobe; Japan*
[84] *AGH University of Science and Technology[(a)], Faculty of Physics and Applied Computer Science, Krakow; Marian Smoluchowski Institute of Physics[(b)], Jagiellonian University, Krakow; Poland*
[85] *Institute of Nuclear Physics Polish Academy of Sciences, Krakow; Poland*
[86] *Faculty of Science, Kyoto University, Kyoto; Japan*
[87] *Kyoto University of Education, Kyoto; Japan*
[88] *Research Center for Advanced Particle Physics and Department of Physics, Kyushu University, Fukuoka; Japan*
[89] *Instituto de Física La Plata, Universidad Nacional de La Plata and CONICET, La Plata; Argentina*
[90] *Physics Department, Lancaster University, Lancaster; United Kingdom*
[91] *Oliver Lodge Laboratory, University of Liverpool, Liverpool; United Kingdom*
[92] *Department of Experimental Particle Physics, Jožef Stefan Institute and Department of Physics, University of Ljubljana, Ljubljana; Slovenia*
[93] *School of Physics and Astronomy, Queen Mary University of London, London; United Kingdom*
[94] *Department of Physics, Royal Holloway University of London, Egham; United Kingdom*
[95] *Department of Physics and Astronomy, University College London, London; United Kingdom*
[96] *Louisiana Tech University, Ruston LA; United States of America*
[97] *Fysiska institutionen, Lunds universitet, Lund; Sweden*
[98] *Centre de Calcul de l'Institut National de Physique Nucléaire et de Physique des Particules (IN2P3), Villeurbanne; France*
[99] *Departamento de Física Teorica C-15 and CIAFF, Universidad Autónoma de Madrid, Madrid; Spain*
[100] *Institut für Physik, Universität Mainz, Mainz; Germany*
[101] *School of Physics and Astronomy, University of Manchester, Manchester; United Kingdom*
[102] *CPPM, Aix-Marseille Université, CNRS/IN2P3, Marseille; France*
[103] *Department of Physics, University of Massachusetts, Amherst MA; United States of America*
[104] *Department of Physics, McGill University, Montreal QC; Canada*
[105] *School of Physics, University of Melbourne, Victoria; Australia*
[106] *Department of Physics, University of Michigan, Ann Arbor MI; United States of America*
[107] *Department of Physics and Astronomy, Michigan State University, East Lansing MI; United States of America*
[108] *B.I. Stepanov Institute of Physics, National Academy of Sciences of Belarus, Minsk; Belarus*
[109] *Research Institute for Nuclear Problems of Byelorussian State University, Minsk; Belarus*
[110] *Group of Particle Physics, University of Montreal, Montreal QC; Canada*
[111] *P.N. Lebedev Physical Institute of the Russian Academy of Sciences, Moscow; Russia*
[112] *National Research Nuclear University MEPhI, Moscow; Russia*
[113] *D.V. Skobeltsyn Institute of Nuclear Physics, M.V. Lomonosov Moscow State University, Moscow; Russia*
[114] *Fakultät für Physik, Ludwig-Maximilians-Universität München, München; Germany*
[115] *Max-Planck-Institut für Physik (Werner-Heisenberg-Institut), München; Germany*

JHEP07(2020)044

[116] *Nagasaki Institute of Applied Science, Nagasaki; Japan*
[117] *Graduate School of Science and Kobayashi-Maskawa Institute, Nagoya University, Nagoya; Japan*
[118] *Department of Physics and Astronomy, University of New Mexico, Albuquerque NM; United States of America*
[119] *Institute for Mathematics, Astrophysics and Particle Physics, Radboud University Nijmegen/Nikhef, Nijmegen; Netherlands*
[120] *Nikhef National Institute for Subatomic Physics and University of Amsterdam, Amsterdam; Netherlands*
[121] *Department of Physics, Northern Illinois University, DeKalb IL; United States of America*
[122] *Budker Institute of Nuclear Physics and NSU[(a)], SB RAS, Novosibirsk; Novosibirsk State University Novosibirsk[(b)]; Russia*
[123] *Institute for High Energy Physics of the National Research Centre Kurchatov Institute, Protvino; Russia*
[124] *Institute for Theoretical and Experimental Physics named by A.I. Alikhanov of National Research Centre "Kurchatov Institute", Moscow; Russia*
[125] *Department of Physics, New York University, New York NY; United States of America*
[126] *Ochanomizu University, Otsuka, Bunkyo-ku, Tokyo; Japan*
[127] *Ohio State University, Columbus OH; United States of America*
[128] *Homer L. Dodge Department of Physics and Astronomy, University of Oklahoma, Norman OK; United States of America*
[129] *Department of Physics, Oklahoma State University, Stillwater OK; United States of America*
[130] *Palacký University, RCPTM, Joint Laboratory of Optics, Olomouc; Czech Republic*
[131] *Institute for Fundamental Science, University of Oregon, Eugene, OR; United States of America*
[132] *Graduate School of Science, Osaka University, Osaka; Japan*
[133] *Department of Physics, University of Oslo, Oslo; Norway*
[134] *Department of Physics, Oxford University, Oxford; United Kingdom*
[135] *LPNHE, Sorbonne Université, Université de Paris, CNRS/IN2P3, Paris; France*
[136] *Department of Physics, University of Pennsylvania, Philadelphia PA; United States of America*
[137] *Konstantinov Nuclear Physics Institute of National Research Centre "Kurchatov Institute", PNPI, St. Petersburg; Russia*
[138] *Department of Physics and Astronomy, University of Pittsburgh, Pittsburgh PA; United States of America*
[139] *Laboratório de Instrumentação e Física Experimental de Partículas - LIP[(a)], Lisboa; Departamento de Física[(b)], Faculdade de Ciências, Universidade de Lisboa, Lisboa; Departamento de Física[(c)], Universidade de Coimbra, Coimbra; Centro de Física Nuclear da Universidade de Lisboa[(d)], Lisboa; Departamento de Física[(e)], Universidade do Minho, Braga; Departamento de Física Teórica y del Cosmos[(f)], Universidad de Granada, Granada (Spain); Dep Física and CEFITEC of Faculdade de Ciências e Tecnologia[(g)], Universidade Nova de Lisboa, Caparica; Instituto Superior Técnico[(h)], Universidade de Lisboa, Lisboa; Portugal*
[140] *Institute of Physics of the Czech Academy of Sciences, Prague; Czech Republic*
[141] *Czech Technical University in Prague, Prague; Czech Republic*
[142] *Charles University, Faculty of Mathematics and Physics, Prague; Czech Republic*
[143] *Particle Physics Department, Rutherford Appleton Laboratory, Didcot; United Kingdom*
[144] *IRFU, CEA, Université Paris-Saclay, Gif-sur-Yvette; France*
[145] *Santa Cruz Institute for Particle Physics, University of California Santa Cruz, Santa Cruz CA; United States of America*
[146] *Departamento de Física[(a)], Pontificia Universidad Católica de Chile, Santiago; Universidad Andres Bello[(b)], Department of Physics, Santiago; Instituto de Alta Investigación[(c)], Universidad de Tarapacá; Departamento de Física[(d)], Universidad Técnica Federico Santa María, Valparaíso; Chile*
[147] *Department of Physics, University of Washington, Seattle WA; United States of America*
[148] *Department of Physics and Astronomy, University of Sheffield, Sheffield; United Kingdom*
[149] *Department of Physics, Shinshu University, Nagano; Japan*

JHEP07(2020)044

[150] Department Physik, Universität Siegen, Siegen; Germany
[151] Department of Physics, Simon Fraser University, Burnaby BC; Canada
[152] SLAC National Accelerator Laboratory, Stanford CA; United States of America
[153] Physics Department, Royal Institute of Technology, Stockholm; Sweden
[154] Departments of Physics and Astronomy, Stony Brook University, Stony Brook NY; United States of America
[155] Department of Physics and Astronomy, University of Sussex, Brighton; United Kingdom
[156] School of Physics, University of Sydney, Sydney; Australia
[157] Institute of Physics, Academia Sinica, Taipei; Taiwan
[158] E. Andronikashvili Institute of Physics[(a)], Iv. Javakhishvili Tbilisi State University, Tbilisi; High Energy Physics Institute[(b)], Tbilisi State University, Tbilisi; Georgia
[159] Department of Physics, Technion, Israel Institute of Technology, Haifa; Israel
[160] Raymond and Beverly Sackler School of Physics and Astronomy, Tel Aviv University, Tel Aviv; Israel
[161] Department of Physics, Aristotle University of Thessaloniki, Thessaloniki; Greece
[162] International Center for Elementary Particle Physics and Department of Physics, University of Tokyo, Tokyo; Japan
[163] Graduate School of Science and Technology, Tokyo Metropolitan University, Tokyo; Japan
[164] Department of Physics, Tokyo Institute of Technology, Tokyo; Japan
[165] Tomsk State University, Tomsk; Russia
[166] Department of Physics, University of Toronto, Toronto ON; Canada
[167] TRIUMF[(a)], Vancouver BC; Department of Physics and Astronomy[(b)], York University, Toronto ON; Canada
[168] Division of Physics and Tomonaga Center for the History of the Universe, Faculty of Pure and Applied Sciences, University of Tsukuba, Tsukuba; Japan
[169] Department of Physics and Astronomy, Tufts University, Medford MA; United States of America
[170] Department of Physics and Astronomy, University of California Irvine, Irvine CA; United States of America
[171] Department of Physics and Astronomy, University of Uppsala, Uppsala; Sweden
[172] Department of Physics, University of Illinois, Urbana IL; United States of America
[173] Instituto de Física Corpuscular (IFIC), Centro Mixto Universidad de Valencia - CSIC, Valencia; Spain
[174] Department of Physics, University of British Columbia, Vancouver BC; Canada
[175] Department of Physics and Astronomy, University of Victoria, Victoria BC; Canada
[176] Fakultät für Physik und Astronomie, Julius-Maximilians-Universität Würzburg, Würzburg; Germany
[177] Department of Physics, University of Warwick, Coventry; United Kingdom
[178] Waseda University, Tokyo; Japan
[179] Department of Particle Physics, Weizmann Institute of Science, Rehovot; Israel
[180] Department of Physics, University of Wisconsin, Madison WI; United States of America
[181] Fakultät für Mathematik und Naturwissenschaften, Fachgruppe Physik, Bergische Universität Wuppertal, Wuppertal; Germany
[182] Department of Physics, Yale University, New Haven CT; United States of America

[a] Also at Borough of Manhattan Community College, City University of New York, New York NY; United States of America
[b] Also at CERN, Geneva; Switzerland
[c] Also at CPPM, Aix-Marseille Université, CNRS/IN2P3, Marseille; France
[d] Also at Département de Physique Nucléaire et Corpusculaire, Université de Genève, Genève; Switzerland
[e] Also at Departament de Fisica de la Universitat Autonoma de Barcelona, Barcelona; Spain
[f] Also at Department of Applied Physics and Astronomy, University of Sharjah, Sharjah; United Arab Emirates

JHEP07(2020)044

[g] Also at Department of Financial and Management Engineering, University of the Aegean, Chios; Greece
[h] Also at Department of Physics and Astronomy, Michigan State University, East Lansing MI; United States of America
[i] Also at Department of Physics and Astronomy, University of Louisville, Louisville, KY; United States of America
[j] Also at Department of Physics, Ben Gurion University of the Negev, Beer Sheva; Israel
[k] Also at Department of Physics, California State University, East Bay; United States of America
[l] Also at Department of Physics, California State University, Fresno; United States of America
[m] Also at Department of Physics, California State University, Sacramento; United States of America
[n] Also at Department of Physics, King's College London, London; United Kingdom
[o] Also at Department of Physics, St. Petersburg State Polytechnical University, St. Petersburg; Russia
[p] Also at Department of Physics, University of Adelaide, Adelaide; Australia
[q] Also at Department of Physics, University of Fribourg, Fribourg; Switzerland
[r] Also at Dipartimento di Matematica, Informatica e Fisica, Università di Udine, Udine; Italy
[s] Also at Faculty of Physics, M.V. Lomonosov Moscow State University, Moscow; Russia
[t] Also at Giresun University, Faculty of Engineering, Giresun; Turkey
[u] Also at Graduate School of Science, Osaka University, Osaka; Japan
[v] Also at Hellenic Open University, Patras; Greece
[w] Also at IJCLab, Université Paris-Saclay, CNRS/IN2P3, 91405, Orsay; France
[x] Also at Institucio Catalana de Recerca i Estudis Avancats, ICREA, Barcelona; Spain
[y] Also at Institut für Experimentalphysik, Universität Hamburg, Hamburg; Germany
[z] Also at Institute for Mathematics, Astrophysics and Particle Physics, Radboud University Nijmegen/Nikhef, Nijmegen; Netherlands
[aa] Also at Institute for Nuclear Research and Nuclear Energy (INRNE) of the Bulgarian Academy of Sciences, Sofia; Bulgaria
[ab] Also at Institute for Particle and Nuclear Physics, Wigner Research Centre for Physics, Budapest; Hungary
[ac] Also at Institute of Particle Physics (IPP), Vancouver; Canada
[ad] Also at Institute of Physics, Azerbaijan Academy of Sciences, Baku; Azerbaijan
[ae] Also at Instituto de Fisica Teorica, IFT-UAM/CSIC, Madrid; Spain
[af] Also at Joint Institute for Nuclear Research, Dubna; Russia
[ag] Also at Louisiana Tech University, Ruston LA; United States of America
[ah] Also at Moscow Institute of Physics and Technology State University, Dolgoprudny; Russia
[ai] Also at National Research Nuclear University MEPhI, Moscow; Russia
[aj] Also at Physics Department, An-Najah National University, Nablus; Palestine
[ak] Also at Physikalisches Institut, Albert-Ludwigs-Universität Freiburg, Freiburg; Germany
[al] Also at The City College of New York, New York NY; United States of America
[am] Also at TRIUMF, Vancouver BC; Canada
[an] Also at Universita di Napoli Parthenope, Napoli; Italy

[*] Deceased

JHEP07(2020)044